Ground-state Cooling and Photon Antibunching in Cavity Optomechanical Systems

Bijita Sarma

A thesis submitted
in Partial Fulfillment of the Requirements
for the Degree of

DOCTOR OF PHILOSOPHY

Department of Physics
Indian Institute of Technology Guwahati
Guwahati-781039, India

May 2018

Ground-state Cooling and Photon Antibunching in Cavity Optomechanical Systems

Bijita Sarma

A thesis submitted
in Partial Fulfillment of the Requirements
for the Degree of
DOCTOR OF PHILOSOPHY

Supervisor
Prof. Amarendra Kumar Sarma

Department of Physics
Indian Institute of Technology Guwahati
Guwahati-781039, India

May 2018

CERTIFICATE

It is certified that the work contained in the thesis entitled "*Ground-state Cooling and Photon Antibunching in Cavity Optomechanical Systems*" by Bijita Sarma, a Ph.D. student in the Department of Physics, IIT Guwahati, was carried out under my supervision and has not been submitted elsewhere for award of any degree.

Prof. Amarendra Kumar Sarma
Department of Physics
Indian Institute of Technology Guwahati
Guwahati-781039, Assam, India
DATE: .....

Dedicated to my family

ACKNOWLEDGMENTS

First and foremost, I would like to express my sincere gratitude towards my Ph.D. advisor, Prof. Amarendra Kumar Sarma, for letting me to conduct my research in the interesting field of cavity optomechanics. I am grateful to him for his consistent guidance, motivation, patience and kindness over these years. His enthusiasm and never-say-die attitude towards research and life as well, has always inspired me to work hard.

I would like to thank my doctoral committee members, Prof. Girish S. Setlur, Dr. Gagan Kumar, and Prof. Sandip Paul, for their encouragement and insightful comments which have helped me to understand many things better.

My sincere gratitude also goes to the current and the former Heads of the department of Physics, Prof. Subhradip Ghosh, Prof. P. Poulose and Prof. Saurabh Basu, for providing all the resources needed for my research, and also all other faculty members of the department, the technical stuff and office members, who provided me help whenever I needed. Without their support it would not have been possible to conduct my research.

I thank my group-mates Koushik, Subhadeep, Jyoti, Monika and Dipti for the stimulating discussions and for all the fun we have had in these years. I would also like to thank all my batchmates, seniors and juniors in the department for their company and help in any direct or indirect ways.

My special gratitude goes to my family for their role in my life. My parents and grandparents have always been an inspiration to me. Their unconditional love, support and trust on me are the most precious gifts that I have. My late grandfather, Uday C. Sarma was the most interesting person to me and he has had immense influence in my life; I am grateful to him for all the memories to treasure. I am thankful to my younger brothers, Tridib and Mitu for being my most favorite company. I am amazed at the way they have evolved from annoying me with their pranks in childhood, to be my greatest emotional support today. I am also grateful to my in-laws for their love and understanding, and for motivating me to pursue my career.

I would like to thank all those inspiring people who have motivated me in one way or another: my friends Dipjyoti, Sonali and Shyni di for their moral support, and specially my school teachers for drawing my interest towards pursuing science as a career.

Last but not the least, I am immensely grateful to my best friend, my husband, Sangkha, for always being there for me. 'Thank you' is such a small word for his unwavering love towards me. His inspiration, understanding and faith on me have been my greatest strengths.

ABSTRACT

Cavity optomechanics aims at understanding the radiation pressure induced interaction between photons and mechanical motion in a cavity. The radiation pressure force, arising due to the momentum carried by light, can displace a movable end mirror of the cavity. This in turn changes the length of the cavity, resulting in modification of the cavity frequency. With the rapid advances in micro and nanofabrication techniques, this nonlinear interaction has led to the exploration of a wide variety of interesting phenomena both theoretically and experimentally, such as squeezing of the light field and mechanical motion, entanglement between optical and mechanical modes, bistability, optomechanical normal mode splitting, optomechanically induced transparency, and so on. However, due to the inevitable coupling of the mechanical resonator to its surrounding, the quantum behavior gets masked by the thermal motion. Therefore, to observe quantum effects in mesoscopic mechanical resonators, it is necessary to cool them down to quantum ground state. In this thesis, we have proposed a scheme to cool the mechanical resonator to its ground state in the unresolved sideband regime by considering the interaction of the optical field with the excitons of a quantum well placed inside the cavity. Also, we have discussed the bistable behavior shown by the optical field and the mechanical motion in an optomechanical cavity, and the controllability of this behavior by coupling it to a feedback cavity containing an atomic ensemble. In the last part of the thesis, we have discussed the phenomena of photon and phonon antibunching in optomechanical setups induced via destructive quantum inference in two-photon and two-phonon excitation pathways.

Table of Contents

CHAPTER 1

INTRODUCTION

1.1 Cavity optomechanics

The field of cavity optomechanics delves into the interactions between photons and the mechanical motion in a cavity, arising due to the radiation pressure. Radiation pressure-induced effects have been studied since as early as the 17th century. The first cognition was offered by Johannes Kepler in 1619, when he observed that the tail of a comet always points away from the Sun. He predicted that this might happen due to the radiation pressure exerted by sunlight [1]. In 1873, J.C. Maxwell suggested that due to the momentum carried by light, it can exert a pressure on material objects during reflection, $P = 2I/c$ (I is the intensity of light and c is the velocity of light in vacuum). The predictions by Maxwell [2] and Bartoli [3] on the strength of the radiation-pressure force were verified experimentally by Lebedev [4], and also Nichols and Hull [5] independently in the early 20th century.

Radiation-pressure effects in the context of gravitational wave interferometers was studied by Braginsky and co-workers in the 1960's and 70's [6]. They analyzed the sensitivity limits imposed by the quantum nature of light and also speculated that the radiation pressure inside a cavity with finite decay time would give rise to damping or antidamping of mechanical motion. In the 1990's the first set of papers discussing the generation of quantum effects through radiation pressure inside an optical cavity were published. These papers discussed the idea of the generation of squeezed light

via the optomechanical Kerr-nonlinearity [7], quantum non-demolition measurements of photon number [8], feedback cooling of mechanical oscillator [9] and generation of nonclassical states of mechanical systems [10] etc., among others. However, initially the required optomechanical interaction strengths were not attainable by the state-of-the-art experiments; with only one exception of an experiment done in 1983 that demonstrated radiation pressure induced bistability in an optical cavity [11]. The feedback cooling of a mechanical mirror mode by radiation pressure was first demonstrated in 1999 [12]. Since then, the field of cavity optomechanics has been established as a feasible approach to realize the quantum regime of mechanical resonators with numerous theoretical and experimental studies [13, 14]. With the rapid advancement in nano- and microfabrication techniques, the availability of high-quality optomechanical devices has been possible. Hence, the early theories on radiation pressure induced quantum effects have become an important basis for exploring quantum optics in this whole new field of cavity optomechanics [15, 16].

The rapid surge of interest into cavity optomechanics is driven by several motivations (Ref. [15, 16] and the references therein). Firstly, optomechanical interaction is a viable tool for highly sensitive detection of small forces and displacements. Another interest is to manipulate mechanical motion in the quantum regime using light and creating nonclassical states of light and mechanical motion. Optomechanical devices could serve as coherent light-matter interfaces for applications in quantum information processing. Another usefulness is the integrability to form hybrid quantum devices by combining different quantum systems. Current research interest in cavity optomechanics includes the generation of squeezed light, quantum non-demolition measurements of photon numbers, ground-state cooling of mechanical motion, entanglement between optical and mechanical modes, and quantum-state transfer between light and mechanical resonator etc., among others.

1.1.1 Optomechanical systems

The prototype of an optomechanical system is an optical cavity with a movable end-mirror as shown in Fig. 1.1. By trapping the photons inside the cavity, the intracavity optical field can be amplified. When driven by a laser, owing to momentum transfer, the photons inside the cavity can exert a radiation pressure force on the movable mirror.

As shown in Fig. 1.1, let us consider the movable end-mirror with frequency ω_m

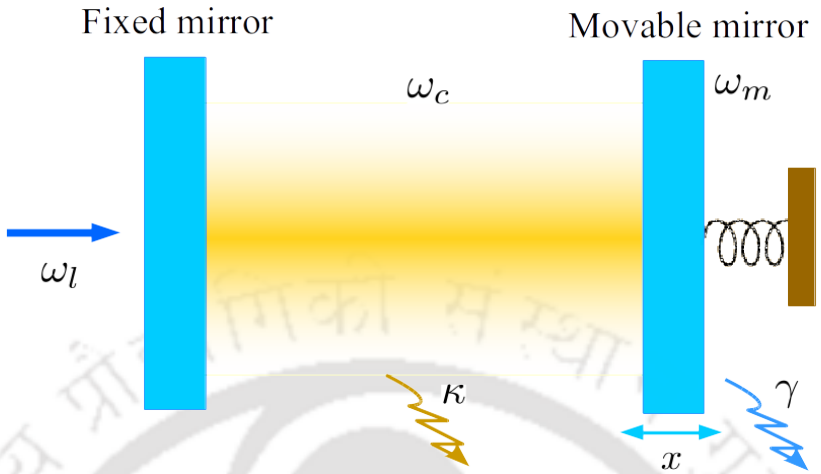

Figure 1.1: A generic optomechanical cavity with one fixed, partially transmitting mirror and one movable, totally reflecting mirror.

and mass m, and the cavity mode with frequency ω_c. In typical optomechanical setups only one of the many optical modes is considered, which is the closest to resonance with the driving laser. Also, the mechanical mirror is designed as a simple harmonic oscillator with only one of the many normal modes [15]. Considering the length of the cavity to be l, the cavity round-trip time is $t = \frac{2l}{c}$, where c is the velocity of light. Let us consider that n photons hit the mechanical mirror in the time-duration t. Then the momentum transfer from these photons to the resonator is $\Delta P = \frac{2n\hbar\omega_c}{c}$. Hence, the radiation pressure force exerted by these photons is given by $F = \frac{n\hbar\omega_c}{l}$, which is proportional to the instantaneous number of photons inside the cavity. Thus, the mirror can move under the action of this force, while also undergoing Brownian motion because of its contact with the environment.

The resonance frequency of the cavity mode is given by $\omega_c = \frac{m\pi c}{l}$, where m is the mode number. The separation of two longitudinal resonances is called the free spectral range (FSR) of the cavity, given by $\Delta\omega_c = \frac{\pi c}{l}$. Considering the optical and the mechanical modes, the Hamiltonian of the system reads (in the unit of $\hbar = 1$)

$$H = \omega_c a^\dagger a + \omega_m b^\dagger b. \tag{1.1}$$

Here, a ($a^\dagger$) and b ($b^\dagger$) are the annihilation (creation) operators for the cavity and mechanical modes respectively. Since the radiation pressure force displaces the mechanical

resonator from its initial position, the resonance frequency of the cavity mode now changes depending upon the changing length of the cavity. Considering that the change in length, $x \ll l$, the cavity frequency can be expanded in the following way:

$$\omega_c(x) = \omega_c + x\frac{\partial \omega_c}{\partial x} + \dots$$

Defining, $g = x_{\mathrm{ZPF}}\frac{\partial \omega_c}{\partial x}$, where $\frac{\partial \omega_c}{\partial x}$ is the optical frequency shift per displacement, we obtain the optomechanical Hamiltonian as follows

$$H = \omega_c a^\dagger a + \omega_m b^\dagger b + g a^\dagger a (b + b^\dagger). \tag{1.2}$$

Here, $x_{\mathrm{ZPF}} = \sqrt{1/(2m\omega_m)}$ is the zero point fluctuation of the mechanical resonator and g is the single-photon optomechanical coupling strength. Now considering the coherent drive into the cavity, the total Hamiltonian in a frame rotating with the laser frequency, ω_l is given by

$$H = \Delta a^\dagger a + \omega_m b^\dagger b + g a^\dagger a (b + b^\dagger) + \Omega(a + a^\dagger), \tag{1.3}$$

where, $\Delta = \omega_c - \omega_l$ is the detuning of the cavity mode from the laser frequency and Ω is the laser drive amplitude. Hence, it is clear from the above deduction that due to the motion of the mirror the length of the cavity gets modified, which in turn gives rise to the modification of the cavity frequency. This is how an optomechanical interaction arises between light and mechanical motion. A more rigorous derivation can be found in Ref. [17]. This optomechanical interaction lies at the heart of several recent developments aiming at the observation of quantum mechanical aspects in nanomechanical resonators [15].

The Hamiltonian derived in Eq. (1.3) is rather general, since it couples two bosonic modes (the optical and the mechanical mode) via the optomechanical coupling. Therefore, the same physics has been tested in a variety of experimental setups developed till now. The optomechanical model with a suspended mirror in a Fabry-Pérot cavity has been studied by several groups [18–22]. One particular instance of such suspended mirrors is the 'laser interferometer gravitational wave observatory' (LIGO) [23], where the arm-lengths are on the order of 4 km. Optomechanical interaction has also been studied in a 'membrane-in-the-middle' setup [24–27]. In such a system, there can be photon tunneling between both sides of the cavity through the membrane, and depending upon the membrane-displacement, either linear or quadratic coupling in position can

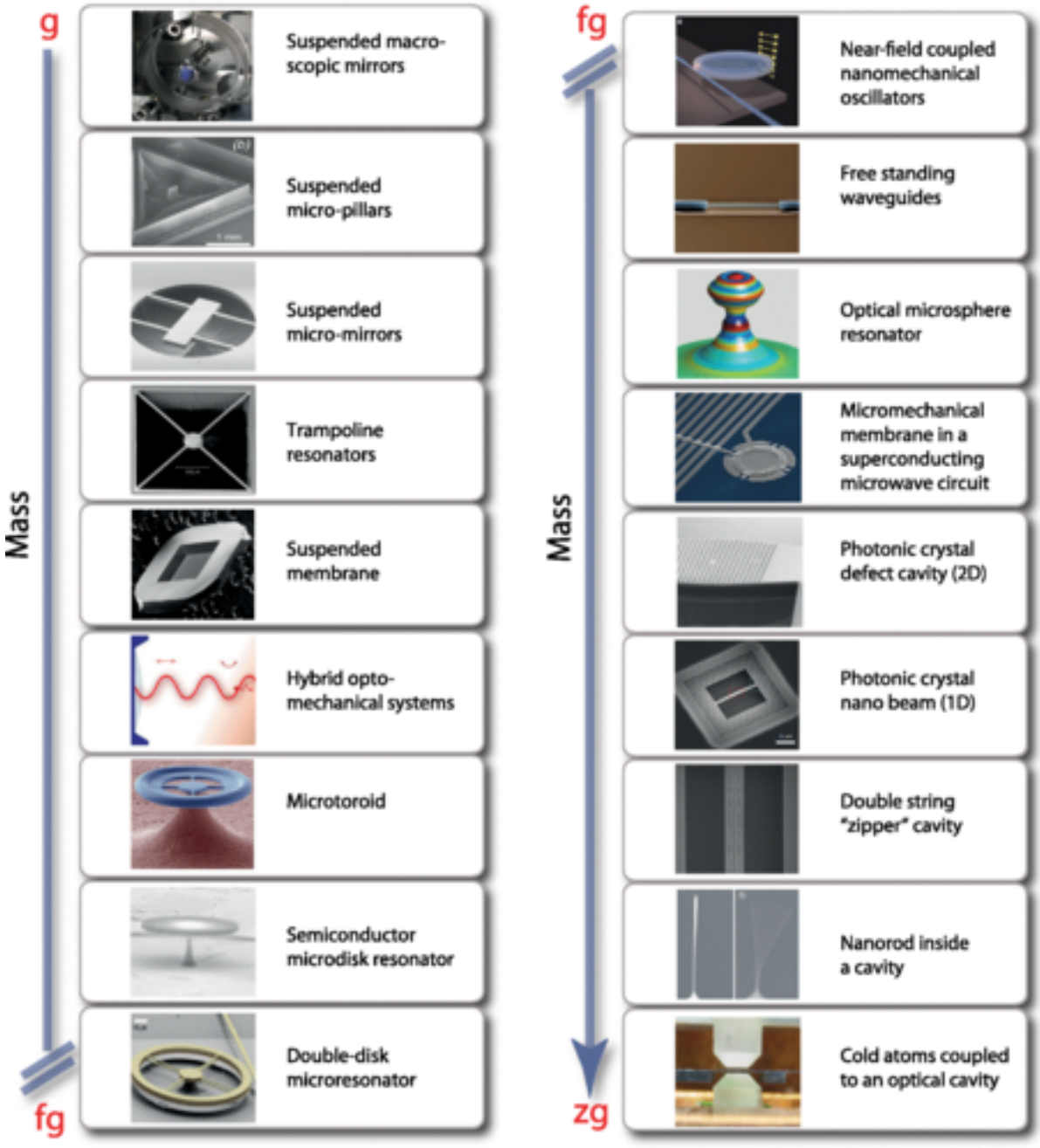

Figure 1.2: Different types of experimental optomechanical setups. Reused with permission from Ref. [15]. ©2014 American Physical Society

be modeled. Whispering gallery mode resonators are another set of analogous systems [28–34], where the optomechanical coupling depends on the change in radius of the resonator. Due to radiation pressure, the radius of the resonator changes which gives rise to a displacement-dependent resonator mode-frequency, $\omega_c(x) = \omega_c(1 - x/r)$, where displacement, $x \ll r$. In this case, the optomechanical coupling is obtained as $g = x_{\mathrm{ZPF}}\omega_c/r$.

Another noteworthy implementation of optomechanical-type coupling is in superconducting microwave LC-circuits, where one of the two parallel plates of the capacitor is movable. Depending on the displacement of the movable plate, x, the capacitance, $C = \epsilon_0 A/(d+x)$, also keeps changing. Here, d is the equilibrium distance of the two plates and A is the area of the plates. Therefore, the resonance frequency of the circuit, which is given by, $\omega_c = 1/\sqrt{LC}$ (L is the inductance of the circuit), becomes a function of the plate displacement. In this case, the optomechanical coupling is obtained as, $g = x_{\mathrm{ZPF}}\omega_c/2d$. This type of microwave setups has been studied by several groups [35–37].

Optomechanical effects have also been studied in optomechanical crystals, which support co-localized optical and mechanical modes [38, 39]. These types of systems possess very low mode-volume and high Q-factor. Therefore, the optomechanical coupling is found to be larger in comparison to other types of optomechanical systems.

Some other experimental setups for studying optomechanics are levitated dielectric objects inside a cavity [40, 41], and trapped ensemble of cold-atoms in a cavity [42–44]. In levitated dielectric systems, the cavity frequency depends on the position of the dielectric object in sinusoidal pattern. In cold-atomic systems, the single-photon optomechanical coupling can be obtained on the order of the cavity decay rate.

Some instances of experimental optomechanical setups studied by various groups are shown in Fig. 1.2.

1.1.2 Optomechanical equations of motion

An optomechanical system can be described by the Lindblad master equation approach or by a formalism called the input-output theory [15]. When one emphasizes only on the internal modes of the cavity, the system can be described by master equation approach. However, if one intends to study the output or reflection from the cavity, input-output theory is used. We briefly describe both the formalism below.

An optomechanical system has to be modeled as an open quantum system as it is

always in contact with a thermal bath. The coupling to the environment acts as a channel for decay of the cavity photons and the phonons on the mechanical resonator. Also, there would be thermal noise entering to the mechanical resonator as it is in equilibrium with the heat bath. This is a typical example of fluctuation-dissipation theorem. Following input-output theory, the dissipative dynamics of the bosonic cavity mode a and the mechanical mode b are given by [16]

$$\begin{aligned} \dot{a} &= -i[a,H] - \frac{\kappa}{2}a - \sqrt{\kappa}a_{\text{in}}, \\ \dot{b} &= -i[b,H] - \frac{\gamma}{2}b - \sqrt{\gamma}b_{\text{in}}. \end{aligned} \tag{1.4}$$

In these equations, the first term is motivated from the Heisenberg formalism for coherent dynamics of operators, the second term incorporates the decay of the bosonic mode and the last term describes the noise entering through the coupling to the environment. The cavity decay rate is κ and the mechanical damping rate is γ. The correlators for the input noise are given by

$$\begin{aligned} \langle a_{\text{in}}(t)\rangle &= 0, \\ \langle b_{\text{in}}(t)\rangle &= 0, \\ \langle a^{\dagger}_{\text{in}}(t)a_{\text{in}}(t')\rangle &= 0, \\ \langle a_{\text{in}}(t)a^{\dagger}_{\text{in}}(t')\rangle &= \delta(t-t'), \\ \langle b^{\dagger}_{\text{in}}(t)b_{\text{in}}(t')\rangle &= n_{\text{th}}\delta(t-t'), \\ \langle b_{\text{in}}(t)b^{\dagger}_{\text{in}}(t')\rangle &= (n_{\text{th}}+1)\delta(t-t'). \end{aligned} \tag{1.5}$$

Here, $n_{\text{th}} = \left[\exp\left(\frac{\omega_m}{k_B T}\right) - 1\right]^{-1}$ is the thermal occupancy of the heat bath with k_B being the Boltzmann constant. For the optical mode with frequency on the order of 10^{14} Hz, the number of thermal photons at 300 K is $\sim 10^{-35}$; whereas for a typical micro- or nano-mechanical resonator with resonance frequency in the range $1-1000$ MHz, the number of thermal phonons at 300 K is found in the range of $10^4 - 10^7$. Therefore, for optomechanical systems at the optical frequency, the thermal photon number can be neglected, but the thermal phonon population has significant effect.

In the Lindblad master equation approach, the dissipative time-evolution of the modes is given by the evolution of the density matrix

$$\dot{\rho} = -i[H,\rho] + \kappa\mathscr{L}[a]\rho + \gamma(n_{\text{th}}+1)\mathscr{L}[b]\rho + \gamma n_{\text{th}}\mathscr{L}[b^{\dagger}]\rho, \tag{1.6}$$

where, $\mathscr{L}[o]\rho = o\rho o^\dagger - \frac{1}{2}o^\dagger o\rho - \frac{1}{2}\rho o^\dagger o$ is the Liouvillian operator for mode 'o'. Since the thermal photon number is negligible, the term $\kappa\mathscr{L}[a]\rho$ describes only the decay of photons from the cavity. However for the mechanical resonator, the term $\gamma\mathscr{L}[b]\rho$ incorporates the damping, whereas the term $\gamma n_{\rm th}\left(\mathscr{L}[b]\rho + \mathscr{L}[b^\dagger]\rho\right)$ incorporates the thermalization due to the environment.

1.2 Optomechanical effects

The Hamiltonian given by Eq. (1.3) exhibits several interesting phenomena in different detuning and coupling regimes. In this thesis, we have studied the phenomena of optomechanical bistability, mechanical resonator-cooling and photon/phonon antibunching in optomechanical systems, which we discuss briefly in the following:

1.2.1 Optomechanical bistability

In order to enhance the radiation pressure induced interaction in an optomechanical cavity, one needs to reach the strong optomechanical coupling regime where $g \gg \kappa, \gamma$. However, it is difficult to achieve strong optomechanical coupling at the single-photon level in experiments, as the force exerted by a single photon on a mechanical resonator is typically very weak. Hence, as an alternate to single-photon strong coupling, one can drive the cavity with a strong laser. Strong coupling using this method has been demonstrated recently [21]. For a strong drive, the intracavity field is amplified, and this in turn can trigger different types of nonlinear effects in the cavity depending on the input laser power and the detuning of the driving laser with respect to the cavity resonance. In the blue-detuned regime, multistability [45, 46] and instability [18] may arise, whereas in the red-detuned regime, bistability [11] of the optical field amplitude and mechanical resonator position occurs.

The name bistability refers to the phenomenon, where for a particular input light intensity, two stable cavity field intensities as well as mechanical positions are possible. To understand it, let us consider the optomechanical Hamiltonian given by Eq. (1.3). The equations of motion are given by the Heisenberg-Langevin equations

$$\begin{aligned} \dot{a} &= -\left[i\left(\Delta + \frac{g}{x_{\rm ZPF}}x\right) + \frac{\kappa}{2}\right]a - i\Omega, \\ \ddot{x} &= -\omega_m^2 x - \frac{g}{m x_{\rm ZPF}}|a|^2 - \gamma\dot{x}, \end{aligned} \tag{1.7}$$

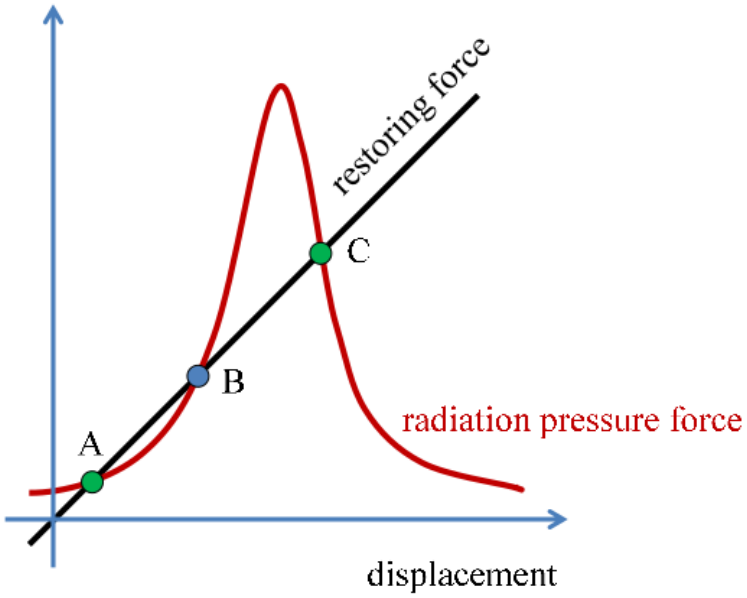

Figure 1.3: At the points A, B and C, the restoring force and the radiation pressure force are equal. Out of these, only A and C are stable, because the rate of growth of restoring force is faster than that of the radiation pressure force [47].

where $x = x_{\mathrm{ZPF}}(b + b^{\dagger})$. From Eq. (1.7), it can be observed that the mechanical resonator acts as a damped harmonic oscillator with restoring force, $m\omega_m^2 x$, and a radiation pressure force, $g|a|^2/x_{\mathrm{ZPF}}$, acting on it. Also, the overall detuning of the cavity changes proportionally to the displacement of the mechanical resonator. In the steady-state, the amplitude of the intracavity optical field and the mechanical resonator position are given by

$$\begin{aligned} a &= \frac{i\Omega}{-i[\Delta + gx/x_{\mathrm{ZPF}}] - \kappa/2} \\ x &= -\frac{g}{m x_{\mathrm{ZPF}} \omega_m}|a|^2. \end{aligned} \tag{1.8}$$

By substituting the second equation into the first one in Eq. (1.8), one obtains a cubic equation in $|a|^2$. Cubic equations can have one real root for some parameter space, or three real roots simultaneously for other parameter spaces. Therefore in the optomechanical cavity, the intracavity optical intensity as well as the mechanical resonator position can possess three different values for certain input parameters. The physics can be understood as follows. When the mechanical resonator in an optomechanical cavity is moved from its equilibrium position, the mechanical restoring force, $m\omega_m^2 x$ increases

linearly with displacement, whereas the radiation pressure force, $g|a|^2/x_{\rm ZPF}$ is maximum only at the cavity resonance. As a result of the competition between these two forces (see Fig. 1.3), for sufficiently high input power, one obtains three displacement values at which these two forces become equal. However, only two of the points are stable. This is how bistability of the intracavity light intensity and mechanical resonator position arises.

Earlier, optical bistability in semiconductor microcavities was demonstrated by Gibbs *et al.* [48] and Baas *et al.* [49]. In fact, bistability was one of the early observations in optomechanical systems. It was demonstrated experimentally by Dorsel *et al.* [11] and Gozzini *et al.* [50]. Recently, the bistable behavior shown by the mean intracavity photon number has been discussed in a generic optomechanical system [47], two-mode optomechanical system [51] as well as optomechanical systems with a Bose-Einstein condensate (BEC) [43], ultracold atoms [52], and a quantum well [53].

1.2.2 Ground-state cooling of a mechanical resonator

In an optomechanical system, the mechanical resonator is always in contact of a thermal environment. Therefore, due to the coupling to the thermal reservoir, the quantum behavior of the resonator is masked by the random thermal motion. In order to observe mechanical quantum effects, one needs to cool the mechanical modes to the quantum ground-state [36].

The optomechanical cooling of mechanical modes could be understood by using the linearization approach. For strong input light, the cavity and the mechanical resonator operators can be expressed as consisting of a classical and a quantum part: $a = a_s + \delta a$, $b = b_s + \delta b$. Then the Langevin equations for the classical and quantum fluctuation parts are given by

$$\begin{aligned}
\dot{a_s} &= -\left(i\Delta' + \frac{\kappa}{2}\right) a_s - i\Omega, \\
\dot{b_s} &= -\left(i\omega_m + \frac{\gamma}{2}\right) b_s - ig|a_s|^2, \\
\dot{\delta a} &= -\left(i\Delta' + \frac{\kappa}{2}\right) \delta a - iga_s(\delta b + \delta b^\dagger) - ig\delta a(\delta b + \delta b^\dagger) - \sqrt{\kappa}\, a_{\rm in}, \\
\dot{\delta b} &= -\left(i\omega_m + \frac{\gamma}{2}\right) \delta b - iga_s(\delta a + \delta a^\dagger) - ig\delta a^\dagger \delta a - \sqrt{\gamma}\, b_{\rm in}.
\end{aligned} \tag{1.9}$$

Here, $\Delta' = \Delta + g(b_s + b_s^*)$, is the modified cavity detuning. For strong optical driving, the terms $ig\delta a(\delta b + \delta b^\dagger)$ and $ig\delta a^\dagger \delta a$ are negligible and can be ignored. Then, the linearized

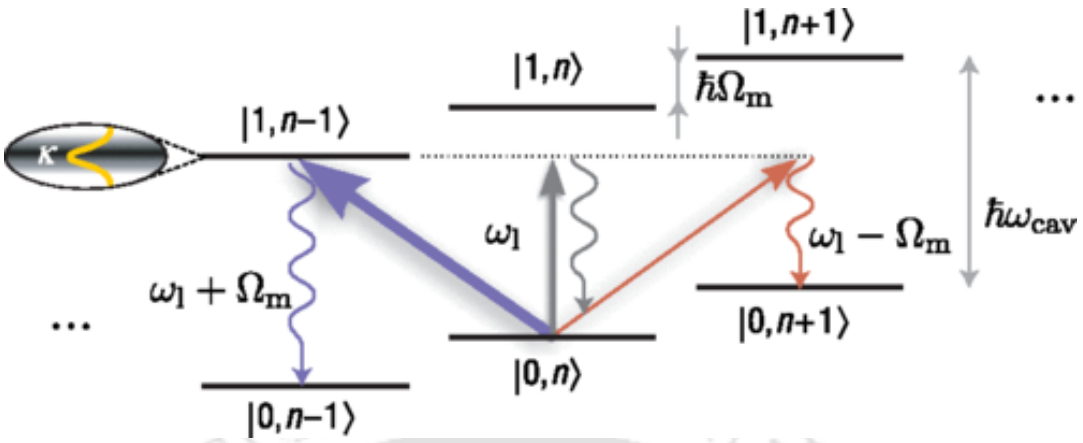

Figure 1.4: Process of cavity-optomechanical sideband cooling. The transitions correspond to the Hamiltonian in Eq. (1.10). Using appropriate detuning one can obtain efficient cooling. Here, Ω_m is our ω_m and ω_{cav} is our ω_c. Adapted and reused with permission from [54]. ©2018 Macmillan Publishers Limited, part of Springer Nature. All rights reserved.

Hamiltonian is obtained as

$$H_L = \Delta' \delta a^\dagger \delta a + \omega_m \delta b^\dagger \delta b + G(\delta a + \delta a^\dagger)(\delta b + \delta b^\dagger), \tag{1.10}$$

where $G = g a_s$ is the enhanced optomechanical coupling due to the coherent input field. The processes described by this linearized Hamiltonian are shown in Fig. 1.4. The basic idea of optomechanical cooling can be understood as follows: in an optomechanical system, the scattering of intra-cavity light from the movable end mirror gives rise to Stokes and anti-Stokes sidebands. If the mechanical mirror absorbs a quantum of energy from the cavity optical field, the Stokes sideband originates leading to heating of the mirror, whereas if the cavity field absorbs energy from the mirror, the anti-Stokes process occurs resulting in cooling of the mirror. In other words, the radiation pressure force exerted by the cavity field reacts with some delay time due to the finite cavity linewidth. Therefore the optical field introduces extra damping for the mechanical mode in an optomechanical cavity.

The effective cooling rate can be calculated as follows. Let us assume that the rate of occurrence of the anti-Stokes process is A_- and that of the Stokes process is A_+. Then, the rates of transition from the phonon state n to the states, $n-1$ and $n+1$ are given by [15]

$$\begin{aligned} \Gamma_{n\to n-1} &= nA_-, \\ \Gamma_{n\to n+1} &= (n+1)A_+. \end{aligned} \tag{1.11}$$

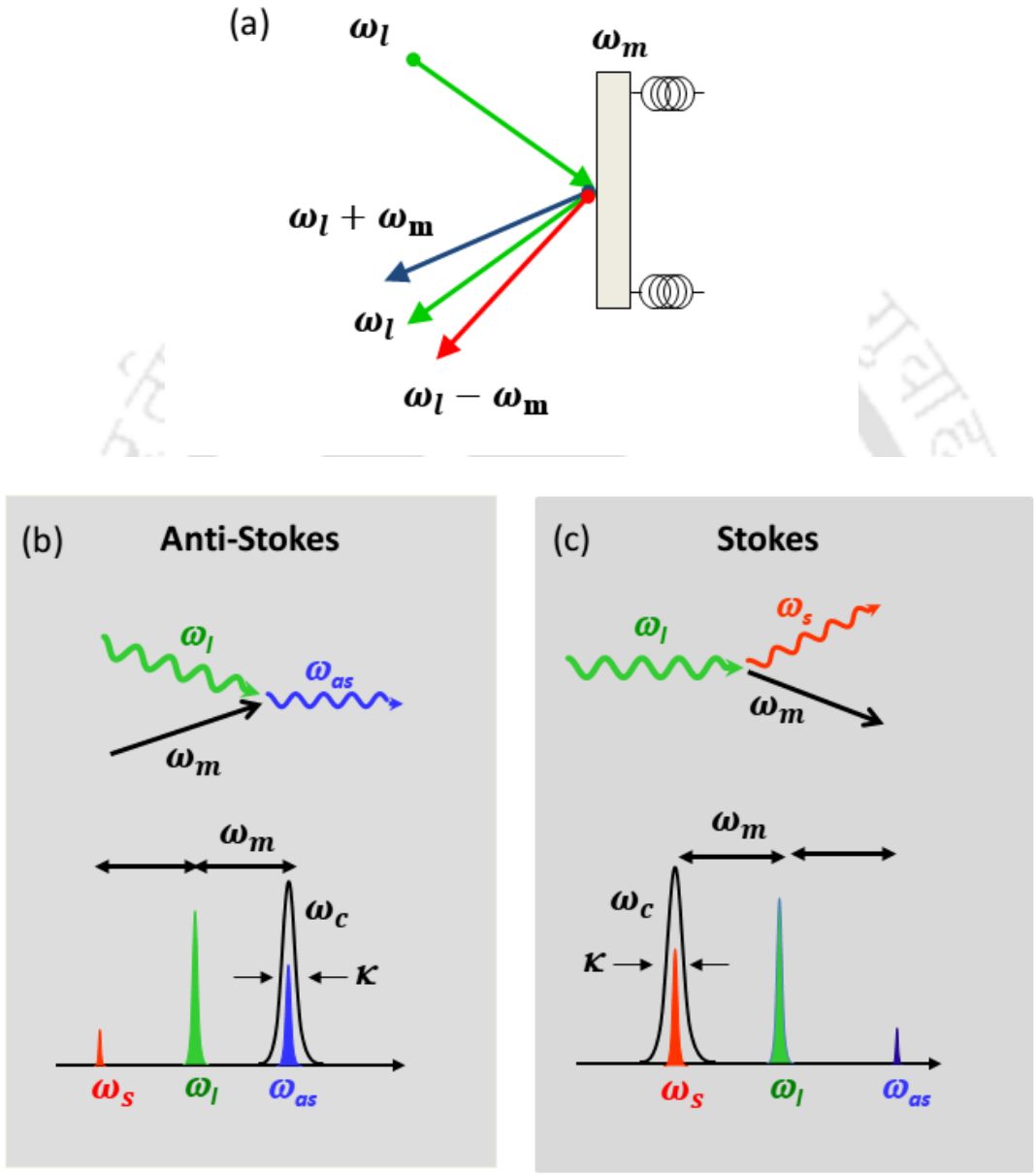

Figure 1.5: (a) The process of producing Stokes and anti-Stokes radiation. (b) and (c) demonstrate the requirement of the resolved-sideband condition.

The optomechanical damping rate is given by the net downward transition rate,

$$\Gamma_{\rm om} = A_- - A_+ \tag{1.12}$$

We assume that the optomechanical system is kept in a thermal environment with average phonon occupancy $n_{\rm th}$. This thermal bath will also give rise to extra transition probabilities from the state n, which are given by

$$A_+^{\rm th} = n_{\rm th}\gamma, \qquad A_-^{\rm th} = (n_{\rm th}+1)\gamma.$$

Therefore, the net rate of change of average phonon occupancy on the mechanical resonator is given by

$$\dot{\bar{n}} = (\bar{n}+1)(A_+ + A_+^{\rm th}) - \bar{n}(A_- + A_-^{\rm th}). \tag{1.13}$$

At the steady-state, which corresponds to $\dot{\bar{n}} = 0$, the average phonon number is given by

$$\bar{n} = \frac{A_+ + n_{\rm th}\gamma}{\gamma_{\rm om}+\gamma} \tag{1.14}$$

The transition rates can be obtained from the Fermi's golden rule as

$$A_\pm = x_{\rm ZPF}^2 S_{FF}(\mp\omega_m) \tag{1.15}$$

where,

$$S_{FF}(\omega) = \int_{-\infty}^{\infty} dt e^{i\omega t}\langle F(t)F(0)\rangle \tag{1.16}$$

is the quantum noise spectrum. To obtain effective cooling of the mechanical mirror, the cooling rate should exceed the heating rate.

In analogy to the laser cooling of ions in the strong-binding regime [55], conventional cavity cooling of mechanical oscillators works in the resolved-sideband regime, where the cavity-mode decay rate is lower than the mechanical oscillator resonance frequency [36, 39, 56], as explained in Fig. 1.5. However, for typical mechanical oscillators with frequency in the range of kHz–MHz, fulfilling this condition is a challenging task. To relax this requirement, few approaches on ground-state cooling in the unresolved sideband regime have been suggested recently, such as cooling using dissipative coupling [57–59], coupling with a high-Q auxiliary cavity [60–62], hybrid atom-optomechanical systems [63–65], and using optomechanically induced transparency [66].

1.2.3 Photon blockade

Once the mechanical resonator in an optomechanical cavity is prepared in or near to its ground state, the system can further be used for quantum information processing related applications. On-demand generation of single photons is a primary requirement in light-based quantum information processing [67]. In recent years, significant progress have been made towards the demonstration of single-photon sources in various platforms, such as single quantum dots integrated with photonic crystal cavities [68], optical fibers [69] or single atoms coupled with micro-cavity systems [70]. One of the ways of obtaining single photons is via the mechanism called photon blockade. It is a quantum optical effect that arises as a result of the quantum anharmonicity ladder in a nonlinear cavity. In most of the studies, the prototype that has been widely explored is cavity quantum electrodynamics. The addition of a Kerr-medium or an atom or quantum dot to a cavity makes it a highly nonlinear system and induces break down of the harmonicity of the energy levels of the cavity. This leads to the phenomenon of photon blockade, where only a single photon can occupy the cavity-atom or cavity-quantum dot system at a time [71, 72]. Presence of one photon prohibits the simultaneous transmission of multiple photons through the cavity and a stream of one-by-one single photons at the output of the device from a coherent light input could be achieved.

There have been proposals for achieving single-photon blockade in several systems such as coupled cavity arrays [73], circuit-QED systems [74], and so on. Recently P. Rabl discussed the idea of realizing photon blockade in an optomechanical system via the optomechanical interaction-induced nonlinearity [75]. Subsequently there were several proposals for photon blockade in optomechanical setups including two-mode optomechanical systems [76], quadratically coupled optomechanical system [77], optomechanical cavity coupled to a two-level sytem [78] etc.

To understand the origin of the photon blockade effect, we consider the optomechanical Hamiltonian given by Eq. (1.3). Now, using a polaron transform, $U = e^{\frac{g}{\omega_m} a^\dagger a (b^\dagger - b)}$, the Hamiltonian can be diagonalized in the absence of coherent driving and bath interactions. In presence of coherent driving, the transformed Hamiltonian is given by

$$H = \Delta a^\dagger a + \Delta_g a^\dagger a^\dagger a a + \omega_m b^\dagger b + \Omega(a + a^\dagger), \tag{1.17}$$

where, $\Delta_g = g^2/\omega_m$. In absence of the driving field, the energy eigenvalues are given by, $E_{nm} = \Delta n - \Delta_g n^2 + \omega_m m$, with eigenstates, $|E_{nm}\rangle = |n\rangle \otimes |m\rangle$. From the energy-levels as shown in Fig. 1.6, it is evident that for a fixed value of m, the energy-levels are not

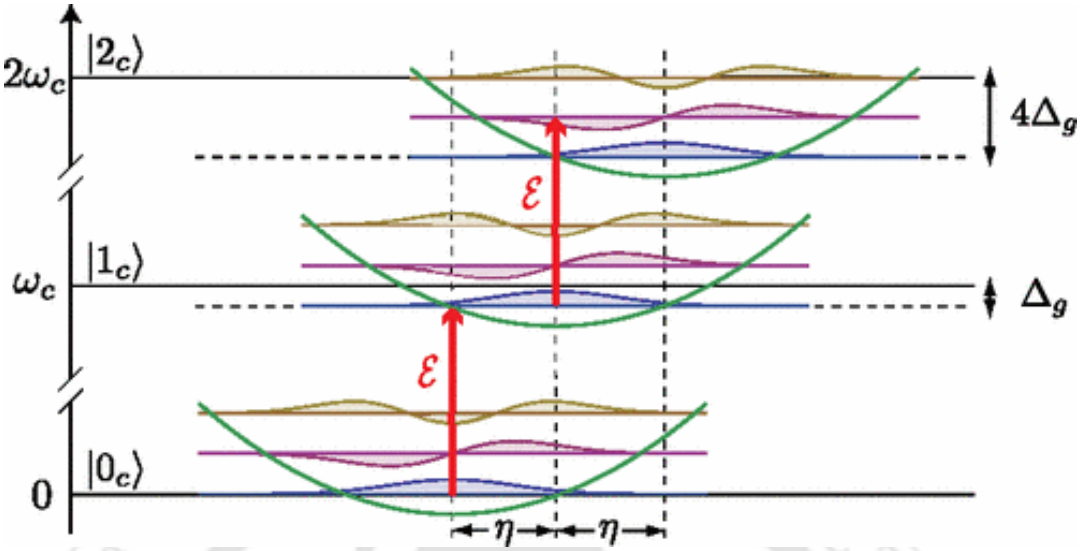

Figure 1.6: Energy-level diagram for an optomechanical system. Here, ε is our Ω, and $\eta = g/\omega_m$. Reused with permission from [75]. ©2011 American Physical Society

equidistant. Therefore, for a resonant coherent driving from $n = 0$ to $n = 1$, the next transition from $n = 1$ to $n = 2$ is off-resonant, which gives rise to photon blockade.

The occurrence of photon blockade is characterized by the observation of sub-Poissonian statistics of the output field [79]. It can be analyzed by means of the zero-time delay second-order correlation function given by

$$g^{(2)}(0) = \frac{\langle a^\dagger(t)a^\dagger(t)a(t)a(t)\rangle}{\langle a^\dagger(t)a(t)\rangle^2}, \tag{1.18}$$

and the two-time correlation function

$$g^{(2)}(\tau) = \frac{\langle a^\dagger(t)a^\dagger(t+\tau)a(t+\tau)a(t)\rangle}{\langle a^\dagger(t)a(t)\rangle^2}. \tag{1.19}$$

For nonclassical light $g^{(2)}(0) < 1$ and $g^{(2)}(\tau) > g^{(2)}(0)$.

As in other nonlinear systems, single-photon blockade in optomechanical system is generally possible only in the single-photon strong coupling regime where, $g \gg \kappa, \gamma$. However, this type of optomechanical coupling where the influence of one photon is enough to control the mechanical motion is difficult to achieve. There is only one exception of optomechanical systems consisting of an ensemble of cold atoms, where this regime has been reached. In a recent work by Liew and Savona [80], a new mechanism was invoked to realize photon blockade, based on quantum interference between photon excitation pathways that is referred to as the unconventional photon blockade. It was

shown that strong antibunching could be achieved even with a weak Kerr nonlinearity in a system consisting of two coupled quantum modes. Realization of unconventional photon blockade has been predicted in a few systems, such as coupled nonlinear photonic molecules [81], coupled single quantum dot–cavity system [82], coupled cavities with third-order nonlinearities [83], and coupled optomechanical systems [84].

1.2.4 Phonon blockade

Photons have been considered as the conventional candidate for the role of transfering and storing quantum information owing to the good integrability to different systems. However, phonons also offer promising role as quantum information carrier due to the low damping rate and the integrability to a wide range of quantum systems such as electric, magnetic and optical systems [85, 86]. In fact, it was noted that the low propagation speed of phonons may enable new dynamic schemes for processing quantum information, and due to the short wavelength of phonon, it may be exploited to explore new regimes of atomic physics that cannot be reached otherwise in photonic systems [87]. Single phonons are the necessary elements in phononic networks. There are several proposals for preparing single phonons such as via two-phonon damping [88], via performing measurements [89] and via heralded measurement of the Stokes photon in optomechanics [90, 91]. In analogy to photon blockade, one can realize phonon blockade as a signature of quantum behavior in nanomechanical resonators. By coupling a mechanical resonator to a qubit or by including a nonlinearity, one can obtain the blockaded state where upon external driving, the number of excitations in the mechanical resonator never exceeds one. There are several proposals in this regard [92–95]. However, the intrinsic nonlinearity in most of the mesoscopic mechanial resonators is very weak [96, 97]. To circumvent this, the idea originally proposed by Liew and Savona [80] in case of photons can be borrowed, where the destructive interference between two-phonon excitation pathways would give rise to phonon blockade. Some of the works in this line has been reported recently [98, 99].

In addition to these phenomena that we discussed here, there are many other intriguing properties shown by optomechanical systems. In the opposite process of cooling, the mechanical resonator motion can be amplified. When the amplification rate exceeds the mechanical damping rate, dynamical instability of the mechanical motion arises and finally one can reach the regime of self-sustained oscillations. This has been studied

in several systems [45, 100–108]. Using the optomechanical interaction one can also realize the analog of electromagnetically induced transparency seen in atomic systems [109–113]. One can also generate entanglement between the optical and the mechanical mode [114–117], squeezing of mechanical modes [118–120] and non-classical mechanical states [121–123].

1.3 Outline of the thesis

In the following, we present the plan of the thesis briefly by including a description of the various problems that have been tackled in the form of different chapters of the thesis.

Chapter 2 discusses the bistable behavior shown by the mean intracavity optical field and the position of the mechanical resonator in an optomechanical cavity, and the effect of optical feedback from a cavity containing an ultracold two-level atomic ensemble on the bistable behavior. We show that the optical bistability can be controlled by tuning the frequency and power of the driving laser and is largely affected by the presence of the atomic ensemble in the feedback cavity. In essence, our work emphasizes the possibility of realization of a controllable optical switch that depends on the hybrid interaction and commands lower threshold power than a single optomechanical cavity.

In *chapter 3*, we discuss the ground-state cooling of a mechanical oscillator in an optomechanical cavity in presence of a quantum well, in the unresolved-sideband regime. Due to the presence of the quantum well, the cavity response gets modified and leads to asymmetric heating and cooling processes. The cooling rate of the mechanical resonator can potentially be enhanced by tuning the cavity-field detuning. We show that even when the cavity is in the unresolved-sideband regime, the effective interaction of the excitons and mechanical mode can bring the system back to an effective resolved-sideband regime. The time evolution of the mean phonon number in the mechanical resonator is studied using the quantum master equation approach. The average phonon occupancy in the mechanical resonator tends to zero with time.

In *chapter 4*, we discuss the occurrence of photon blockade in optomechanical systems via destructive quantum interference between two-photon excitation pathways. First, we consider an optomechanical system in which two weakly nonlinear optical modes interact with a mechanical mode via three-mode resonance. We show that through the three-mode interaction, distinct pathways can be created that leads to two-photon excitation in the higher frequency optical mode. This may lead to the phenomenon of photon

antibunching via destructive quantum interference. We derive the optimal conditions for unconventional photon blockade and numerical analysis also holds these results. We also discuss the photon blockade effect in an optomechanical cavity containing a degenerate optical parametric amplifier. We show that for optimal values of the amplifier pump amplitude and phase, strong photon antibunching can be realized.

Chapter 5 discusses the phenomenon of phonon blockade in a system of two weakly nonlinear coupled mechanical resonators. We show that via the effect of destructive quantum interference between the paths leading to two-phonon excitation, phonon blockade can be realized in the system. We also show that in comparison to a single drive applied on a single mechanical resonator, driving both the mechanical resonators can be beneficial in terms of temperature sensitivity of phonon blockade. Also, we discuss the aspect of detection of phonon blockade via connecting it to an optomechanical cavity where the radiation pressure force can be exploited to obtain the photon correlation as a measure of phonon blockade.

Chapter 6 concludes the thesis with a summary of the major findings of the research works carried out, and a brief outline on the scope for future studies.

CHAPTER 2

OPTOMECHANICAL BISTABILITY

In this chapter, we study the bistable behavior shown by the mean intracavity optical field in an optomechanical cavity, and the effect of optical feedback from a cavity containing an ultracold two-level atomic ensemble on the bistable behavior. It is observed that the optical bistability can be controlled by tuning the frequency and power of the driving laser and it is largely affected by the presence of the atomic ensemble in the feedback cavity. In essence, our work emphasizes the possibility for realization of a controllable optical switch that depends on the hybrid interaction and commands lower threshold power than a single optomechanical cavity.

Optical bistability inside a cavity with finite decay time, arising due to the dynamic backaction induced by radiation pressure has been studied in various optomechanical systems [43, 47, 51–53, 124–127]. In this work, we consider a hybrid optomechanical system consisting of two cavities, one optomechanical and the other containing an ultracold two level atomic ensemble, coupled by a single pump laser. Currently hybrid optomechanical systems [63, 65, 128–133] are highly in focus due to the versatility of both optical and mechanical components in coupling to different systems such as spins, cold atoms, superconducting qubits etc. In particular, we study the bistable behavior shown by the cavity optical field in the optomechanical cavity with and without feedback

An article based on this chapter is published in *J. Opt. Soc. Am. B*, vol. **33**, No. 7, year 2016, pages 1335-1340; title: "*Controllable optical bistability in a hybrid optomechanical system*"; authors: Bijita Sarma and Amarendra K. Sarma. Selected contents are reproduced with permission. ©2016 Optical Society of America.

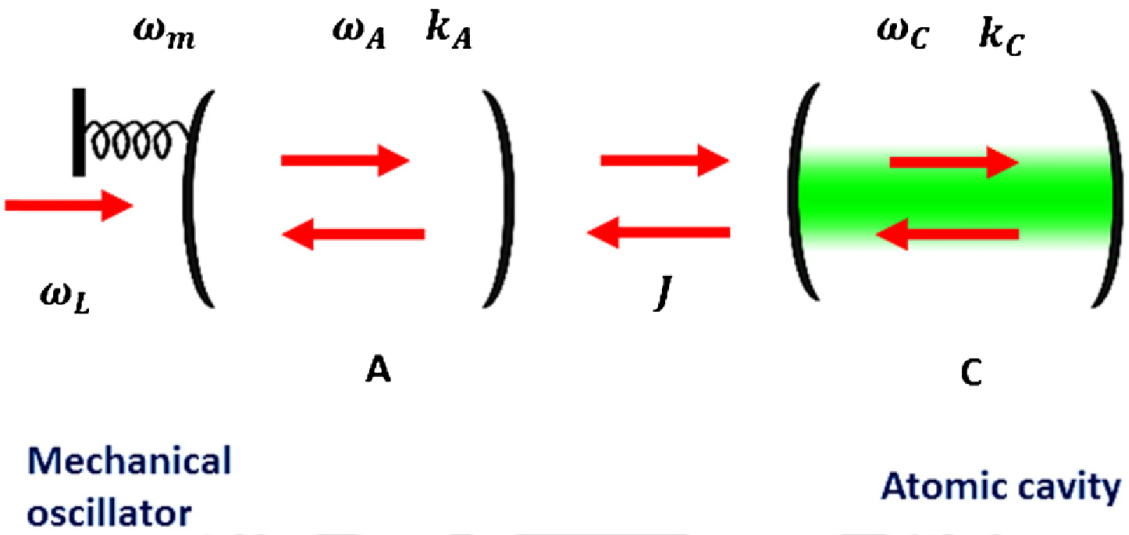

Figure 2.1: A hybrid optomechanical cavity setup with an optomechanical cavity A and a feedback cavity C containing ultracold atomic ensemble, coupled optically.

from the atomic cavity. We discuss the controllability of the bistable behavior of the mean intracavity optical intensity in the optomechanical cavity depending on the system parameters provided by the feedback cavity.

2.1 Model and theory

We consider a hybrid optomechanical system consisting of two cavities A and C as shown schematically in Fig. 2.1. Cavity C, with both the end mirrors fixed contains an ensemble of ultracold two-level atoms. Cavity A consists of one fixed end mirror and another movable end mirror with resonance frequency ω_m, effective mass m and decay rate γ_m. Cavity A is driven by an intense pump laser of frequency ω_L , which exerts a radiation pressure force on the movable end mirror. The output optical field from the cavity A drives the cavity C, and the output from cavity C is again fed back into cavity A.

The Hamiltonian of the whole system, in a frame rotating with the driving laser frequency ω_L, is given by,

$$\begin{aligned} H &= \hbar\Delta_A a^\dagger a + \hbar\Delta_C c^\dagger c + \frac{p^2}{2m} + \frac{1}{2}m\omega_m^2 q^2 + \frac{1}{2}\hbar\Delta_{\rm at}\sigma_3 + \hbar g_{\rm at}\left(c^\dagger\sigma_{12} + c\sigma_{21}\right) \\ &\quad - \hbar g_{\rm OM} a^\dagger a q + \hbar J\left(c^\dagger a + a^\dagger c\right) + i\hbar\varepsilon_A\left(a^\dagger - a\right), \end{aligned} \tag{2.1}$$

where the first and second terms represent the free energy of the cavity modes in

the two cavities, A and C respectively. $\Delta_A = \omega_A - \omega_L$ and $\Delta_C = \omega_C - \omega_L$ are the cavity detunings with ω_A and ω_C being the corresponding cavity resonance frequencies. The third and fourth terms give the energy of the mechanical oscillator expressed in terms of the position and momentum operators q and p satisfying the commutation relation $[q,p] = i\hbar$. The fifth term is the energy of the two-level atomic ensemble trapped inside the cavity C where, $\Delta_{\text{at}} = \omega_{\text{at}} - \omega_L$, is the detuning of the atomic resonance from the laser drive. σ_{ij} 's are the atomic operators with $\sigma_{ij} = |i\rangle\langle j|$ and we have denoted $\sigma_{22} - \sigma_{11}$ as σ_3, where σ_{22} and σ_{11} are the atomic populations in the excited and ground levels respectively. The sixth term describes the interaction of the atomic ensemble with the optical field in the cavity C, g_{at} being the single atom-photon coupling constant. The seventh term is the optomechanical interaction term, where, $g_{\text{OM}} = \omega_A/L$, is the optomechanical coupling between the cavity field and the mechanical oscillator in cavity A. The eighth term accounts for the coupling between the two cavities where J is the coupling strength [134–138]. The last term represents the effect of the driving pump laser with frequency ω_L and amplitude $\varepsilon_A = \sqrt{\frac{2k_A P_{in,A}}{\hbar\omega_L}}$, on the optomechanical cavity where $P_{in,A}$ is the input laser power.

To study the effect of feedback into cavity A, we first need to analyze the cavity field dynamics in cavity C. The time evolution of the system operators are given by nonlinear Heisenberg-Langevin equations:

$$\frac{dc}{dt} = -(k_C + i\Delta_C)c - ig_{\text{at}}\sigma_{12} - iJa + \sqrt{2k_C}\,c_{\text{in}}(t), \tag{2.2a}$$

$$\frac{d\sigma_{12}}{dt} = -\left(\gamma_{\text{at}} + i\Delta_{\text{at}}\right)\sigma_{12} + ig_{\text{at}}c\sigma_3 + \sqrt{2\gamma_{\text{at}}}\,c_{\text{in}}(t), \tag{2.2b}$$

where, γ_{at} is the atomic coherence decay rate and c_{in} is the input vacuum noise operator with zero mean value and nonzero correlation function given by [139]

$$\langle c_{\text{in}}(t)\, c_{\text{in}}^{\dagger}\left(t'\right)\rangle = \delta\left(t - t'\right). \tag{2.3}$$

Assuming the system operators under mean field approximation and considering $\langle\sigma_{22}\rangle = 0$ and $\langle\sigma_{11}\rangle = N$, i.e. atoms populating only the ground state, the steady state operators are given by

$$c_S = \frac{-iJa}{k_C + i\Delta_C + \frac{g_{\text{at}}^2 N}{\gamma_{\text{at}} + i\Delta_{\text{at}}}}, \tag{2.4a}$$

$$\sigma_{12,S} = \frac{-ig_{\text{at}}c_S N}{\gamma_{\text{at}} + i\Delta_{\text{at}}} \tag{2.4b}$$

Now, defining the dimensionless position and momentum operators, $Q = \sqrt{\frac{m\omega_m}{\hbar}}\, q$ and $P = \sqrt{\frac{1}{m\hbar\omega_m}}\, p$, satisfying the commutation relation $[Q,P] = i$, the equations of motion for the operators for cavity A are given by

$$\frac{dQ}{dt} = \omega_m P, \tag{2.5a}$$

$$\frac{dP}{dt} = \omega_m \chi a^\dagger a - \omega_m Q - \gamma_m P + \xi, \tag{2.5b}$$

$$\frac{da}{dt} = -i\Delta a - \left(k_A + \frac{J^2}{k_C + i\Delta_C + \frac{g_{\rm at}^2 N}{\gamma_{\rm at} + i\Delta_{\rm at}}} \right) a + \varepsilon_A + \sqrt{2k_A}\, a_{\rm in}, \tag{2.5c}$$

where, $\chi = \frac{\omega_A}{\omega_m L}\sqrt{\frac{\hbar}{m\omega_m}} = \frac{g}{\omega_m}\sqrt{\frac{\hbar}{m\omega_m}}$, is the scaled coupling constant, and $\Delta = \Delta_A - \omega_m \chi Q_S$ is the effective detuning in the optomechanical cavity. $a_{\rm in}$ is the input vacuum noise operator for cavity A, given by [139]

$$\left\langle a_{\rm in}(t) a_{\rm in}^\dagger\left(t'\right)\right\rangle = \delta\left(t - t'\right). \tag{2.6}$$

ξ is the Brownian noise operator associated with the damping of the mechanical oscillator, with zero mean value and nonzero correlation function given by [140]

$$\langle \xi(t)\xi(t')\rangle = \frac{1}{2\pi}\frac{\gamma_m}{\omega_m}\int \omega e^{-i\omega(t-t')}\left[1 + \coth\left(\frac{\hbar\omega}{2k_B T}\right)\right] d\omega. \tag{2.7}$$

2.2 Bistability of the intracavity field and mirror position

Bistability is a ubiquitous phenomenon observed in many nonlinear systems. The inherent nonlinearity in the equations of motion of our system indicates observation of such effects through optomechanical coupling. Considering that the mean values of the system operators can be factorized, one derives the steady state solutions of the equations (2.5) as

$$Q_S = \chi |a_S|^2, \tag{2.8a}$$

$$P_S = 0, \tag{2.8b}$$

$$a_S = \frac{\varepsilon_A}{k_A + \frac{J^2}{k_C + i\Delta_C + \frac{g_{\rm at}^2 N}{\gamma_{\rm at} + i\Delta_{\rm at}}} + i\Delta}. \tag{2.8c}$$

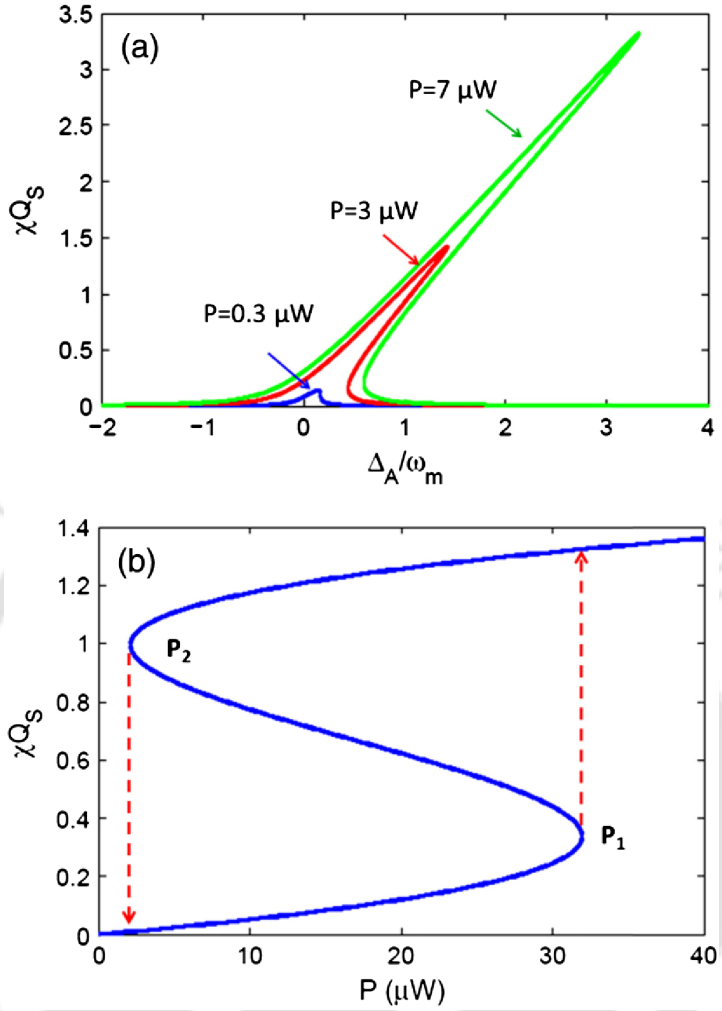

Figure 2.2: Plot of (a) χQ_S vs $\frac{\Delta_A}{\omega_m}$ for $P = 0.3\ \mu W$ (blue solid line), $3\ \mu W$ (red solid line) and $7\mu W$ (green solid line), (b) χQ_S vs P for optomechanical cavity detuning $\Delta_A = \omega_m$. Other system parameters used are $L = 1mm$, $m = 10\ ng$, $\lambda = 794.98\ nm$, $\omega_m = 10\ MHz$, $k_A = 0.1\ \omega_m$, $Q = 10^7$.

Simplifying Eq. (2.8)(a)-(c) , we get the following expression for $|a_S|^2$, that indicates the occurrence of bistable behavior

$$|a_S|^2 \left[k_{\text{new}}^2 + \left(\Delta_{\text{new}} - \omega_m \chi^2 |a_S|^2\right)^2\right] = |\varepsilon_A|^2, \tag{2.9}$$

where, $k_{\text{new}} = k_A + \frac{J^2(\gamma_{\text{at}} A_1 + \Delta_{\text{at}} A_2)}{A_1^2 + A_2^2}$, and $\Delta_{\text{new}} = \Delta_A + \frac{J^2(\Delta_{\text{at}} A_1 - \gamma_{\text{at}} A_2)}{A_1^2 + A_2^2}$, are the modified optomechanical cavity decay rate and detuning in presence of the atomic cavity; with $A_1 = g_{\text{at}}^2 N + k_C\ \gamma_{\text{at}} - \Delta_C \Delta_{\text{at}}$ and $A_2 = \Delta_C \gamma_{\text{at}} + k_C \Delta_{\text{at}}$. Now, to observe bistability, one

must have $\frac{\partial|\varepsilon_A|^2}{\partial|a_S|^2} = 0$, which results in the condition for our system

$$\left(k_{\text{new}}^2 + \Delta_{\text{new}}^2\right) - 4\Delta_{\text{new}}\omega_m\chi^2|a_S|^2 + 3\omega_m^2\chi^4|a_S|^4 = 0. \tag{2.10}$$

Equation (2.10) is a quadratic equation in $|a_S|^2$ that will have two distinct roots when the discriminant is positive: $\omega_m^2\chi^4(\Delta_{\text{new}}^2 - 3k_{\text{new}}^2) > 0$. This expression clearly shows that for $\chi = 0$, i.e. when there is no optomechanical coupling, bistability disappears. For nonzero χ, the condition for bistability is given by: $\Delta_{\text{new}}^2 - 3k_{\text{new}}^2 > 0$, or,

$$\begin{aligned}\Delta_{\text{A}}^2 - 3k_A^2 + \frac{J^4}{\left(A_1^2+A_2^2\right)^2}\left(\Delta_{\text{at}}A_1 - \gamma_{\text{at}}A_2\right)^2 - 3\,\frac{J^4}{\left(A_1^2+A_2^2\right)^2}\left(\gamma_{\text{at}}A_1 + \Delta_{\text{at}}A_2\right)^2 \\ - 6k_A\frac{J^2}{(A_1^2+A_2^2)}\left(\gamma_{\text{at}}A_1 + \Delta_{\text{at}}A_2\right) + 2\Delta_A\frac{J^2}{(A_1^2+A_2^2)}\left(\Delta_{\text{at}}A_1 - \gamma_{\text{at}}A_2\right) > 0.\end{aligned} \tag{2.11}$$

To analyze the bistability behavior of intracavity optical field in the optomechanical cavity, first we consider the case for $J = 0$, i.e. without coupling to the atomic cavity. In absence of the atomic cavity, the condition in equation (2.11) reduces to $\Delta_{\text{A}}^2 - 3k_A^2 > 0$. Fig. 2.2(a) shows the behavior of intracavity optical intensity and mechanical resonator position in the optomechanical cavity denoted in terms of χQ_S with respect to normalized cavity detuning in the optomechanical cavity, Δ_A/ω_m. The parameters used are: $L = 1mm$, $m = 10\ ng$, $\lambda = 794.98\ nm$, $\omega_m = 10\ MHz$, $k_A = 0.1\ \omega_m$, $Q = 10^7$ [141]. The cavity is pumped at the red sideband, $\Delta_A = \omega_m$. For driving laser power $P = 0.3\ \mu W$, the mean intracavity intensity curve is nearly Lorentzian. With increasing power of the driving laser, bistable behavior is seen to occur after crossing a critical value of the input laser power. It is also noted that for higher laser power, bistability occurs at larger cavity detuning. Fig. 2.2(b) exhibits the hysteresis curve for the mean intracavity intensity with respect to varying input power, without feedback from the atomic cavity. This curve clearly indicates the bistable behavior of the intracavity photon intensity. If one starts scanning from a low driving power and gradually increases the driving laser power, the intracavity intensity initially follows the lower stable branch. When it reaches the first bistable point P_1, it jumps to the upper stable branch and continues to follow that branch for further increasing laser power. Now, if one starts decreasing the input laser power, the intracavity intensity is observed to decrease following the upper stable branch at first; however when it reaches the second bistable point P_2, it will jump down to the lower stable branch and continue to decrease along that branch for further decrease in the input laser power.

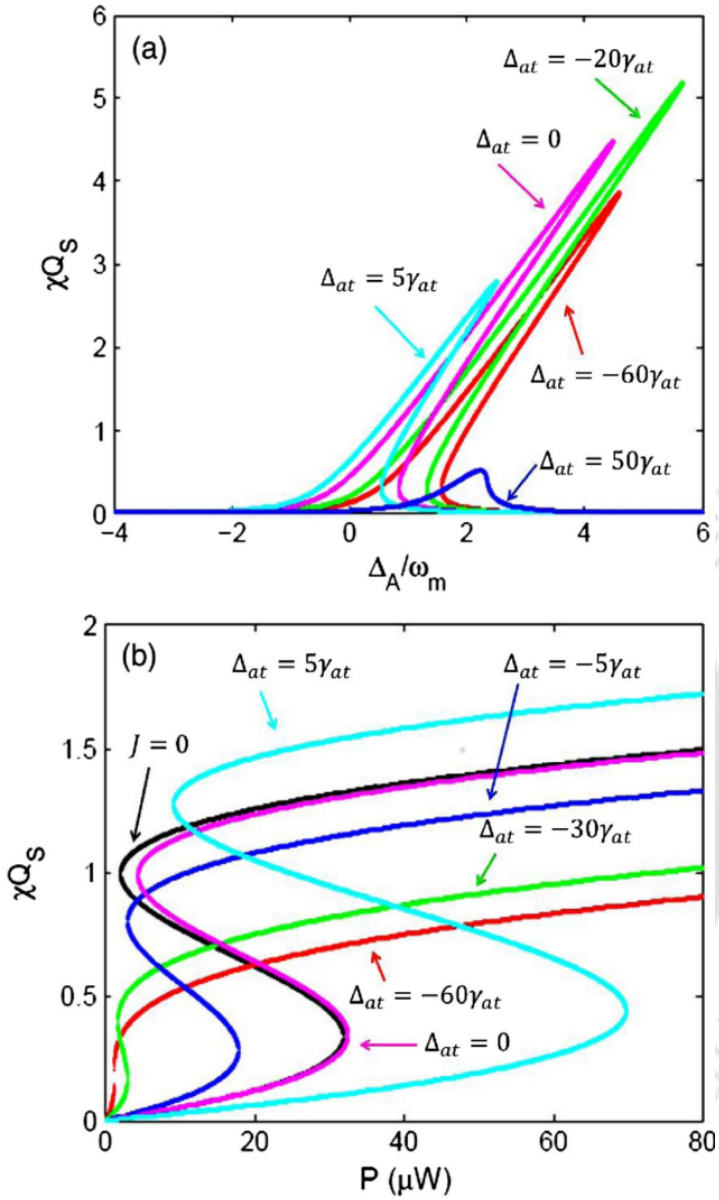

Figure 2.3: (a) Plot of χQ_S vs Δ_A/ω_m, with driving power $P = 20\ \mu W$, (b) Plot of χQ_S vs P, with cavity detuning $\Delta_A = \omega_m$; for different values of Δ_{at}. Other parameters used are: $J = \omega_m$, $g_{\text{at}} = 2\pi\ kHz$, $k_C = 0.1\omega_m$, $N = 10^8$, $\gamma_{\text{at}} = 2\pi \times 2.875\ MHz$, $\Delta_C = \omega_m$, others same as in Fig. 2.2.

Next, we proceed to study the bistability behavior of the intracavity optical field in the optomechanical cavity in presence of the atomic cavity. The effect of the presence of the atomic ensemble is shown in Fig. 2.3. The parameters considered are: $g_{\text{at}} = 2\pi\ kHz$, $k_C = 0.1\omega_m$, $N = 10^8$, $\gamma_{\text{at}} = 2\pi \times 2.875\ MHz$, $\Delta_C = \omega_m$ and $J = \omega_m$ [62, 137, 142]. Fig. 2.3(a)

shows the bistable behavior shown by the intracavity optical intensity with respect to the detuning in the optomechanical cavity for different values of Δ_{at}, and Fig. 2.3(b) shows the hysteresis curves. From Fig. 2.3(a), it is evident that the bistable behavior is dependent on the atom-field detuning Δ_{at}. We get different operating frequency range for bistability for the same input power if we have different atom-field detunings. As can be seen from Fig. 2.3(a), for higher atom-field detuning, the intracavity optical field curve is nearly Lorentzian. Therefore for higher values of atom-field detuning bistability vanishes. It should be noted that the mean intracavity intensity is highly system specific. In order to satisfy the condition for bistability, the contribution from all the terms in the LHS of Eq. (2.11) should add up to give a positive number. The bistability behavior also depends on the atom-cavity coupling g_{at} and the coupling between the two cavities J, as indicated in Eq. (2.11).

Fig. 2.3(b) shows the hysteresis curve for the intracavity optical field. It shows that, for increasing value of atom-field detuning, the operating power range for bistability becomes wider. For the parameters considered in Fig. 2.3(b), it can be trivially shown that for the system to exhibit bistability, Δ_{at} should be approximately higher than $-60\gamma_{at}$, which is the threshold value for $\Delta_{at}$for the specific parameters. The threshold power for observing bistability can be calculated to be: $P_{th} = \frac{\hbar\omega_L}{2k_A}|a_S|^2_{th}[k^2_{new} + (\Delta_{new} - \omega_m\chi^2|a_S|^2_{th})]$, where, $|a_S|^2_{th} = \left(2\Delta_{new} - \sqrt{\Delta^2_{new} - 3k^2_{new}}\right)/(3\omega_m\chi^2)$, is the intra-cavity photon number at the threshold power. For $\Delta_{at} = 0$, the threshold power needed for bistability is almost equal to that for the single optomechanical cavity; and if the detuning is increased to more positive value, the threshold value of input power further shows an increase as seen from Fig. 2.3(b). Significantly, for negative values of Δ_{at}, the threshold input power for the hybrid system appears to be lower than the generic single cavity case, as shown in Fig. 2.3(b). The threshold power, P_{th} also depends on the decay rate of the feedback cavity k_C.

The variation of P_{th} with respect to k_C and Δ_{at} is shown in Fig. 2.4. This shows that for a range of Δ_{at} and k_C, the threshold power is lower than that for the single cavity optomechanical system, which is calculated to be 31.9 μW for the experimental parameters considered in this work. Lower value of threshold power is obtained for lower values of k_C as can be seen from Fig. 2.4. The occurrence of bistability at low input power can be attributed to the additional feedback field from the atomic cavity. Lower decay rate of the atomic cavity ensures more feedback intensity to the optomechanical cavity.

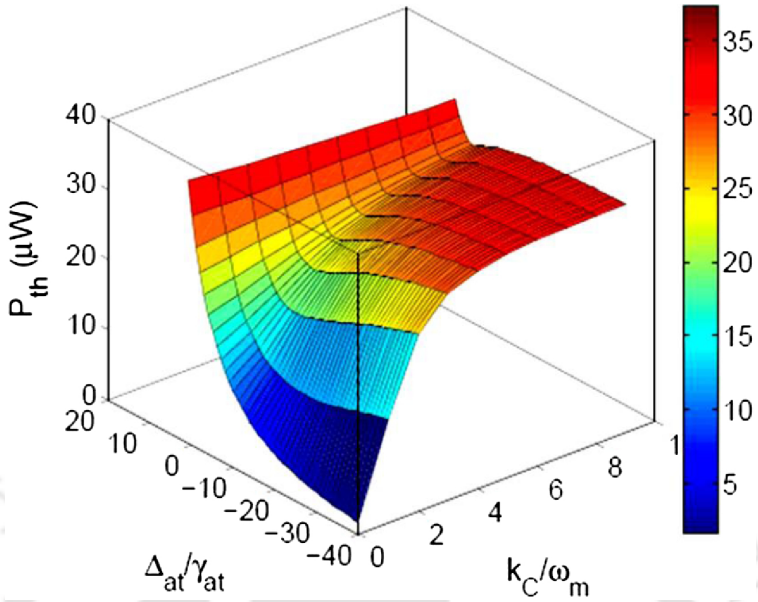

Figure 2.4: Variation of threshold power for bistability as a function of $\Delta_{\rm at}/\gamma_{\rm at}$ and k_C/ω_m.

Therefore, by coupling a feedback cavity with optimum parameters to the optomechanical cavity, one can observe bistability for lower input power. Conclusively, we find that the system has the following three externally controllable parameters: power of the single driving laser, cavity-field detuning in the optomechanical cavity and the atom-field detuning in the atomic cavity. The extra controlling parameters provided by the feedback from the atomic cavity modify the condition for bistability. This presents us with more flexibility in switching the intracavity intensity in the optomechanical cavity, between the two stable branches.

2.3 Summary

In conclusion, we have studied a hybrid system consisting of an optomechanical cavity and another cavity containing ultracold two level atomic ensemble serving as a feedback to the first cavity; with a special emphasize on bistability shown by the optical field in the optomechanical cavity, emerging due to the effect of radiation pressure force. It turns out that the bistable behavior of the intracavity field in the optomechanical cavity can be controlled by tuning the power of the single driving laser as well as by changing the frequency of the driving laser that can control the cavity-field detuning in the optomechanical cavity and the atom-field detuning in the atomic cavity. This allows more

flexibility in controlling bistability compared to the single cavity optomechanical system. In addition, by coupling the atomic cavity with the optomechanical cavity, one can obtain bistability for much lower threshold power compared to the generic optomechanical cavity system.

CHAPTER 3

GROUND-STATE COOLING OF A MECHANICAL RESONATOR IN THE UNRESOLVED-SIDEBAND REGIME

This chapter discusses the ground-state cooling of a mechanical resonator in an optomechanical cavity induced by a quantum well, in the unresolved-sideband regime. Due to the presence of the quantum well, the cavity response gets modified and leads to asymmetric heating and cooling processes. The cooling rate of the mechanical resonator can potentially be enhanced by tuning the cavity-field detuning. It is demonstrated that, even when the cavity is in the unresolved-sideband regime, the effective interaction of the excitons and mechanical mode can bring the system back to an effective resolved-sideband regime. The time evolution of the mean phonon number in the mechanical resonator is studied using the quantum master equation. The average phonon occupancy in the mechanical resonator tends to zero with time.

3.1 Brief overview

In the previous chapter, we studied the bistable behavior shown by the mean intracavity optical field and mechanical mirror position, which is a classical nonlinear optomechani-

An article based on this chapter is published in *Phys. Rev. A*, vol. **93**, No. 3, year 2016, pages 033845:1-7; title: "*Ground-state cooling of micromechanical oscillators in the unresolved-sideband regime induced by a quantum well*"; authors: Bijita Sarma and Amarendra K. Sarma. Selected contents are reproduced with permission ©2016 American Physical Society.

cal effect. In this chapter, we analyze the phenomenon of mechanical resonator-cooling which essentially occurs in the regime of linearized quantum optomechanics [15]. For observing quantum effects in optomechanical systems, ground state cooling of the mechanical oscillator is an essential condition [36, 39, 56, 143]. In an optomechanical system, the light scattered from the movable end mirror gives rise to Stokes and anti-Stokes sidebands. During the Stokes process, the mirror absorbs a quantum of energy from the cavity optical field, leading to heating of the mirror; whereas during the anti-Stokes process, the cavity field absorbs energy from the mirror resulting in cooling of the mirror. To obtain an effective cooling of the mechanical mirror, cooling rate should be higher than the heating rate. Therefore, in analogy to the laser cooling of ions in the strong binding regime [55], conventional cavity cooling of mechanical oscillators requires the condition of resolved-sideband regime, where the cavity mode decay rate is lower than the mechanical oscillator resonance frequency [56, 144, 145]. However, in practical situations, for typical mechanical oscillators of frequency in the range of kHz-MHz; fulfilling this condition is a challenging task, that poses serious constraints experimentally. To relax this requirement, few different approaches have been suggested such as cooling using dissipative coupling [57–59, 146, 147], coupling with high-Q auxiliary cavity [60–62], hybrid atom-optomechanical systems [63–65, 148–151], and using optomechanically induced transparency [66, 152]. Here, in this chapter, we consider the cavity cooling of a micromechanical mirror, with a quantum well (QW) having lower exciton decay rate, placed inside the optomechanical cavity. This type of solid-state systems has their own advantages over atomic cavity systems. The engineerable emission frequency, fixed position and potential for integration with cavities and waveguides using developed semiconductor fabrication techniques [149, 153, 154] make them unique tool for exploring optomechanics further [15, 30, 155, 156]. The same type of system has been studied in the context of nonlinear effects like bistability and squeezing of the output field [53, 157]. It is also predicted in such a system that the interaction between the exciton and mechanical modes through the cavity field may lead to entanglement between the two [158].

We explore the aspect of ground state cooling of the mechanical oscillator in the unresolved-sideband regime. In this regime, by coupling the mechanical oscillator to a quantum well placed at the anti-node of the cavity field, one can modify the noise spectrum. This illustrates mode structuring around the sidebands, due to the inhibition of the heating process, while enhancing the cooling process through quantum interference.

In order to study the cooling effect in the mechanical oscillator, we use an effective exciton-phonon interaction model that is analogous to dark mode formation, which has been studied extensively in optomechanics, in connection to state transfer protocols [159, 160]. The dark mode in optomechanics is similar to coherent-population trapped state or the dark state in atomic physics [161]. The similarity to the so-called stimulated Raman adiabatic passage (STIRAP) is also notable.

3.2 Model and theory

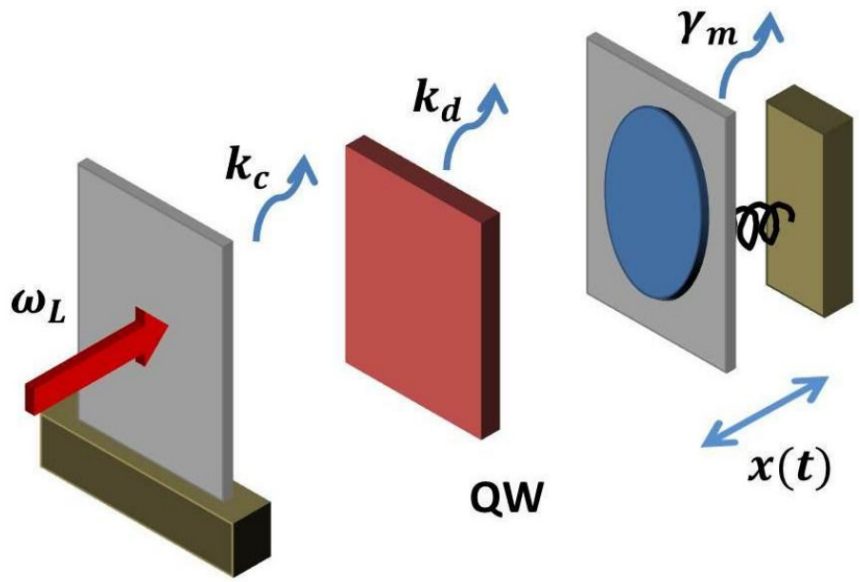

Figure 3.1: An optomechanical cavity containing a Quantum Well (QW) placed at the antinode of the cavity field.

We consider an optomechanical cavity containing a QW as shown schematically in Fig. 3.1. The movable end mirror has resonance frequency ω_m, effective mass m and decay rate γ_m. The cavity is driven by an intense pump laser of frequency ω_L, which exerts a radiation pressure force on the movable end mirror. The Hamiltonian of the system is given by (in the unit of $\hbar = 1$)

$$H = H_{\text{free}} + H_{\text{o-m}} + H_{\text{o-d}} + H_{\text{drive}} \tag{3.1}$$

The first term H_{free} in Eq. (3.1) describes the free Hamiltonian of the system, given by $H_{\text{free}} = \omega_c c^\dagger c + \omega_d d^\dagger d + \omega_m b^\dagger b$, where, ω_c, ω_d and ω_m are the resonance frequencies of the cavity optical field, the QW excitons and the mechanical oscillator respectively. Since we are dealing with quasi-resonant coherent excitation, higher lying exciton states of the QW are neglected. The optomechanical interaction between the cavity mode and the mechanical oscillator is described by the second term, $H_{\text{o-m}} = g_{\text{OM}} c^\dagger c \left(b^\dagger + b\right)$. Here, g_{OM} is the single-photon optomechanical coupling strength between the cavity field and the mechanical oscillator. The third term in Eq. (3.1) accounts for the coupling between the cavity mode and the exciton mode in the QW, given by $H_{\text{o-d}} = g\left(c^\dagger d + d^\dagger c\right)$, with interaction strength, g. The last term represents the pump laser driving, given by, $H_{\text{drive}} = \varepsilon_p \left(c^\dagger e^{-i\omega_L t} + c e^{i\omega_L t}\right)$, with pump laser frequency, ω_l, and amplitude, $\varepsilon_p = \sqrt{\frac{\kappa_c P_{\text{in}}}{\omega_L}}$; P_{in} and κ_c being the input power and cavity decay rate respectively. In the frame rotating with the input laser frequency, ω_L, one can obtain the Hamiltonian of the system as

$$H = -\Delta_c c^\dagger c - \Delta_d d^\dagger d + \omega_m b^\dagger b + g_{\text{OM}} c^\dagger c \left(b^\dagger + b\right) + g\left(c^\dagger d + d^\dagger c\right) + \varepsilon_p \left(c^\dagger + c\right), \tag{3.2}$$

where, $\Delta_c = \omega_L - \omega_c$, and $\Delta_d = \omega_L - \omega_d$, are the detunings of the cavity mode and the exciton mode respectively. The time evolution of the system operators are given by the nonlinear Heisenberg-Langevin equations

$$\dot{c} = \left(i\Delta_c - \frac{\kappa_c}{2}\right) c - i g_{\text{OM}} c \left(b^\dagger + b\right) - i g d - i\varepsilon_p - \sqrt{\kappa_c}\, c_{\text{in}}(t), \tag{3.3a}$$

$$\dot{d} = \left(i\Delta_d - \frac{\kappa_d}{2}\right) d - i g c - \sqrt{\kappa_d}\, d_{\text{in}}(t), \tag{3.3b}$$

$$\dot{b} = \left(-i\omega_m - \frac{\gamma_m}{2}\right) b - i g_{\text{OM}} c^\dagger c - \sqrt{\gamma_m}\, b_{\text{in}}(t), \tag{3.3c}$$

where, κ_c, κ_d and γ_m are the decay rates of the optical mode, exciton mode and the mechanical mode respectively. Here, c_{in}, d_{in} and b_{in} are the corresponding input vacuum noise operators with zero mean value and nonzero correlation functions given by [139]:

$$\left\langle c_{\text{in}}(t)\, {c_{\text{in}}}^\dagger\left(t'\right)\right\rangle = \delta(t - t'),$$
$$\left\langle d_{\text{in}}(t)\, {d_{\text{in}}}^\dagger\left(t'\right)\right\rangle = \delta(t - t'),$$
$$\left\langle b_{\text{in}}(t)\, {b_{\text{in}}}^\dagger\left(t'\right)\right\rangle = (n_{\text{th}} + 1)\delta(t - t'),$$
$$\left\langle b_{\text{in}}^\dagger(t)\, b_{\text{in}}\left(t'\right)\right\rangle = n_{\text{th}}\delta(t - t'),$$

where, n_{th} is the environmental thermal phonon number given by, $n_{\text{th}} = [\exp(\omega_m/k_B T) - 1]^{-1}$, with, k_B being the Boltzmann constant, and T being the environmental temperature.

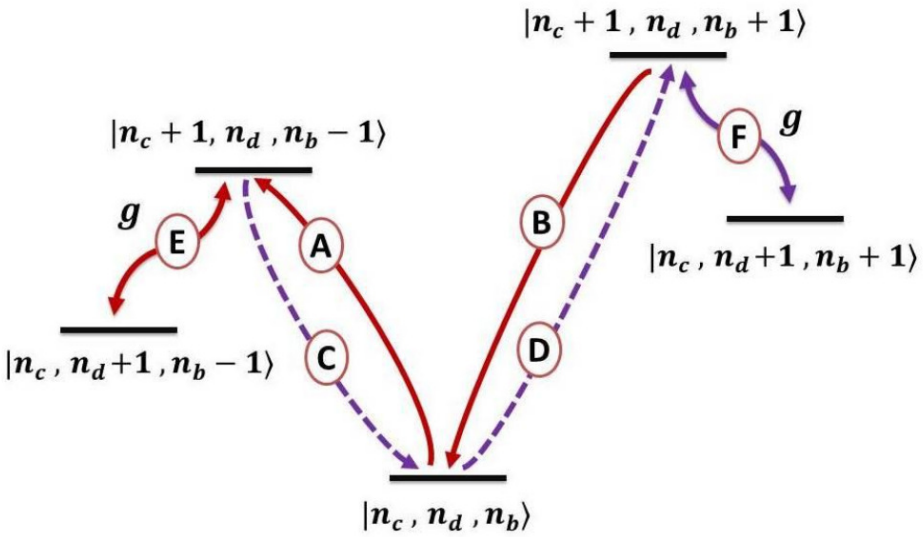

Figure 3.2: Level diagram for the linearized Hamiltonian [Eq. (3.6)] and different coupling routes in displaced frame where $|n_c,n_d,n_b\rangle$ denotes the state with n_c number of photons, n_d number of excitons and n_b number of phonons. The solid, red curve $A(B)$ denote the cooling process due to energy swapping (counter-rotating-wave interaction). The dashed, purple curve $C(D)$ denote the heating process due to energy swapping (quantum back-action). The energy swapping due to exciton-cavity coupling is denoted by solid curves E and F.

3.3 Cooling of the mechanical resonator

Assuming a strong driving condition, Eqs. (3.3)(a)-(c) can be linearized around the steady state mean values by expressing the system operators to be comprising of the mean value O_S, and a small fluctuating term δO: $O = O_S + \delta O$. The Langevin equations for the fluctuation terms are given by:

$$\dot{\delta c} = \left(i\Delta_c' - \frac{\kappa_c}{2}\right)\delta c - iG\left(\delta b^\dagger + \delta b\right) - igd - \sqrt{\kappa_c}\,c_{\rm in}(t), \tag{3.5a}$$

$$\dot{\delta d} = \left(i\Delta_d - \frac{\kappa_d}{2}\right)\delta d - ig\delta c - \sqrt{\kappa_d}\,d_{\rm in}(t), \tag{3.5b}$$

$$\dot{\delta b} = \left(-i\omega_m - \frac{\gamma_m}{2}\right)\delta b - iG(\delta c^\dagger + \delta c) - \sqrt{\gamma_m}\,b_{\rm in}(t). \tag{3.5c}$$

Then the linearized Hamiltonian of the system is given by:

$$H_L = -\Delta'_c \delta c^\dagger \delta c - \Delta_d \delta d^\dagger \delta d + \omega_m \delta b^\dagger \delta b + G\left(\delta c^\dagger + \delta c\right)\left(\delta b^\dagger + \delta b\right) + g\left(\delta c^\dagger \delta d + \delta d^\dagger \delta c\right), \tag{3.6}$$

where, $G = g_{\rm OM} c_S$, is the enhanced optomechanical coupling strength due to the driving optical field, and, $\Delta'_c = \Delta_c - g_{\rm OM}(b_s + b_s^\dagger)$ is the modified cavity detuning. Fig. 3.2 displays the level diagram of the linearized Hamiltonian and all the coupling routes among states denoted by $|n_c, n_d, n_b\rangle$ in the displaced frame; where n_c, n_d and n_b are the photon, exciton and phonon numbers respectively. Different kinds of cooling and heating processes may occur due to the optomechanical interaction [162]. The cooling processes associated with energy swapping and counter-rotating-wave interaction are illustrated by solid (red) curves A and B respectively. The heating processes are denoted by the dashed (purple) curves, corresponding to swap heating (C) and quantum backaction heating (D). The energy swapping due to the extra exciton-cavity coupling is shown by curves E and F. In order to achieve efficient mechanical motion cooling, one needs to enhance the cooling effect while suppressing the heating. Eqs. (3.5) (a)-(c) can be solved in the frequency domain to obtain the expression for $\widetilde{\delta b}(\omega)$ as follows:

$$\widetilde{\delta b}(\omega) = \frac{\sqrt{\gamma_m}\,\widetilde{b_{\rm in}}(\omega) - i\sqrt{\kappa_c}\,A(\omega) - \sqrt{\kappa_d}\,B(\omega)}{i\omega - i\left[\omega_m + \Sigma(\omega)\right] - \frac{\gamma_m}{2}}, \tag{3.7}$$

where,

$$\begin{aligned} A(\omega) =& G[\chi(\omega)\,\widetilde{c_{\rm in}}(\omega) + \chi^*(-\omega)\,\widetilde{c_{\rm in}}^\dagger(\omega)], \\ B(\omega) =& gG[\chi(\omega)\chi_d(\omega)\widetilde{d_{\rm in}}(\omega) - \chi^*(-\omega)\chi_d^*(-\omega)\widetilde{d_{\rm in}}^\dagger(\omega)]. \end{aligned}$$

Here, $\Sigma(\omega) = -iG^2[\chi(\omega) - \chi^*(-\omega)]$, is the optomechanical self-energy, where $\chi(\omega) = \left[\{\chi_c(\omega)\}^{-1} + g^2\chi_d(\omega)\right]^{-1}$ is the total response function of the optomechanical cavity with the QW. And $\chi_c(\omega) = \left[-i\left(\omega + \Delta'_c\right) + \frac{\kappa_c}{2}\right]^{-1}$, $\chi_d(\omega) = \left[-i(\omega + \Delta_d) + \frac{\kappa_d}{2}\right]^{-1}$ and $\chi_m(\omega) = \left[-i(\omega - \omega_m) + \frac{\gamma_m}{2}\right]^{-1}$, are the response functions of the optical mode, the exciton mode and the mechanical mode respectively. The radiation pressure force, in an optomechanical system, arising due to the interaction term, $H_{\rm int}$, is given by, $F = -\frac{\delta H_{\rm int}}{\delta x}$. Using this, the radiation pressure force for our system is estimated as, $F = -G\,[\delta c^\dagger + \delta c]/x_{\rm ZPF}$, where, $x_{\rm ZPF}$ is the zero-point fluctuation of the mechanical oscillator. The quantum noise spectrum is calculated using: $S_{FF}(\omega) = \int dt e^{i\omega t}\langle F(t)F(0)\rangle$ [15]. The spectral density, in our

system is calculated to be:

$$S_{FF}(\omega) = \frac{G^2|\chi(\omega)|^2}{x_{ZPF}^2}\left[\kappa_c + \kappa_d g^2 |\chi_d(\omega)|^2\right]. \tag{3.8}$$

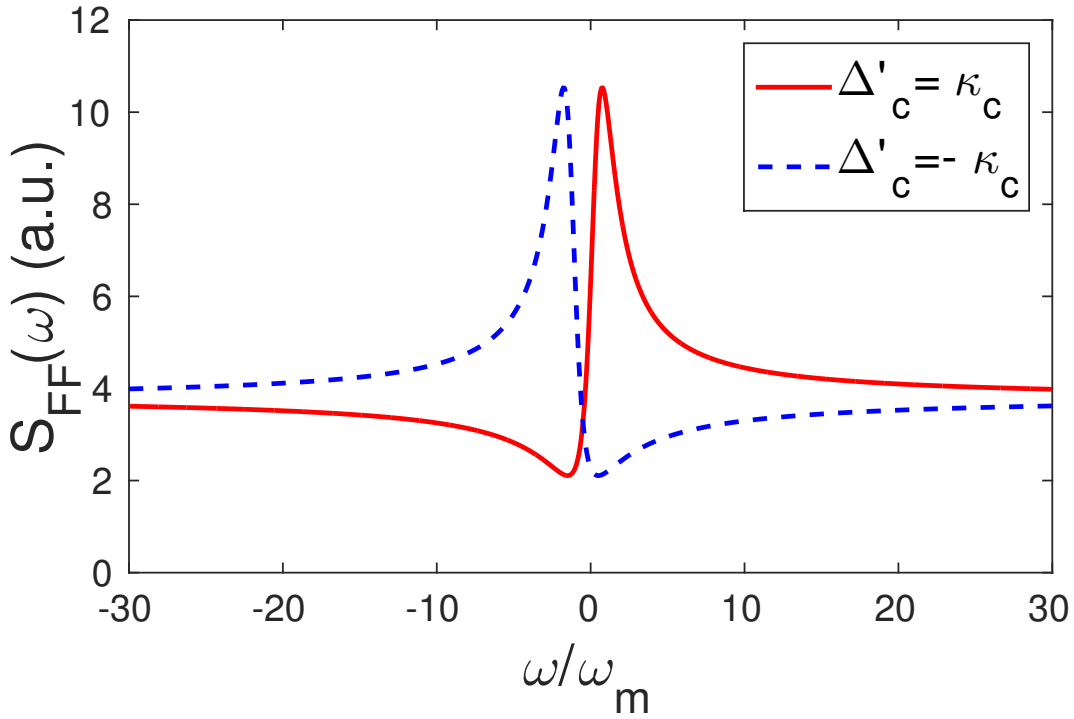

Figure 3.3: Plot of noise spectrum S_{FF} vs. normalized frequency ω/ω_m for $\Delta_c' = \kappa_c$ (red solid), $\Delta_c' = -\kappa_c$ (blue dashed). Other parameters are $\Delta_d = 0.5\omega_m$, $\gamma_m = 10^{-5}\omega_m$, $\kappa_c = 10^4\omega_m$, $\kappa_d = \omega_m$, $g = 100\omega_m$, $G = 50\omega_m$ and $n_{\rm th} = 10^4$ [163].

The cooling rate of the mechanical resonator is given by, $A_- = S_{FF}(\omega_m)x_{ZPF}^2$, while the heating rate is given by, $A_+ = S_{FF}(-\omega_m)x_{ZPF}^2$. Due to the dynamical back-action induced by the radiation pressure force, the spring constant (and thereby the effective oscillation frequency) and the damping rate of the mechanical oscillator get modified. The extra damping of the mechanical oscillator due to the optomechanical interaction is given by, $\gamma_{\rm OM} = A_- - A_+ = -2{\rm Im}[\Sigma(\omega_m)]$ and the mechanical frequency shift is given by, $\delta\omega_m = {\rm Re}[\Sigma(\omega_m)]$. In Fig. 3.3, we have plotted the noise spectrum for different values of modified cavity-field detuning in the unresolved-sideband regime. In a generic optomechanical cavity, in the unresolved-sideband regime, the noise spectrum reduces to, $S_{FF}(\omega) = \frac{G^2|\chi(\omega)|^2}{x_{ZPF}^2}\kappa_c$. This gives rise to a Lorentzian curve illustrating equal heating and cooling

rates of the mechanical resonator. Nevertheless, the noise spectrum for the system considered here as depicted in Fig. 3.3, shows asymmetric Fano lineshapes that arise as a result of interference between resonant and nonresonant processes [57]. This indicates that the presence of the QW modulates the cavity profile to show asymmetry in cooling and heating processes. For $\Delta_c' = \kappa_c$, there is an increase in cooling rate while the heating rate is reduced, and for $\Delta_c' = -\kappa_c$, the opposite happens. Therefore, by tuning the cavity-field detuning, the cooling rate of the mechanical resonator can potentially be enhanced while reducing the heating rate. This is possible due to the interaction of the high-Q QW with the mechanical mode through the cavity field. Intuitively, the asymmetry in cooling and heating rates can be pictured as an outcome of quantum interference. As can be observed from Fig. 3.2, due to the presence of the exciton-cavity coupling, g, there are two different pathways leading to the same cooling or heating process. Therefore, one can harness the interference to overpower the heating effect while enhancing the cooling effect.

In the highly unresolved regime, $\kappa_c \gg \omega_m$, and for $\kappa_c \gg (k_d,\ \gamma_m)$, $\Delta_c' \gg \Delta_d$, the three-mode system can be reduced to a two-mode system by considering the cavity mode as perturbation. Integrating Eqs. (3.5) (a)-(c), we get the time dependent form of the operators as follows:

$$\begin{aligned}\delta c(t) &= \delta c(0)\exp\left(i\Delta_c' t - \frac{\kappa_c}{2}t\right) + \exp\left(i\Delta_c' t - \frac{\kappa_c}{2}t\right)\int_0^t [-iG\delta b^\dagger(\tau) - iG\delta b(\tau) - ig\delta d(\tau) \\ &\quad - \sqrt{\kappa_c}\, c_{\rm in}(\tau)] \times \exp\left(-i\Delta_c'\tau + \frac{\kappa_c}{2}\tau\right) d\tau, \qquad (3.9a)\\ \delta d(t) &= \delta d(0)\exp\left(i\Delta_d t - \frac{\kappa_d}{2}t\right) + \exp\left(i\Delta_d t - \frac{\kappa_d}{2}t\right)\int_0^t [-ig\delta c(\tau) - \sqrt{\kappa_d}\, d_{\rm in}(\tau)] \\ &\quad \times \exp\left(-i\Delta_d\tau + \frac{\kappa_d}{2}\tau\right) d\tau, \qquad (3.9b)\\ \delta b(t) &= \delta b(0)\exp\left(-i\omega_m t - \frac{\gamma_m}{2}t\right) + \exp\left(-i\omega_m t - \frac{\gamma_m}{2}t\right)\int_0^t [-iG\delta c^\dagger(\tau) - iG\delta c(\tau) \\ &\quad - \sqrt{\gamma_m}\, b_{\rm in}(\tau)]\exp\left(i\omega_m\tau + \frac{\gamma_m}{2}\tau\right) d\tau. \qquad (3.9c)\end{aligned}$$

Now considering the effect of the cavity mode as perturbation, the expressions for the time dependent exciton mode and mechanical mode operators are approximated as

$$\delta d(t) \cong \delta d(0)\exp\left(i\Delta_d t - \frac{\kappa_d}{2}t\right) + D_{\rm in}(t), \qquad (3.10a)$$

$$\delta b(t) \cong \delta b(0)\exp\left(-i\omega_m t - \frac{\gamma_m}{2}t\right) + B_{\rm in}(t), \qquad (3.10b)$$

where, the effect of the cavity mode is included in the noise terms $D_{\text{in}}(t)$ and $B_{\text{in}}(t)$. Substituting Eqs. (3.10)(a) and (b) back into Eq. (3.9)(a), and under the assumptions, $\left|\Delta'_c\right| \gg \Delta_d, \kappa_c \gg (\kappa_d, \gamma_m)$, we obtain:

$$\delta c(t) \cong -\frac{iG\left[\delta b(t) + \delta b^{\dagger}(t)\right]}{-i\Delta'_c + \frac{\kappa_c}{2}} - \frac{ig\delta d(t)}{-i\Delta'_c + \frac{\kappa_c}{2}} + \delta c(0)\exp\left(i\Delta'_c t - \frac{\kappa_c}{2}t\right) + C_{\text{in}}(t). \tag{3.11}$$

And substituting $\delta c(t)$ into Eqs. (3.5)(b) and (3.5)(c), we get the equation for the exciton mode as:

$$\begin{aligned}\dot{\delta d} \;=\; & \left(i\Delta_d - \frac{\kappa_d}{2}\right)\delta d + ig\left[\frac{iG\left[\delta b(t) + \delta b^{\dagger}(t)\right]}{-i\Delta'_c + \frac{\kappa_c}{2}} + \frac{ig\delta d(t)}{-i\Delta'_c + \frac{\kappa_c}{2}}\right] - \sqrt{\kappa_d}\, d_{\text{in}}(t) \\ & - ig[\delta c(0)\exp\left(i\Delta'_c t - \frac{\kappa_c}{2}t\right) + C_{\text{in}}(t)].\end{aligned} \tag{3.12}$$

Comparing this with the generic single-cavity optomechanical system, we can derive the parameters for the effective exciton-mechanical mode interaction as, $\Delta_{\text{eff}} = \Delta_d - \eta^2\Delta'_c$, $k_{\text{eff}} = \kappa_d + \eta^2\kappa_c$, $G_{\text{eff}} = \eta G$, where $\eta = g/\sqrt{\Delta'^2_c + \left(\frac{\kappa_c}{2}\right)^2}$, that can be approximated to $\eta = g/\Delta'_c$ for $\Delta'_c \gg \kappa_c$. Analogous to the single cavity optomechanical system, the steady-state cooling limits are approximated as, $n_{\text{f}} = n_{\text{classical}} + n_{\text{quantum}}$ [162, 164]. Here, $n_{\text{classical}} = \frac{4G_{\text{eff}}^2 + k_{\text{eff}}^2}{4G_{\text{eff}}^2 k_{\text{eff}}}\gamma_m n_{\text{th}} \approx \frac{k_{\text{eff}}}{4|G_{\text{eff}}|^2}\gamma_m n_{\text{th}}$ is the classical steady-state cooling limit and $n_{\text{quantum}} = \frac{k_{\text{eff}}^2 + 8G_{\text{eff}}^2}{16(\omega_m^2 - 4G_{\text{eff}}^2)} \approx \frac{k_{\text{eff}}^2}{16\omega_m^2}$ is the quantum limit of cooling for effective resolved sideband ($k_{\text{eff}} \ll \omega_m$) and the effective weak coupling regime ($G_{\text{eff}} < k_{\text{eff}}$). In Figs. 3.4(a)-(b) the variations of steady-state cooling limit as functions of normalized cavity detuning and the thermal phonon number are shown. As seen from Fig. 3.4(a), ground state cooling is not possible for a generic optomechanical cavity in the unresolved-sideband regime. Nevertheless, in case of the QW coupled system, ground state cooling can be achieved for a range of high cavity detuning near $10^4\omega_m$. For large detuning, dark modes with respect to the low-Q cavity mode (c) are formed via linear combination of the mechanical mode (b), and high-Q exciton mode (d). This dark-mode is responsible for an effective cooling [159, 160]. It is worth to be noted that in case of a single optomechanical cavity without the QW, cooling occurs in the red detuned regime only. But, with the QW inside the cavity, the damping is significantly enhanced in the blue-detuned regime as illustrated in Fig. 3.3. The effective detuning term, Δ_{eff} contains both Δ'_c and Δ_d. Hence, it is possible to tune these blue-detuned terms to get a red-detuned, Δ_{eff} at high value of Δ'_c, that

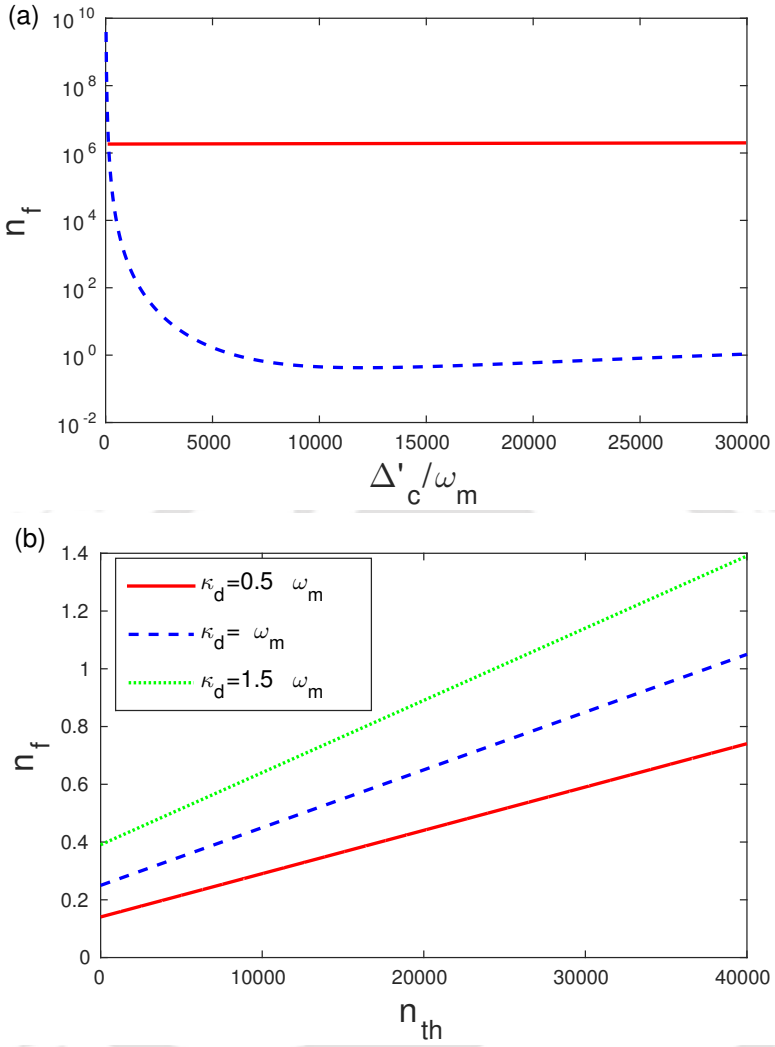

Figure 3.4: Plot of steady-state cooling limit as function of (a) Δ'_c/ω_m, with $\kappa_d = \omega_m$ and $n_{\rm th} = 10^4$. The red solid line denotes the final phonon number in the mechanical oscillator for a generic optomechanical cavity, whereas the blue dotted line shows the phonon number in presence of the QW in the cavity; (b) $n_{\rm th}$ with $\Delta'_c = 10^4\omega_m$. Other unspecified parameters are: $\gamma_m = 10^{-5}\omega_m$, $\kappa_c = 10^4\omega_m$, $g = 100\omega_m$, $G = 50\omega_m$, $\Delta_d = 0.5\omega_m$.

results in cavity cooling. Fig. 3.4(b) depicts the variation of the steady-state cooling limit as a function of the bath phonon number for different values of κ_d. The plots show that, for ground state cooling of the mechanical resonator, high values of bath phonon number is tolerable. For example, for $\kappa_d = \omega_m$, the maximum tolerable bath phonon number is approximately equal to 37×10^3. It is also to be noted that more bath phonon number is tolerable for ground state cooling with lower decay rate of the QW excitons.

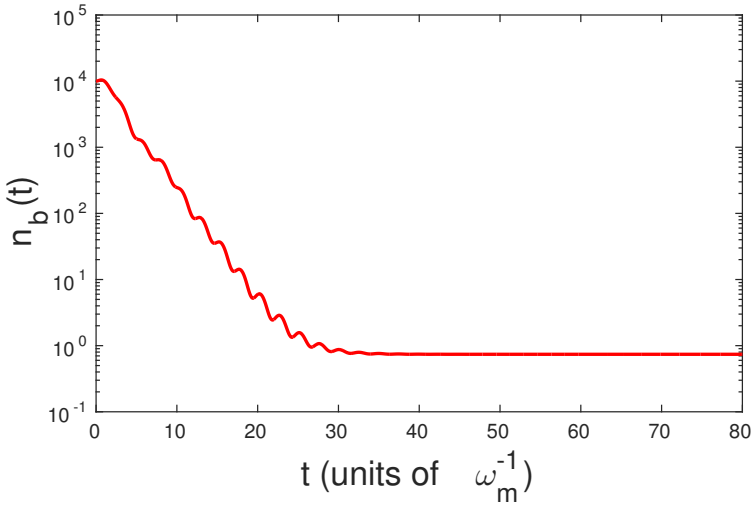

Figure 3.5: Time evolution of the mean phonon number in the mechanical resonator in presence of the QW, starting from $n_{\text{th}} = 10^4$. Parameters considered are $\kappa_c = 10^4\omega_m$, $\kappa_d = \omega_m$, $\Delta_c' = 10^4\omega_m$, $\Delta_d = 0.5\omega_m$, $\gamma_m = 10^{-5}\omega_m$, $g = 100\omega_m$ and $G = 50\omega_m$.

It is important to have an idea about the optimum range of the optomechanical coupling, G, and the exciton-cavity coupling, g to be used for efficient mechanical mode cooling. The optimum value of g can be determined analytically by maximizing the cooling rate, that is found to be, $g = \sqrt{\left(\frac{\Delta_c'+\omega_m}{\Delta_d+\omega_m}\right)\left(\frac{\kappa_d}{2}\right)^2 + (\Delta_c'+\omega_m)(\Delta_d+\omega_m)}$. For the stability of the system, the effective coupling must follow, $G_{\text{eff}} < \omega_m/2$, as observed from the quantum limit of cooling. Therefore, the condition for the optomechanical coupling, G, and the exciton-cavity coupling, g simplifies to, $gG < \omega_m\sqrt{\Delta_c'^2 + \left(\frac{\kappa_c}{2}\right)^2}\Big/2$. For $\Delta_c' \cong \kappa_c$, the requirement for the approximate value of the couplings give $gG < \omega_m\kappa_c/2$.

In order to study the time evolution of the mean phonon number in the mechanical resonator, we use the Lindblad master equation approach. The quantum master equation of the system reads:

$$\begin{aligned}\dot{\rho} &= i\left[\rho, H_L\right] + \frac{\kappa_c}{2}\left(2\delta c\rho\delta c^\dagger - \delta c^\dagger\delta c\rho - \rho\delta c^\dagger\delta c\right) + \frac{\kappa_d}{2}\left(2\delta d\rho\delta d^\dagger - \delta d^\dagger\delta d\rho - \rho\delta d^\dagger\delta d\right) \\ &+ \frac{\gamma_m}{2}(n_{\text{th}}+1)\left(2\delta b\rho\delta b^\dagger - \delta b^\dagger\delta b\rho - \rho\delta b^\dagger\delta b\right) + \frac{\gamma_m}{2}n_{\text{th}}(2\delta b^\dagger\rho\delta b - \delta b\delta b^\dagger\rho - \rho\delta b\delta b^\dagger)\end{aligned} \tag{3.13}$$

We use the covariance approach to find out the time evolution of the mean phonon number $n_b(t) = \langle\delta b^\dagger\delta b\rangle(t)$ [162]. For this, we solve a linear system of differential equations $\partial_t\langle\hat{o}_i\hat{o}_j\rangle = \text{Tr}\left(\dot{\rho}\hat{o}_i\hat{o}_j\right) = \sum_{m,n}\mu_{m,n}\langle\hat{o}_m\hat{o}_n\rangle$, where, $\hat{o}_i$, $\hat{o}_j$, $\hat{o}_m$, $\hat{o}_n$ are one of the operators:

$\delta b^\dagger$, $\delta c^\dagger$, $\delta d^\dagger$, δb, δc and δd; and $\mu_{m,n}$ are the corresponding coefficients. Solving these, we can find out the mean values of all the time-dependent second-order moments: $\langle \delta b^\dagger \delta b \rangle$, $\langle \delta b^\dagger \delta c \rangle$, $\langle \delta b^\dagger \delta d \rangle$, $\langle \delta c^\dagger \delta c \rangle$, $\langle \delta c^\dagger \delta d \rangle$, $\langle \delta d^\dagger \delta d \rangle$, $\langle \delta b^2 \rangle$, $\langle \delta b \delta c \rangle$, $\langle \delta b \delta d \rangle$, $\langle \delta c^2 \rangle$, $\langle \delta c \delta d \rangle$ and $\langle \delta d^2 \rangle$. In Fig. 3.5, we show the time evolution of the mean phonon number. The environmental phonon number is assumed to be 10^4. The cavity is considered to be in highly unresolved sideband regime. Initially the phonon number in the mechanical oscillator is equal to the environmental phonon number. All other second order moments are considered to be zer initially. The plot shows that with increasing time, the average phonon occupancy in the mechanical resonator is cooled down to below one. This indicates ground state cooling of the resonator mode in the highly unresolved sideband regime.

3.4 Summary

To summarize, we have studied the sideband cooling of a mechanical resonator in an optomechanical cavity containing a quantum well. It is worthwhile to note that such semiconductor structures, with well-developed semiconductor fabrication techniques, are easily integrable with cavities and waveguides making them a unique tool for exploiting optomechanics. The exciton and mechanical modes are not coupled directly, but their interaction with the cavity optical field gives rise to an indirect coupling between them. This specific configuration of the system can lead to cooling of the mechanical oscillator in the unresolved sideband regime. Due to the presence of the high-Q element in the cavity, the noise spectrum is modified and leads to asymmetric cooling and heating rates. Even when the cavity is in the highly unresolved-sideband regime, the effective interaction between the exciton and mechanical modes can bring the system back to effective resolved-sideband regime. Hence the requirement of the resolved-sideband condition for cooling is relaxed significantly. The cooling rate of the mechanical resonator can be enhanced by tuning the cavity-field detuning. The time evolution of the mean phonon number in the mechanical resonator is studied using the quantum master equation. It is found that, with increasing time, the average phonon occupancy in the mechanical resonator tends towards zero exhibiting dynamic controllability of cavity dissipation. This might open up the possibility of manipulation of semiconductor integrated mechanical systems in the quantum mechanical regime.

CHAPTER 4

PHOTON BLOCKADE

In this chapter we discuss the occurrence of photon blockade in optomechanical systems via destructive quantum interference between two-photon excitation pathways. First, we consider an optomechanical system in which two weakly nonlinear optical modes interact with a mechanical mode via three-mode coupling. It is shown that through the three-mode interaction, distinct pathways can be created that leads to two-photon excitation in the higher frequency optical mode. These pathways may lead to the phenomenon of photon antibunching via destructive quantum interference. We derive the optimal conditions for photon blockade, and subsequent numerical analysis also agree with the analytical results. In the second part of this chapter, we discuss the photon blockade effect in an optomechanical cavity containing a degenerate optical parametric amplifier. We show via analytical and numerical calculations, that for optimal values of the amplifier pump amplitude and phase, strong photon antibunching can be realized in the cavity.

This chapter is based on two articles: (1) *Phys. Rev. A*, vol. **96**, No. 5, year 2017, pages 053827:1-6; title: "*Quantum-interference-assisted photon blockade in a cavity via parametric interactions*"; authors: Bijita Sarma and Amarendra K. Sarma. Selected contents are reproduced with permission ©2017 American Physical Society, (2) *Phys. Rev. A*, vol. **98**, No. 1, year 2018, pages 013826:1-7; title: "*Unconventional photon blockade in three-mode optomechanics*"; authors: Bijita Sarma and Amarendra K. Sarma. Selected contents are reproduced with permission ©2018 American Physical Society.

4.1 Brief overview

Following the early theories on cavity optomechanical cooling of mechanical resonators, recent progress in optomechanical experiments has enabled the realization of mechanical resonators near to the ground state [18, 19, 39, 54, 165–170]. This has opened up newer avenues for quantum applications of optomechanical systems [131, 171, 172]. Recently, cavity optomechanical systems have been studied for its inherent nonlinear coupling to achieve photon blockade [75, 173].

Photon blockade arises from the anharmonicity in energy eigenvalues of an optical mode, which can be introduced via nonlinear interactions. Due to the anharmonicity, resonant excitation of one photon prohibits other photons from simultaneous excitation, giving rise to sub-Poissonian light. The early theories and experiments on photon blockade dealt with atom-coupled cavities [71, 174], or quantum dot-coupled cavity QED systems [72], or cavities with Kerr-type nonlinearity [175]. After that, there have been several studies on photon blockade in optical waveguides [176], coupled cavities [73, 177, 178], qubit-cavity systems [179], circuit-QED [74, 180, 181], gain cavity [182], four-wave mixing in weakly nonlinear system [183], and multiphoton blockade in some systems [184–186]. Numerous possible quantum device designs such as: single-photon transistors [187], quantum repeaters [188], quantum gates [189], quantum-optical Josephson interferometer [190], fermionization of photons [191], and crystallization of polaritons [192] rely on the phenomenon of photon blockade. In fact, generation of single photons plays a central role in light-based quantum computation and cryptography [67, 193–195].

Photon blockade in an optomechanical system was studied recently, where due to the photon-phonon nonlinear interaction, realization of antibunched sub-Poissonian light was predicted [75]. Subsequently, photon blockade [76–78], as well as phonon blockade [92–94] have been studied in various optomechanical and nanomechanical systems. However, similar to the cavity-QED systems, realization of optomechanical photon blockade demands the criterion of strong-coupling, where the single-photon optomechanical coupling is strong enough to overcome system losses, in order to produce sufficient anharmonicity in the energy-levels [75]. Reaching this strong-coupling regime is a long-sought-after goal in cavity optomechanics, however only with a few realizations like cold-atomic clouds in optomechanical cavity [43, 196], where this requirement has been met till date.

Recently, another mechanism for photon blockade which does not require the strong-

coupling condition to hold, is invoked by Liew and Savona in coupled-polaritonic systems [80]. This method, named as the unconventional photon blockade, is based on quantum interference, in which strong photon antibunching was predicted with nonlinearity much smaller than the decay rate of the photonic modes [81]. Afterwards, it has been studied in other systems including coupled nonlinear photonic molecules [81], coupled cavities with Kerr-type nonlinearity [83, 197–201], coupled optomechanical cavities [84, 202], coupled quantum dot-cavity system [82], bimodal cavity [203, 204], weakly nonlinear photonic molecules [205], Gaussian squeezed states [206], a double quantum well embedded in a micropillar optical cavity [207],and with second-order nonlinearity [208, 209]. Recently, unconventional photon blockade has also been realized experimentally in a quantum dot cavity system [210].

4.2 Photon blockade in a three-mode optomechanical cavity

Here, we study photon correlations in a nonlinear optomechanical cavity containing two optical modes and one mechanical mode which are cross-coupled by a three-mode interaction. We show that even when the Kerr-nonlinearities in the optical modes are weak, due to the three-mode interaction, distinct two-photon excitation pathways arise which gives rise to strong photon antibunching via unconventional photon blockade. We describe the model and derive the optimal conditions for photon blockade.We calculate the equal-time second-order correlation function as well as the two-time correlation function for the higher-frequency cavity mode and analyze the photon blockade characteristics. We also discuss the effects of temperature and pure-dephasing induced decoherences.

4.2.1 Model and theory

We consider a nonlinear optomechanical system as shown in Fig. 4.1(a), that contains two cavity modes with frequencies, ω_1 and ω_2, and one mechanical mode with frequency ω_m. The Hamiltonian of the system reads

$$\begin{aligned} H_0 &= \omega_1 a_1^\dagger a_1 + \omega_2 a_2^\dagger a_2 + \omega_m b^\dagger b + U a_1^\dagger a_1^\dagger a_1 a_1 \\ &\quad + U a_2^\dagger a_2^\dagger a_2 a_2 + g(a_1^\dagger a_2 + a_2^\dagger a_1)(b + b^\dagger) \\ &\quad + \Omega_1(a_1^\dagger e^{-i\omega_l t} + a_1 e^{i\omega_l t}) + \Omega_2(a_2^\dagger e^{-i\omega_l t} + a_2 e^{i\omega_l t}), \end{aligned} \tag{4.1}$$

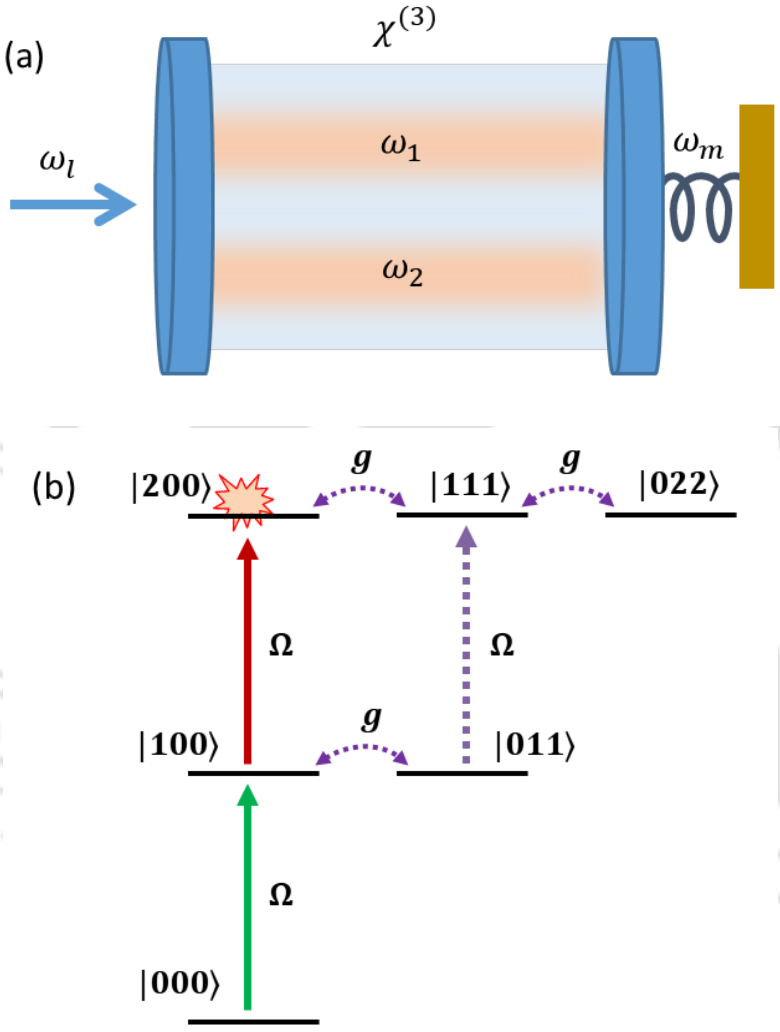

Figure 4.1: (a) Schematic diagram of the optomechanical cavity with two optical modes and a single mechanical mode, (b) The low energy-levels of the system for a weak drive and low temperature.

where a_1 ($a_1^\dagger$), a_2 ($a_2^\dagger$), and b ($b^\dagger$) are the annihilation (creation) operators for the two cavity modes with decay rates κ_1 and κ_2, and the mechanical mode with damping rate γ, respectively. Here, U is the strength of the Kerr-nonlinearity experienced by both the optical modes. We assume the difference between the two cavity mode frequencies to be equal to the mechanical frequency, i.e. $\omega_1 - \omega_2 = \omega_m$, so that the cavity modes can be cross-coupled by the optomechanical interaction [211]. The coupling is characterized by the rate, g, and is also proportional to the mechanical displacement. The last two terms in Eq. (4.1) describe the driving input fields and its interaction with the two cavity modes. For simplicity, we will assume that $\kappa_1 = \kappa_2 = \kappa$, for the rest of the analysis.

In a rotating frame at the laser frequency, ω_l, the Hamiltonian is transformed to

$$\begin{aligned} H &= \Delta a_1^\dagger a_1 + (\Delta - \omega_m) a_2^\dagger a_2 + \omega_m b^\dagger b + U a_1^\dagger a_1^\dagger a_1 a_1 \\ &\quad + U a_2^\dagger a_2^\dagger a_2 a_2 + g(a_1^\dagger a_2 + a_2^\dagger a_1)(b + b^\dagger) \\ &\quad + \Omega_1(a_1^\dagger + a_1) + \Omega_2(a_2^\dagger + a_2), \end{aligned} \tag{4.2}$$

where, $\Delta = \omega_1 - \omega_l$, is the detuning of the cavity mode a_1 from the laser drive. Now, we transform the Hamiltonian to a frame defined by the unitary transformation, $U = \exp[-i\omega_m t(b^\dagger b - a_2^\dagger a_2)]$. Assuming that the coupling rate is much lower in comparison to the mechanical resonator frequency, i.e. $\omega_m \gg g$, under a rotating-wave approximation, the transformed Hamiltonian is obtained as:

$$\begin{aligned} H &= \Delta(a_1^\dagger a_1 + a_2^\dagger a_2) + U a_1^\dagger a_1^\dagger a_1 a_1 + U a_2^\dagger a_2^\dagger a_2 a_2 \\ &\quad + g(a_1^\dagger a_2 b + a_1 a_2^\dagger b^\dagger) + \Omega_1(a_1^\dagger + a_1). \end{aligned} \tag{4.3}$$

This Hamiltonian indicates a three-mode interaction among the two optical modes and the mechanical mode, in which one photon from the mode, a_1, is annihilated to create one photon in the mode, a_2, and one phonon in the mechanical mode, b. In the reverse process, one photon from the mode, a_2, and one phonon in the mode, b of the mechanical resonator are annihilated to create one photon in the mode, a_1. In the following, we intend to study the photon antibunching effect in the mode, a_1, arising as a result of this three-wave mixing Hamiltonian.

Photon antibunching would be studied by analyzing the normalized zero-time-delay second-order correlation function, given by

$$g_a^{(2)}(0) = \frac{\langle a_1^\dagger(t) a_1^\dagger(t) a_1(t) a_1(t) \rangle}{\langle a_1^\dagger(t) a_1(t) \rangle^2}. \tag{4.4}$$

This quantity characterizes the joint probability of detecting two photons at the same time, which can be calculated numerically from the Lindblad master equation. The master equation for the driven-dissipative system is given by

$$\dot{\rho} = i[\rho, H] + L_1(\rho) + L_2(\rho) + L_b(\rho), \tag{4.5}$$

where, $L_1(\rho) = \frac{\kappa}{2}(2a_1\rho a_1^\dagger - a_1^\dagger a_1\rho - \rho a_1^\dagger a_1)$, $L_2(\rho) = \frac{\kappa}{2}(2a_2\rho a_2^\dagger - a_2^\dagger a_2\rho - \rho a_2^\dagger a_2)$, and $L_b(\rho) = \frac{\kappa}{2}(n_{\rm th}+1)(2b\rho b^\dagger - b^\dagger b\rho - \rho b^\dagger b) + \frac{\kappa}{2}n_{\rm th}(2b^\dagger\rho b - bb^\dagger\rho - \rho bb^\dagger)$, are the Liouvillian operators for the two optical modes and the mechanical mode respectively. Here, $n_{\rm th} = 1/[\exp(\omega_m/k_BT) - 1]$ denotes the thermal phonon number in the mechanical mode at the bath temperature, T. The steady-state value of $g_a^{(2)}(0)$ can be found numerically by solving the master equation and then from the steady state density matrix operator as, $g_a^{(2)}(0) = {\rm Tr}(\rho a_1^\dagger a_1^\dagger a_1 a_1)/[{\rm Tr}(\rho a_1^\dagger a_1)]^2$. For this, we have used the Quantum Optics Toolbox in MATLAB [212] and QuTiP (Quantum Toolbox in Python) [213, 214].

In addition to the master equation approach, optimal conditions for photon blockade can be determined in the following manner. When the driving field is very weak in comparison to the Kerr nonlinearity, and the temperature is also very low, then, only the lower energy levels of the cavity and the mechanical modes are occupied [78], as shown in Fig. 4.1(b). Considering the allowed low-energy transitions given by the Hamiltonian in Eq. (4.3), the truncated state of the system is given by [81]

$$\begin{aligned}|\psi\rangle = {} & C_{000}|000\rangle + C_{100}|100\rangle + C_{011}|011\rangle \\ & + C_{200}|200\rangle + C_{111}|111\rangle + C_{022}|022\rangle,\end{aligned} \tag{4.6}$$

where, $C_{a_1a_2b}$'s are the amplitudes of the quantum states for which the corresponding occupation probability is given by $|C_{a_1a_2b}|^2$. The values of the coefficients can be determined by solving the Schrödinger equation, $i\frac{d|\psi\rangle}{dt} = H'|\psi\rangle$, where H' is the non-Hermitian Hamiltonian containing the optical decay and mechanical damping terms

$$\begin{aligned}H' = {} & (\Delta - i\frac{\kappa}{2})(a_1^\dagger a_1 + a_2^\dagger a_2) - i\frac{\gamma}{2}b^\dagger b + Ua_1^\dagger a_1^\dagger a_1 a_1 \\ & + Ua_2^\dagger a_2^\dagger a_2 a_2 + g(a_1^\dagger a_2 b + a_1 a_2^\dagger b^\dagger) + \Omega_1(a_1^\dagger + a_1).\end{aligned} \tag{4.7}$$

For a weak drive, a set of equations for the coefficients is obtained from the Schrödinger

equation

$$\begin{aligned}
i\frac{\partial C_{100}}{\partial t} &= \left(\Delta - i\frac{\kappa}{2}\right)C_{100} + gC_{011} + \Omega(C_{000} + \sqrt{2}C_{200}),\\
i\frac{\partial C_{011}}{\partial t} &= \left(\Delta - i\frac{\kappa+\gamma}{2}\right)C_{011} + gC_{100} + \Omega C_{111},\\
i\frac{\partial C_{200}}{\partial t} &= 2\left(\Delta + U - i\frac{\kappa}{2}\right)C_{200} + \sqrt{2}gC_{111} + \sqrt{2}\Omega C_{100},\\
i\frac{\partial C_{111}}{\partial t} &= \left[2\left(\Delta - i\frac{\kappa}{2}\right) - i\frac{\gamma}{2}\right]C_{111} + g(2C_{022} + \sqrt{2}C_{200})\\
&\quad + \Omega C_{011},\\
i\frac{\partial C_{022}}{\partial t} &= 2\left(\Delta + U - i\frac{\kappa+\gamma}{2}\right)C_{022} + 2gC_{111}.
\end{aligned} \tag{4.8}$$

Under the weak driving assumption, one can consider that $\{C_{111}, C_{022}, C_{200}\} \ll \{C_{100}, C_{011}\} \ll C_{000}$. In steady-state, to solve the coupled equations, we follow the iterative method prescribed by Bamba et. al [81]. The optimal condition for complete photon blockade corresponds to the case, when the probability of a photon in the state $|200\rangle$ equals zero. Therefore, at steady-state, the equations for C_{100} and C_{011} are given by

$$\begin{aligned}
\left(\Delta - i\frac{\kappa}{2}\right)C_{100} + gC_{011} + \Omega C_{000} &= 0,\\
\left(\Delta - i\frac{\kappa+\gamma}{2}\right)C_{011} + gC_{100} &= 0.
\end{aligned} \tag{4.9}$$

These two equations give the coefficints C_{100} and C_{011} as

$$\begin{aligned}
C_{100} &= -\frac{\Omega(\Delta - i\frac{\kappa+\gamma}{2})}{(\Delta - i\frac{\kappa}{2})(\Delta - i\frac{\kappa+\gamma}{2}) - g^2}C_{000},\\
C_{011} &= \frac{\Omega g}{(\Delta - i\frac{\kappa}{2})(\Delta - i\frac{\kappa+\gamma}{2}) - g^2}C_{000}.
\end{aligned} \tag{4.10}$$

Now, the equations for the other coefficients are reduced to

$$\begin{aligned}
gC_{111} + \Omega C_{100} &= 0,\\
\left[2\left(\Delta - i\frac{\kappa}{2}\right) - i\frac{\gamma}{2}\right]C_{111} + 2gC_{022} + \Omega C_{011} &= 0,\\
2\left(\Delta + U - i\frac{\kappa+\gamma}{2}\right)C_{022} + 2gC_{111} &= 0.
\end{aligned} \tag{4.11}$$

Now, considering $\gamma \ll \kappa$ for typical optomechanical systems, the necessary and sufficient condition for the existence of nontrivial solutions of Eqs. (4.11) gives the optimal

parameters for complete photon antibunching in the mode a_1:

$$\begin{aligned}\Delta_{\rm opt} &= \pm\frac{1}{2}\sqrt{2\sqrt{g^2(5g^2+2\kappa^2)}-4g^2-\kappa^2},\\ U_{\rm opt} &= \frac{\Delta(4\Delta^2+2g^2+5\kappa^2)}{2(2g^2-\kappa^2)}.\end{aligned} \tag{4.12}$$

These optimal conditions correspond to the situation, where different transition paths leading to two-photon excitation in the mode a_1 interferes destructively, as shown in Fig. 4.1(b).

4.2.2 Results

In the following, we discuss the numerical results for $g_a^{(2)}(0)$ obtained from solving Eq. (4.5). In Fig. 4.2(a), we show $g_a^{(2)}(0)$ as a function of Δ/κ with different moderate values of g. The values of U is considered to be $U_{\rm opt}$. For the values of g considered in the plot, the optimal parameters from Eq. (4.12) are obtained as, for $g/\kappa = 1$: $\Delta_{\rm opt}/\kappa = 0.27$, $U_{\rm opt}/\kappa = 0.98$; for $g/\kappa = 1.5$: $\Delta_{\rm opt}/\kappa = 0.47$, $U_{\rm opt}/\kappa = 0.71$; for $g/\kappa = 2$: $\Delta_{\rm opt}/\kappa = 0.66$, $U_{\rm opt}/\kappa = 0.69$; for $g/\kappa = 2.5$: $\Delta_{\rm opt}/\kappa = 0.84$, $U_{\rm opt}/\kappa = 0.74$. It can be observed from Fig. 4.2(a) that, as predicted from the optimal conditions calculated analytically, $g_a^{(2)}(0)$ shows a strong antibunching effect at the optimal values of Δ/κ.

Fig. 4.2(b), demonstrates the two-time second-order correlation function $g_a^{(2)}(\tau)$ which is calculated as:

$$g_a^{(2)}(\tau) = \frac{\langle a_1^\dagger(t)a_1^\dagger(t+\tau)a_1(t+\tau)a_1(t)\rangle}{\langle a_1^\dagger(t)a_1(t)\rangle^2}. \tag{4.13}$$

This quantity, $g_a^{(2)}(\tau)$ is proportional to the joint probability of detecting one photon at time, $(t+\tau)$, provided another photon was detected at time, t, at that position [215]. The plots show $g_a^{(2)}(\tau)$ under the optimal conditions for different values of J. We can observe that at $\tau = 0$, $g_a^{(2)}(0) \approx 0$, and for other delay times $g_a^{(2)}(\tau) > g_a^{(2)}(0)$. Therefore, it clearly demonstrates that the emitted photons are antibunched and sub-Poissonian in nature. From Figs. 4.2(a) and (b), one can observe that for the values of U falling in the weak coupling regime, i.e. $U < \kappa$, photon blockade can be realized owing to the quatum interference-inducing interaction, as verified by the optimal parameters.

In order to visualize the photon blockade effects more clearly, we show the contour plots of $g_a^{(2)}(0)$ in Fig. 4.3, as functions of normalized detuning, Δ/κ and normalized nonlinear strength, U/κ. In Figs. 4.3(a)-(d), the values of g/κ are considered as: $g/\kappa = 1$ in

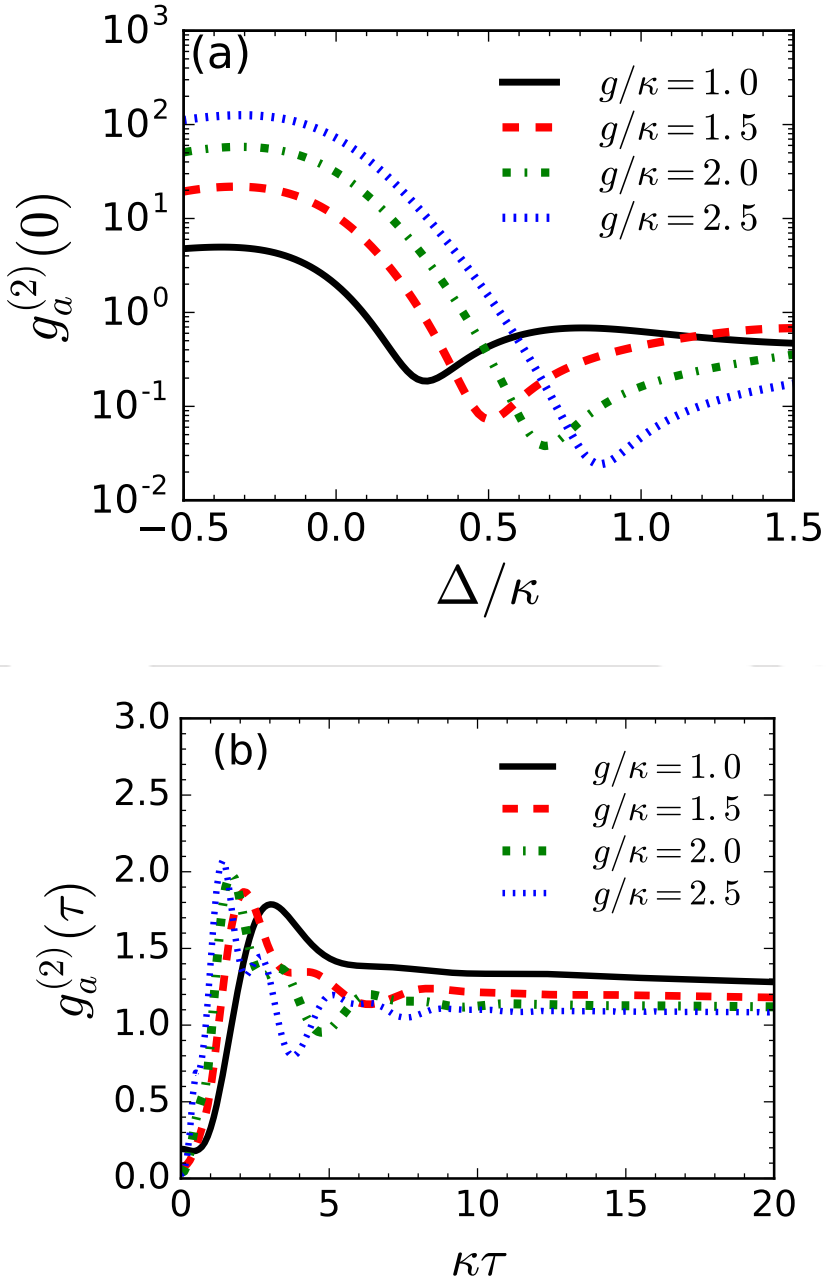

Figure 4.2: Plot of second-order correlation function, $g_a^{(2)}(0)$ at $T = 0$ as a function of normalized detuning Δ/κ for different values of g/κ. The nonlinearity is considered to be $U_{\text{opt}}/\kappa = 0.98$, 0.71, 0.69, and 0.74 for the normalized values of coupling, $g/\kappa = 1$, 1.5, 2 and 2.5 respectively. (b) Plot of two-time correlation function, $g_a^{(2)}(\tau)$. The values of U is considered same as in (a). The nonlinear strength is considered as $\Delta_{\text{opt}}/\kappa = 0.27$, 0.47, 0.66, and 0.84 respectively.

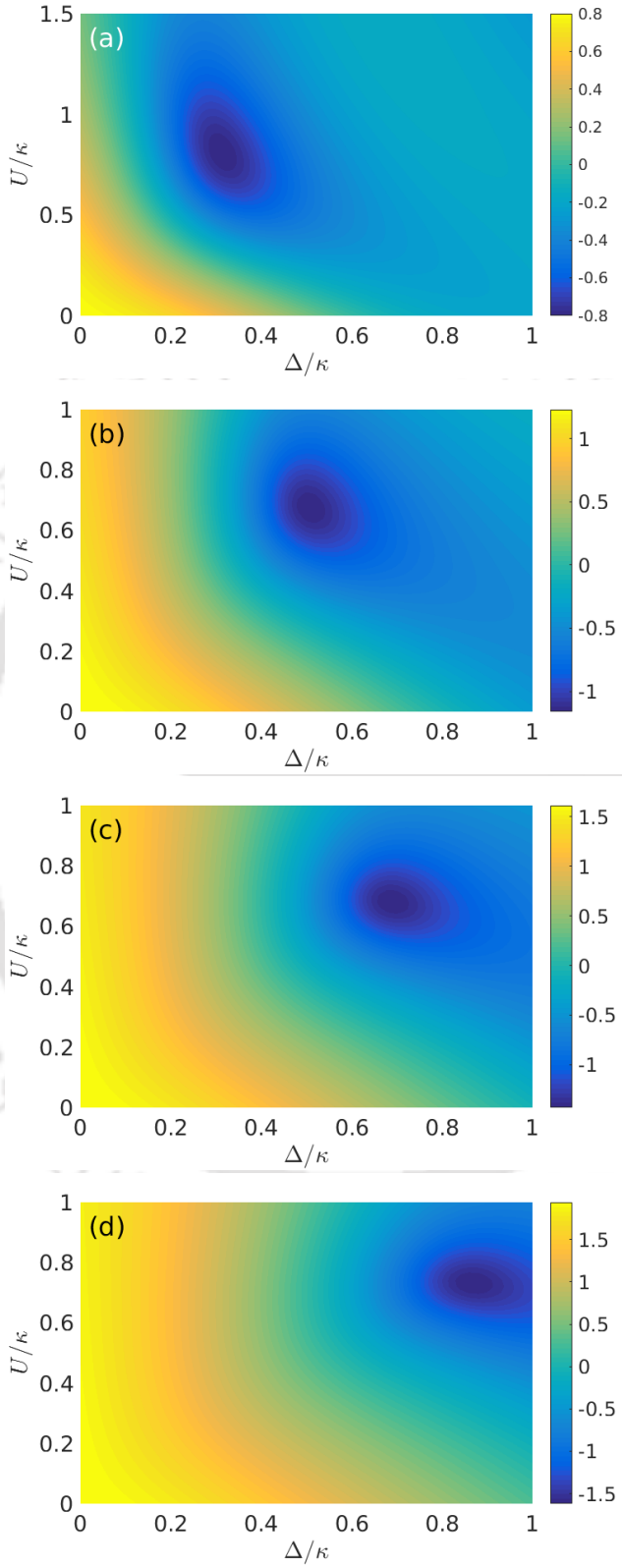

Figure 4.3: Contour plots showing the variation of $\log_{10} g_a^{(2)}(0)$ as functions of Δ/κ and U/κ, for different values of g/κ considered as: $g/\kappa = 1$ in (a), $g/\kappa = 1.5$ in (b), $g/\kappa = 2$ in (c), and $g/\kappa = 2.5$ in (d).

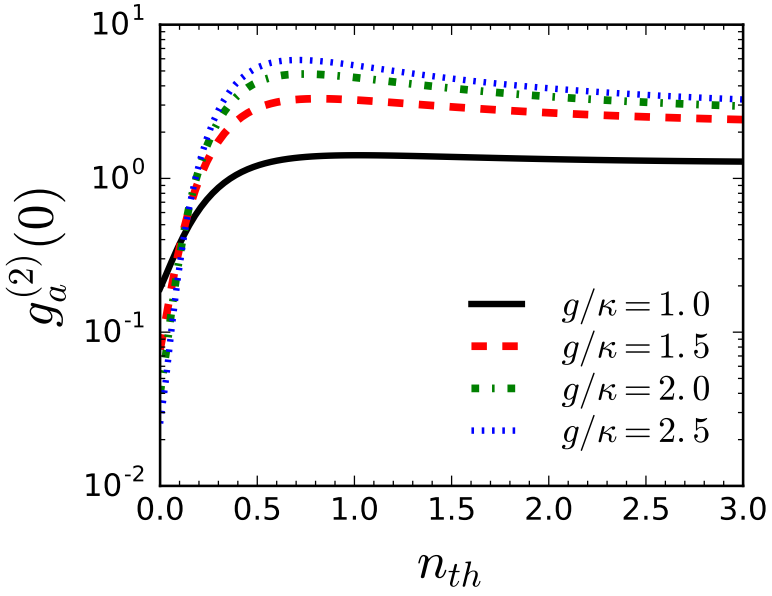

Figure 4.4: Plot of $g_a^{(2)}(0)$ as a function of thermal phonon number, $n_{\rm th}$ for various values of g/κ.

(a), $g/\kappa = 1.5$ in (b), $g/\kappa = 2$ in (c), and $g/\kappa = 2.5$ in (d). The plots show that strong photon antibunching occurs exactly at the values predicted from the analytical calculations, in Eq. (4.12).

Next, we want to study the influence of environmental phonon population on the photon blockade characteristics. In Fig. 4.4, we demonstrate $g_a^{(2)}(0)$ as a function of the bath phonon number, $n_{\rm th}$. For $g/\kappa = 1$, $g_a^{(2)}(0)$ reaches 1 at $n_{\rm th} \approx 0.5$, whereas, for $g/\kappa = 1.5$, 2 and 2.5, $g_a^{(2)}(0) \leq 1$ upto $n_{\rm th} \approx 0.25$. Therefore, it is evident that the environmental thermal phonon population has undesirable effect on the observation of photon blockade.

Till now, in our analysis, we have not considered the effect of pure dephasing induced decoherences. Pure dephasing may arise from the instability of the laser drive, or coupling of the cavity modes to other mechanical modes, and due to this there can be perturbing effect on polarization, linewidth, transmittance, and photon statistics [202]. Therefore in the following, we analyze the effect of pure-dephasing on the antibunching properties of the cavity photons. The effects of pure dephasing can be modeled by adding another Lindblad term of the form $L_p(\rho) = \frac{\gamma_p}{2} \sum_{j=1,2} [2a_j^\dagger a_j \rho a_j^\dagger a_j - (a_j^\dagger a_j)^2 \rho - \rho (a_j^\dagger a_j)^2]$, into the master equation, where γ_p is the pure dephasing rate for the cavity modes. Figs. 4.5(a)-

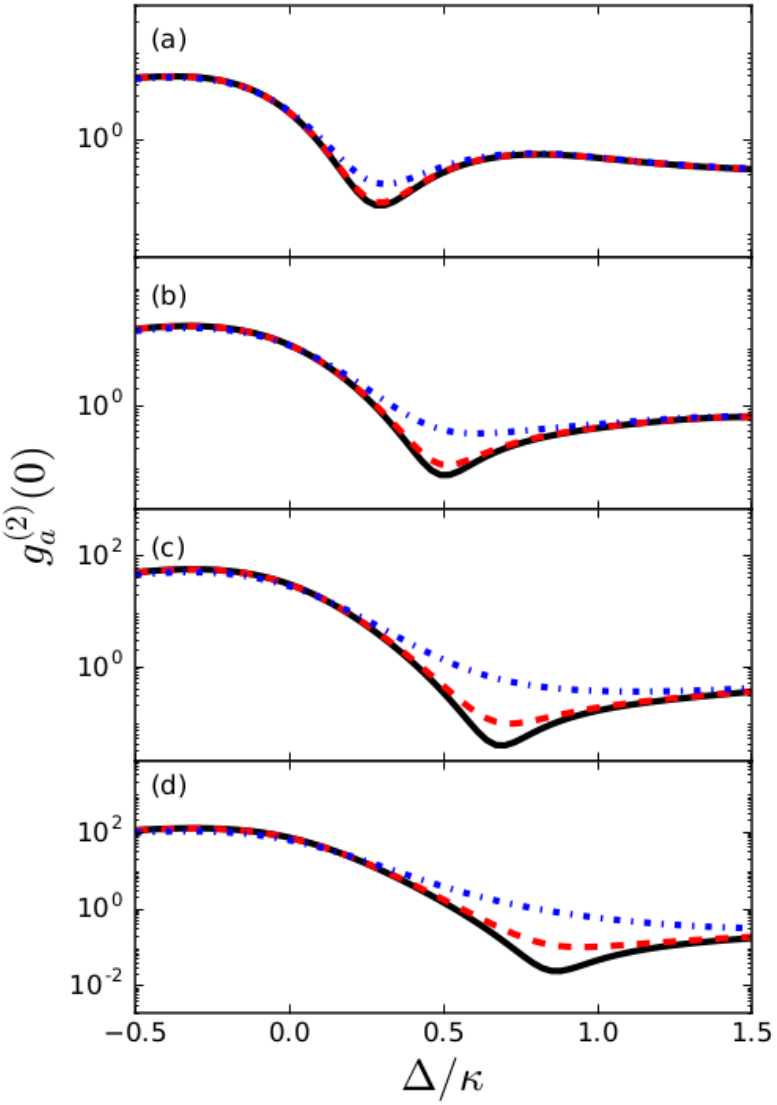

Figure 4.5: Effect of pure dephasing. The black solid line represents $\gamma_p/\kappa = 0$, red dashed line is for $\gamma_p/\kappa = 0.001$ and the blue dash-dotted line denotes $\gamma_p/\kappa = 0.01$.

(d) show the second-order correlation function $g_a^{(2)}(0)$ for different pure dephasing rates with different sets of optimized values. The values of g is considered as: $g/\kappa = 1$ in (a), $g/\kappa = 1.5$ in (b), $g/\kappa = 2$ in (c), and $g/\kappa = 2.5$ in (d). The black solid line represents $\gamma_p/\kappa = 0$, red dashed line is for $\gamma_p/\kappa = 0.001$ and the blue dash-dotted line denotes $\gamma_p/\kappa = 0.01$. With increase in the pure dephasing rate, $g_a^{(2)}(0)$ increases near the optimal detuning. For higher values of pure-dephasing rates eg. $\gamma_p = 0.01\kappa$, $g_a^{(2)}(0)$ approaches classical Poissonian statistics.

4.2.3 Summary

In conclusion, we analyzed the photon statistics in terms of the second-order correlation function, in a weakly driven optomechanical system, where two optical modes and one mechanical mode interact via a three-mode mixing. Due to this coupling, additional two-photon excitation pathways are created in the higher-frequency optical mode, which can be exploited to obtain the desired photon blockade characteristics in the system via quantum interference. We derived the optimal parameters required for strong photon blockade by solving the non-Hermitian Schrödinger equation containing the terms corresponding to damping and decay present in the system. The numerical calculations of the second-order correlation function obtained from solving the master equation show agreement with the analytical calculations. It is observed that even when the Kerr-type nonlinearity is weak, under the optimal conditions necessary for the fulfillment of the quantum-interference effect, photon blockade is possible in the system.

4.3 Photon blockade in an optomechanical cavity with a degenerate optical parametric amplifier

Next, we study the possibility of realizing unconventional photon blockade in an optomechanical cavity that includes a degenerate optical parametric amplifier (OPA). Introducing the OPA, one can create new paths for photon excitation, that may lead to destructive quantum interference in the two-photon excitation pathway. We find out the optimal conditions for achieving this. The validity of the optimal conditions are also confirmed via numerical calculations. We also analyze the effects of pure dephasing induced decoherence on the unconventional photon blockade.

4.3.1 Model and theory

We study an optomechanical cavity containing an optical parametric amplifier (OPA), which can be modeled schematically as shown in Fig. 4.6(a). The Hamiltonian for the system in a frame rotating at the pump frequency is given by

$$H = \Delta a^\dagger a + \omega_m b^\dagger b + g a^\dagger a \left(b + b^\dagger\right) + iG(e^{i\theta} a^{\dagger 2} - e^{-i\theta} a^2) + \Omega(a^\dagger + a), \tag{4.14}$$

where a ($a^\dagger$) and b ($b^\dagger$) are the annihilation (creation) operators for optical and mechanical modes respectively. Also, $\Delta = \omega_a - \omega_l$ is the cavity detuning, where ω_a is the

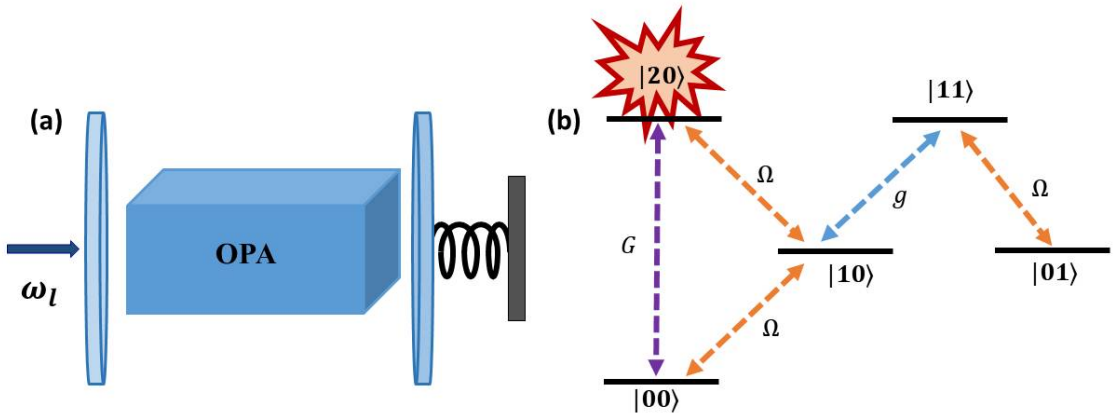

Figure 4.6: (a) Schematic diagram of the optomechanical system with an OPA medium, (b) Transition paths of the system for quantum interference.

resonance frequency of the cavity field and ω_l is the driving laser frequency, and ω_m is the resonance frequency of the mechanical resonator. The single-photon optomechanical coupling strength between the cavity field and the mechanical resonator is denoted by g, G is the OPA coupling term, and Ω is the driving laser amplitude.

First, we will derive the optimal conditions for unconventional photon blockade analytically. In the weak driving condition ($\Omega \ll \kappa$) and for low temperature, the photon number and phonon number Hilbert space can be truncated to low values. Considering a Fock-state basis, $|m,n\rangle$ in Hilbert space, where m and n are the photon and the phonon numbers respectively, the state of the system can be expressed as [81]:

$$|\psi\rangle = C_{00}|00\rangle + C_{01}|01\rangle + C_{10}|10\rangle + C_{11}|11\rangle + C_{20}|20\rangle, \tag{4.15}$$

where C_{mn} are the amplitudes of the quantum states and the corresponding occupation probability is given by $|C_{mn}|^2$. In terms of the probability coefficients, the second-order correlation function for the optical mode can be written as:

$$g^{(2)}(0) = \frac{2|C_{20}|^2}{(|C_{10}|^2 + |C_{11}|^2)^2}. \tag{4.16}$$

The coefficients C_{mn} can be obtained by solving the Schrödinger equation:

$$i\frac{d|\psi\rangle}{dt} = H'|\psi\rangle, \tag{4.17}$$

where H' is the effective non-Hermitian Hamiltonian that takes into account the dissipations in the system:

$$H' = \Delta' a^\dagger a + \omega'_m b^\dagger b + g a^\dagger a(b + b^\dagger) + iG(e^{i\theta}a^{\dagger 2} - e^{-i\theta}a^2) + \Omega(a^\dagger + a), \tag{4.18}$$

with $\Delta' = \Delta - i\kappa/2$ and $\omega_m' = \omega_m - i\gamma/2$. Using Eq. (4.15) for the state $|\psi\rangle$ and Eq. (4.18) for the Hamiltonian H' in the Schrödinger equation, $i\frac{d|\psi\rangle}{dt} = H'|\psi\rangle$, we get a set of equations for the coefficients:

$$\begin{aligned}
i\frac{\partial C_{00}}{\partial t} &= \Omega C_{10} - i\sqrt{2}GC_{20}e^{-i\theta} \\
i\frac{\partial C_{01}}{\partial t} &= \omega_m' C_{01} + \Omega C_{11} \\
i\frac{\partial C_{10}}{\partial t} &= \Delta' C_{10} + gC_{11} + \Omega(C_{00} + \sqrt{2}C_{20}) \\
i\frac{\partial C_{11}}{\partial t} &= (\Delta' + \omega_m')C_{11} + gC_{10} + \Omega C_{01} \\
i\frac{\partial C_{20}}{\partial t} &= 2\Delta' C_{20} + \sqrt{2}\Omega C_{10} + i\sqrt{2}Ge^{i\theta}C_{00}
\end{aligned} \tag{4.19}$$

The steady-state solution can be found by solving the coupled equations for the coefficients. Under the weak driving condition, the first equation in Eqs. (4.19) is always approximately satisfied. Therefore, we only consider the last four equations for further calculations:

$$\begin{aligned}
\omega_m' C_{01} + \Omega C_{11} &= 0 \\
\Delta' C_{10} + gC_{11} + \Omega(C_{00} + \sqrt{2}C_{20}) &= 0 \\
(\Delta' + \omega_m')C_{11} + gC_{10} + \Omega C_{01} &= 0 \\
2\Delta' C_{20} + \sqrt{2}\Omega C_{10} + i\sqrt{2}Ge^{i\theta}C_{00} &= 0
\end{aligned} \tag{4.20}$$

For complete photon blockade, the probability of a photon in state $|20\rangle$ should be approximately zero. Therefore, we consider $C_{20} = 0$ in Eqs. (4.20) for photon blockade. After finding out the necessary and sufficient conditions for these equations to have a solution, more simplifications lead us to the following optimum conditions:

$$\begin{aligned}
G_{\text{opt}} &= \frac{\Omega^2}{\cos\theta(\frac{\kappa}{2} + \frac{g^2 A}{A^2+B^2}) + \sin\theta(-\Delta + \frac{g^2 B}{A^2+B^2})}, \\
\theta_{\text{opt}} &= \arctan\left(-\frac{\Delta + \frac{g^2 B}{A^2+B^2}}{\frac{\kappa}{2} + \frac{g^2 A}{A^2+B^2}}\right),
\end{aligned} \tag{4.21}$$

where, $A = \frac{1}{2}\left(\kappa + \gamma + \frac{\Omega^2\gamma}{\omega_m^2 + (\frac{\gamma}{2})^2}\right)$, and $B = \Delta + \omega_m - \frac{\Omega^2\omega_m}{\omega_m^2 + (\frac{\gamma}{2})^2}$.

Interestingly, these conditions depend on the cavity-detuning, the driving laser amplitude and the cavity linewidth. Since the optimal conditions correspond to the

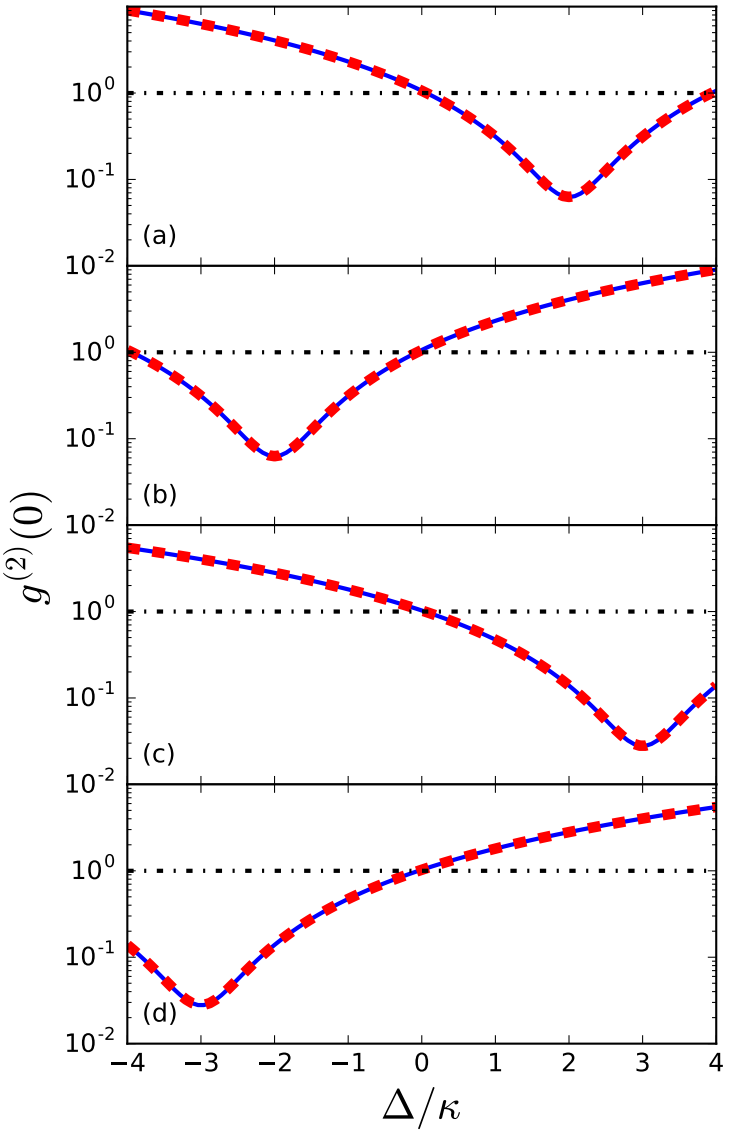

Figure 4.7: Numerical and analytical results for the zero-time-delay second order correlation function, $g^{(2)}(0)$ as function of normalized detuning Δ/κ. Other parameters are considered as: $\omega_m/\kappa = 10$ (resolved sideband limit), $\Omega/\kappa = 0.01$, $\gamma/\kappa = 0.01$ $g/\kappa = 0.5$, and $n_{\text{th}} = 0$. OPA parameters are: $G/\kappa = 4.89 \times 10^{-5}$, $\theta/\pi = -0.42$ in (a), $G/\kappa = 4.77 \times 10^{-5}$, $\theta/\pi = 0.42$ in (b), $G/\kappa = 3.30 \times 10^{-5}$, $\theta/\pi = -0.44$ in (c) and $G/\kappa = 3.25 \times 10^{-5}$, $\theta/\pi = 0.44$ in (d).

parameters of the pump field driving the OPA, these are expected to be controlled by tuning the OPA pump field.

The statistical properties of the cavity field can be described by the normalized

zero-time-delay second-order correlation function given by:

$$g^{(2)}(0) = \frac{\langle a^\dagger(t)a^\dagger(t)a(t)a(t)\rangle}{\langle a^\dagger(t)a(t)\rangle^2}. \tag{4.22}$$

For photon blockade, we assume that the cavity is driven by a weak classical field. The master equation of the density operator ρ for the driven system reads as:

$$\dot{\rho} = i[\rho, H] + L_a(\rho) + L_b(\rho), \tag{4.23}$$

where $L_a(\rho) = \frac{\kappa}{2}(2a\rho a^\dagger - a^\dagger a\rho - \rho a^\dagger a)$ and $L_b(\rho) = \frac{\gamma}{2}(n_{\rm th}+1)(2b\rho b^\dagger - b^\dagger b\rho - \rho b^\dagger b) + \frac{\gamma}{2}n_{\rm th}(2b^\dagger\rho b - bb^\dagger\rho - \rho bb^\dagger)$, are the Liouvillian operators for the optical and the mechanical modes respectively. Here, $n_{\rm th}$ is the thermal phonon number given by $n_{\rm th} = 1/[e^{\omega_m/(k_B T)} - 1]$. It is worth to be noted that due to the high frequency of optical radiation, thermal photon number is considered to be zero at low temperature. The steady-state value of $g^{(2)}(0)$ can be found numerically by solving the master equation and from the steady state density matrix operator as [212–214]:

$$g^{(2)}(0) = \frac{{\rm Tr}(\rho a^\dagger a^\dagger a a)}{[{\rm Tr}(\rho a^\dagger a)]^2}. \tag{4.24}$$

We also derive an analytic expression for the zero-delay time second-order correlation function and compare it with the numerical solution. In the weak pumping limit, it can be assumed that the ground state population is unity and population in other levels is negligible. In that case, we may assume that $C_{00} \approx 1$. Then Eqs. (4.20) transform to:

$$\begin{aligned}
\omega_m' C_{01} + \Omega C_{11} &= 0,\\
\Delta' C_{10} + g C_{11} + \Omega(1 + \sqrt{2}C_{20}) &= 0,\\
(\Delta' + \omega_m') C_{11} + g C_{10} + \Omega C_{01} &= 0,\\
2\Delta' C_{20} + \sqrt{2}\Omega C_{10} + i\sqrt{2}G e^{i\theta} &= 0.
\end{aligned} \tag{4.25}$$

Solving these equations, the coefficients to be used for the calculation of $g^{(2)}(0)$ are obtained as:

$$\begin{aligned}
C_{10} &= \frac{\Omega(1 - iGe^{i\theta}/\Delta')}{-\Delta' + \frac{\Omega^2}{\Delta'} + \frac{g^2}{\Delta' + \omega_m' - \frac{\Omega^2}{\omega_m'}}}\\
C_{11} &= -\frac{gC_{10}}{\Delta' + \omega_m' - \frac{\Omega^2}{\omega_m'}}\\
C_{20} &= -\frac{(iGe^{i\theta} + \Omega C_{10})}{\sqrt{2}\Delta'}
\end{aligned} \tag{4.26}$$

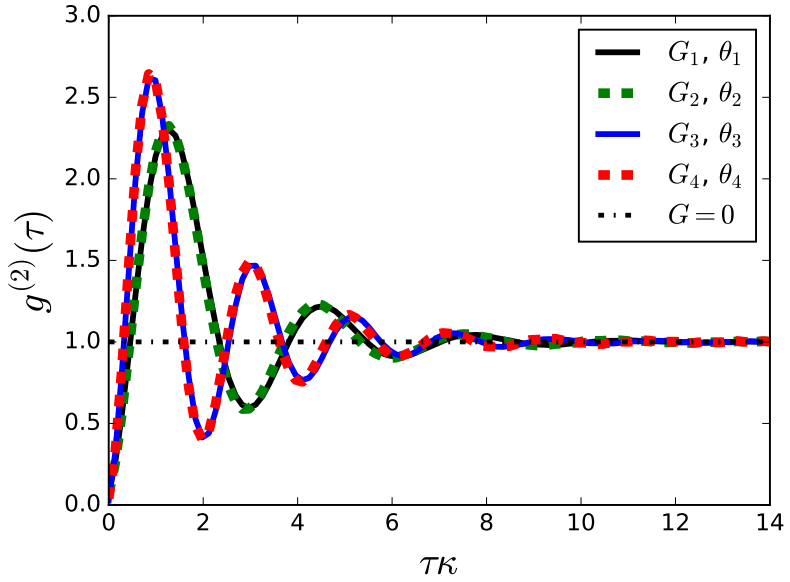

Figure 4.8: Time evolution of the second-order correlation function, $g^{(2)}(\tau)$. The OPA parameters are: $G_1 = 4.89 \times 10^{-5}\kappa$, $\theta_1 = -0.42\pi$, $G_2 = 4.77 \times 10^{-5}\kappa$, $\theta_2 = 0.42\pi$, $G_3 = 3.30 \times 10^{-5}\kappa$, $\theta_3 = -0.44\pi$ and $G_4 = 3.25 \times 10^{-5}\kappa$, $\theta_4 = 0.44\pi$.

4.3.2 Results

In the following, we solve the quantum master equation numerically using the analytical optimum conditions, and compare with the approximate analytical results. For the entire calculations, we have considered $\Omega/\kappa = 0.01$ for the weak driving condition. In Fig. 4.7, we have discussed the variation of the second-order correlation function at zero-time delay, $g^{(2)}(0)$ as a function of the normalized detuning Δ/κ, for optimal values of G and θ. The red dots show the numerical simulation results. In Fig. 4.7(a), the optimized values are, $G_{opt} = 4.89 \times 10^{-5}\kappa$ and $\theta_{opt} = -0.42\pi$ that correspond to the optimum values for $\Delta/\kappa = 2$. As expected, $g^{(2)}(0)$ shows a strong antibunching effect at an exact value of $\Delta/\kappa = 2$, as precisely predicted by the optimal parameters calculated analytically. In Fig. 4.7(b), optimized values are $G/\kappa = 4.77 \times 10^{-5}$, $\theta/\pi = 0.42$ for $\Delta/\kappa = -2$. In this case also, $g^{(2)}(0)$ shows a strong antibunching effect at an exact value of $\Delta/\kappa = -2$. For Fig. 4.7(c) and (d), G and θ values are considered to satisfy the optimal parameter calculations for $\Delta/\kappa = 3$ and -3 respectively.

Figure 4.8 shows the time evolution of the second-order correlation function $g^{(2)}(\tau)$,

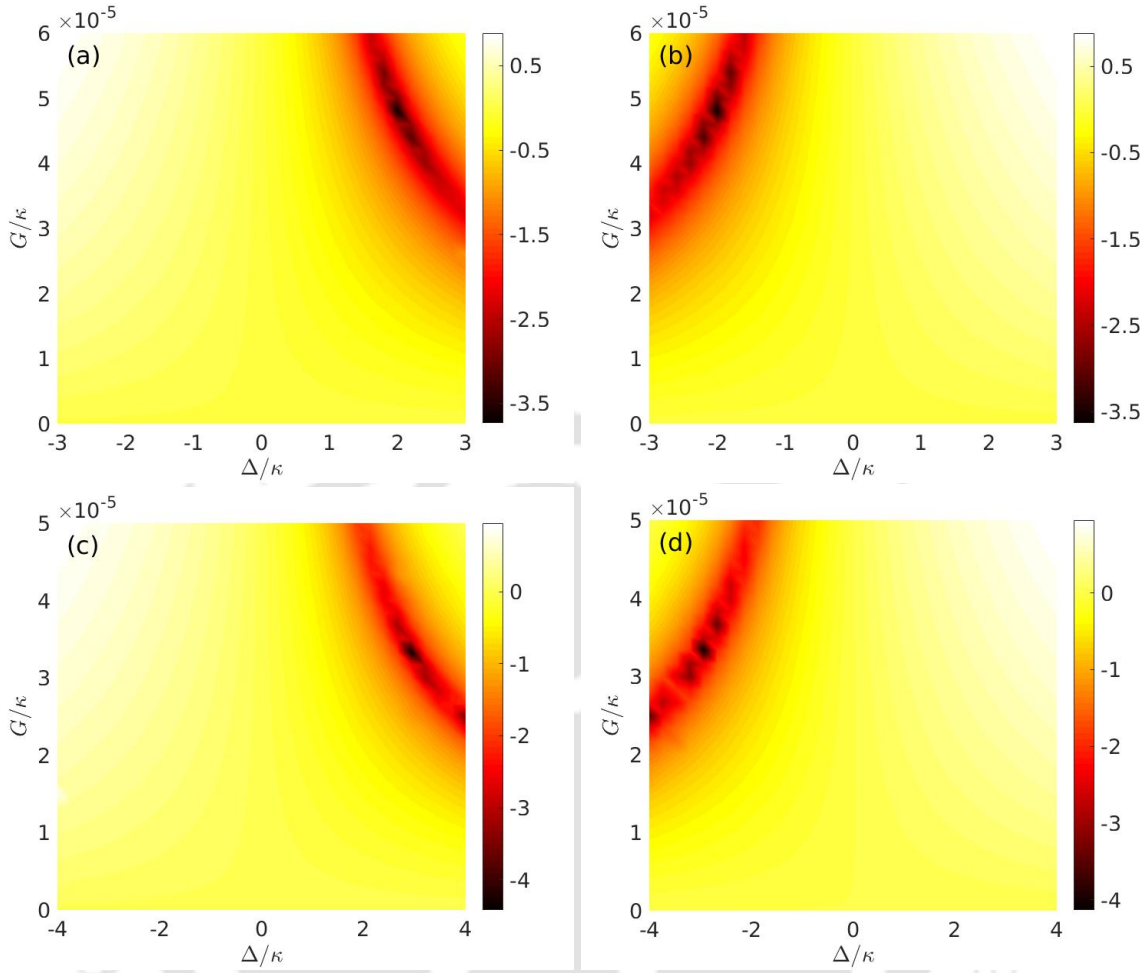

Figure 4.9: Numerical results for $\log_{10} g^{(2)}(0)$ as functions of normalized detuning Δ/κ and OPA coupling G/κ for $g/\kappa = 0.01$. In (a) $\theta/\pi = -0.42$, in (b) $\theta/\pi = 0.42$, in (c) $\theta/\pi = -0.44$ and in (d) $\theta/\pi = 0.44$.

that is calculated as:

$$g^{(2)}(\tau) = \frac{\langle a^\dagger(t)a^\dagger(t+\tau)a(t+\tau)a(t)\rangle}{\langle a^\dagger(t)a(t)\rangle^2}. \tag{4.27}$$

$g^{(2)}(\tau)$ is proportional to the joint probability of detecting one photon at time $t = \tau$, provided another photon was detected at time $t = 0$, at that position [215]. The plots show $g^{(2)}(\tau)$ for different optimal conditions. We can observe that at $\tau = 0$, $g^{(2)}(0) = 0$ and for other delay times $g^{(2)}(\tau) > g^{(2)}(0)$. Therefore, it clearly demonstrates that the emitted photons are antibunched and sub-Poissonian in nature.

To further investigate the antibunching effects, we calculated $g^{(2)}(0)$ as a function of cavity-light detuning Δ/κ and OPA gain G/κ with optimized values of θ. In Fig. 4.9(a), the

phase is assumed to be -0.42π, that corresponds to the optimum value for $\Delta/\kappa = 2$. As expected, a strong photon blockade occurs near the red detuning with $\Delta \approx \kappa$, and it occurs at $G/\kappa \approx 4.85 \times 10^{-5}$ as optimized precisely in Eq. (4.21). However for the blue detuned regime with $\Delta \approx -\kappa$, there is no strong antibunching because the phase of $\theta = -0.42\pi$ is not an optimized value in this case. In Fig. 4.9(b), $\theta/\pi = 0.42$ corresponding to $\Delta/\kappa = -2$. Here also, a strong antibunching occurs near the blue detuned regime with $\Delta \approx -2\kappa$ again at $G/\kappa \approx 4.85 \times 10^{-5}$; whereas there is no photon blockade in the red detuning regime in this case. Fig. 4.9(c)-(d) depict the behavior for $\theta/\pi = -0.44$ and 0.44 corresponding to $\Delta/\kappa = 3$ and -3 respectively.

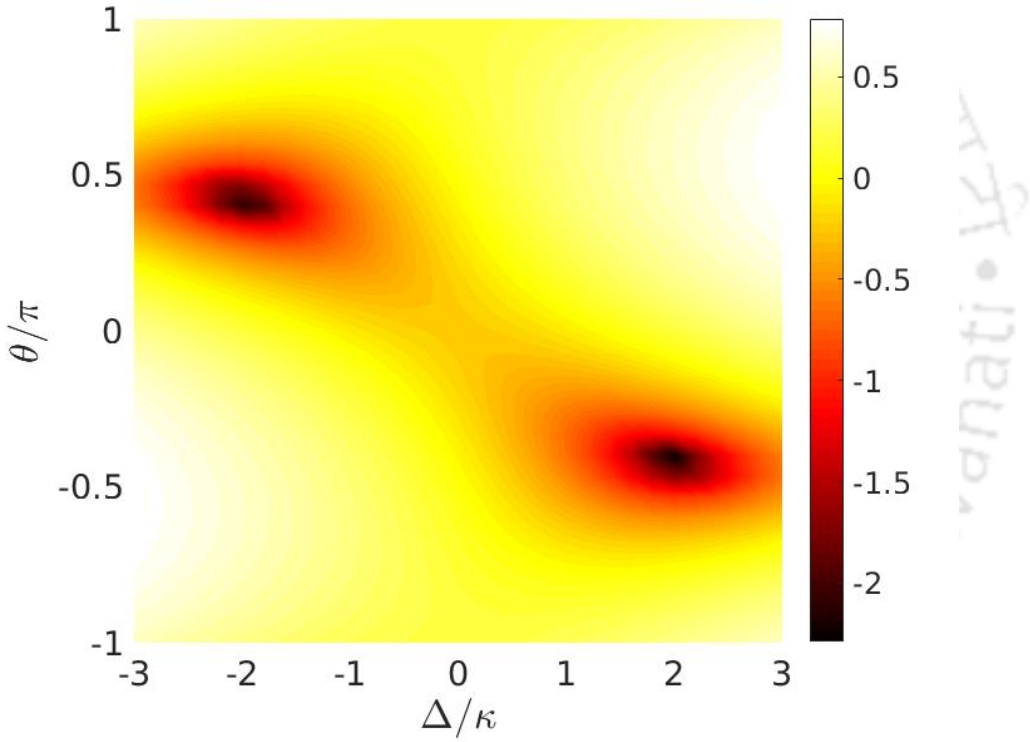

Figure 4.10: Numerical results for $\log_{10} g^{(2)}(0)$ as a function of normalized detuning Δ/κ and θ/π for $G/\kappa = 4.85 \times 10^{-5}$.

Fig. 4.10 illustrates the variation of $g^{(2)}(0)$ as a function of the cavity-light detuning Δ/κ and the OPA pump phase θ with an optimized coupling strength $G/\kappa = 4.85 \times 10^{-5}$. A red-blue detuning asymmetric feature for $g^{(2)}(0)$ is observed, that is related to the OPA phase θ. For $\Delta \approx \kappa$ in the red detuning regime, $g^{(2)}(0)$ exhibits a strong sub-Poissonian quantum statistics at a phase of $\theta/\pi \approx -0.42$. For this θ value, $g^{(2)}(0)$ does not show any antibunching in the blue detuning regime. Similar features can be observed for the blue

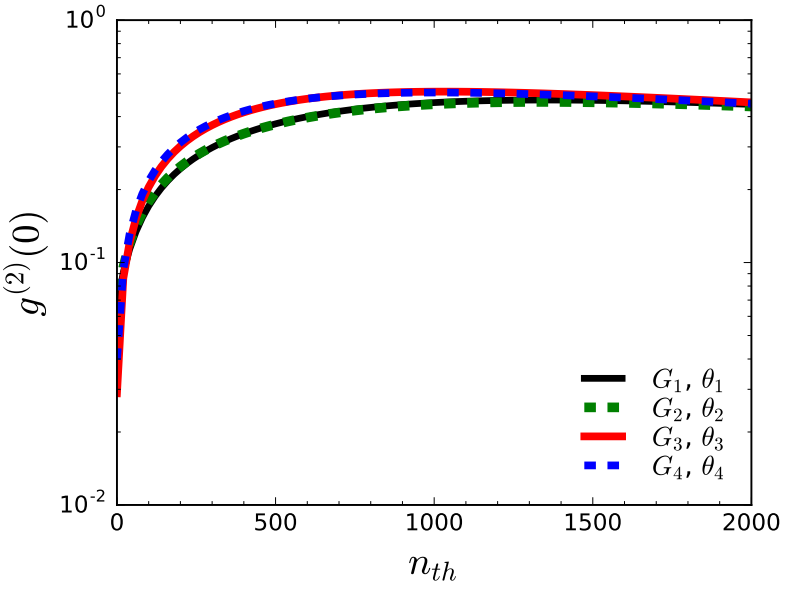

Figure 4.11: Temperature dependence of $g^{(2)}(0)$ corresponding to different optimal parameters: $G_1 = 4.89 \times 10^{-5}\kappa$, $\theta_1 = -0.42\pi$; $G_2 = 4.77 \times 10^{-5}\kappa$, $\theta_2 = 0.42\pi$; $G_3 = 3.30 \times 10^{-5}\kappa$, $\theta_3 = -0.44\pi$; and $G_4 = 3.25 \times 10^{-5}\kappa$, $\theta_4 = 0.44\pi$.

detuning case with $\Delta \approx \kappa$ with phases at $\theta/\pi \approx 0.42$. This proves that the OPA pump phase has an important role in achieving strong photon antibunching.

In Fig. 4.11, we show the temperature dependence of photon blockade. For all the optimal values, $g^{(2)}(0)$ is on the order of 0.1 upto a value of $n_{\text{th}} \approx 20$ showing strong antibunching characteristics.

Now, we analyze the effect of pure-dephasing on the antibunching properties of the cavity photons. The effects of pure dephasing can be modeled by solving the master equation after adding another Lindblad term of the form $L_p(\rho) = \frac{\gamma_p}{2}(2a^\dagger a \rho a^\dagger a - (a^\dagger a)^2\rho - \rho(a^\dagger a)^2)$, in the master equation, where γ_p is the pure dephasing rate for the cavity mode. Figs. 4.12(a)-(d) show the second-order correlation function $g^{(2)}(0)$ for different pure dephasing rates with different sets of optimized values: $G/\kappa = 4.85 \times 10^{-5}$, $\theta/\pi = -0.42$ in (a), $G/\kappa = 4.85 \times 10^{-5}$, $\theta/\pi = 0.42$ in (b), $G/\kappa = 3.28 \times 10^{-5}$, $\theta/\pi = -0.44$ in (c) and $G/\kappa = 3.28 \times 10^{-5}$, $\theta/\pi = 0.44$ in (d). It can be shown that $g^{(2)}(0)$ still maintains the red-blue detuning asymmetry. In Fig. 4.12(a), for a typical pure dephasing rate of 0.01κ, the value of $\log_{10} g^{(2)}(0)$ at the red detuning with $\Delta \approx \kappa$ is -1. With increase in the pure dephasing rate, $g^{(2)}(0)$ increases near the red detuning at $\Delta \approx 2\kappa$. Similar feature is shown in Fig. 4.12(b)-(d) for $\Delta \approx -2\kappa$, 3κ and -3κ respectively. For higher values of

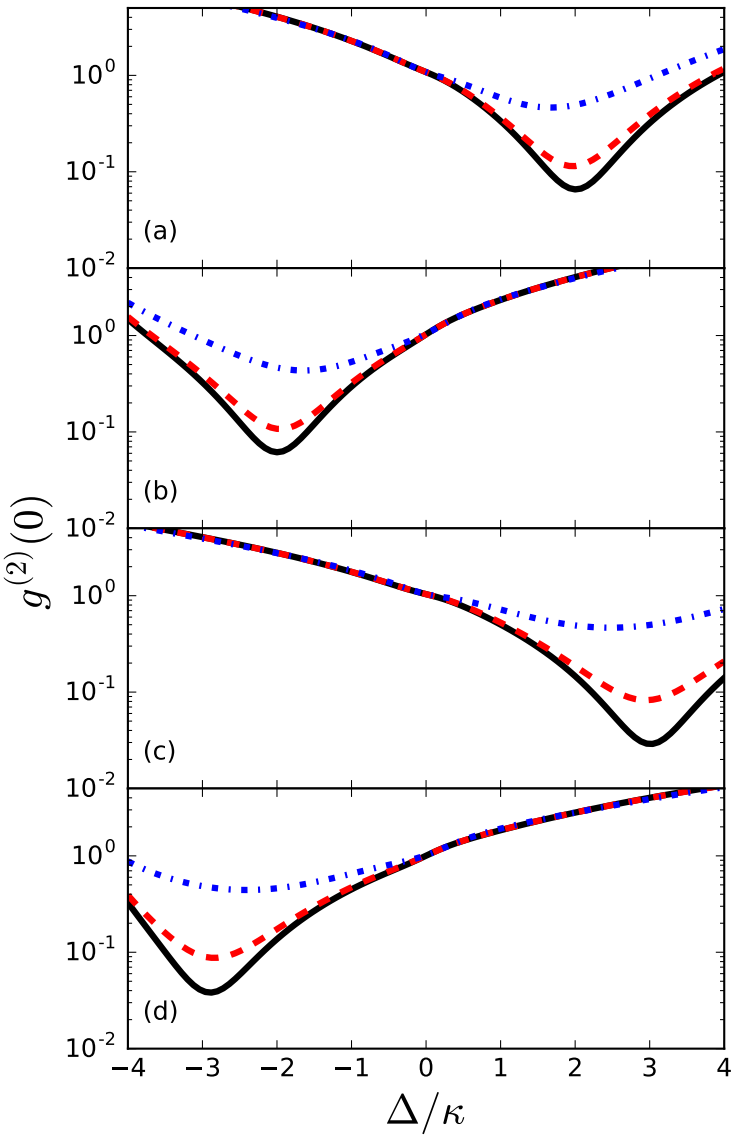

Figure 4.12: Plot of $g^{(2)}(0)$ for different pure-dephasing rates. The black solid line is for $\gamma_p = 0$ case, i.e. without any pure-dephasing. The red and blue dashed lines are for $\gamma_p = 0.01\kappa$ and 0.1κ respectively. OPA parameters are: $G/\kappa = 4.85 \times 10^{-5}$, $\theta/\pi = -0.42$ in (a), $G/\kappa = 4.85 \times 10^{-5}$, $\theta/\pi = 0.42$ in (b), $G/\kappa = 3.28 \times 10^{-5}$, $\theta/\pi = -0.44$ in (c) and $G/\kappa = 3.28 \times 10^{-5}$, $\theta/\pi = 0.44$ in (d).

pure-dephasing rates, $g^{(2)}(0)$ approaches the classical Poissonian statistics similar to a thermal source.

4.3.3 Summary

In conclusion, we have proposed a model to realize a strong unconventional photon blockade by placing an OPA medium inside an optomechanical cavity under weak pump driving with $G \ll \omega_a$. We studied the photon correlations in terms of the second-order correlation function. Using analytical calculations, we derive the conditions for optimized photon antibunching in terms of OPA pump phase θ and the OPA gain G. We find that the optimal parameters depend on the cavity-light detuning. Under the optimal parameters, the system can be used to generate sub-Poissonian light. A red-blue detuning asymmetry for pump phase θ has been observed. We find that the analytical expressions are consistent with the numerical solutions. We hope that the proposed scheme may provide us with a way to control the photon blockade exactly and it could be used as a single-photon source on-demand.

CHAPTER 5

PHONON BLOCKADE

In this chapter, we show that phonon blockade could be achieved in a system of two weakly nonlinear mechanical resonators coupled by a Coulomb interaction. The optimal blockade arises as a result of the destructive quantum interference between paths leading to two-phonon excitation. It is observed that, in comparison to a single drive applied on one mechanical resonator, driving both the resonators could be beneficial in many aspects; such as, in terms of the temperature sensitivity of phonon blockade and also with regard to the tunability, by controlling the amplitude and the phase of the second drive externally. We also show that via a radiation pressure induced coupling in an optomechanical cavity, phonon correlations can be measured indirectly in terms of photon correlations of the cavity mode.

5.1 Brief overview

Reaching the quantum regime of micro- and nanomechanical resonators has significance in weak force detection [216, 217] as well as quantum information processing [86, 218, 219]. Quantum effects can be realized when the mechanical resonator is cooled to its motional ground state, i.e. when its vibrational energy is higher than or comparable to the thermal noise. Once the quantum regime of a mechanical resonator is reached, it can

This chapter is based on the article "*Tunable phonon blockade in weakly nonlinear coupled mechanical resonators via Coulomb interaction*"; arXiv:1803.10403, authors: Bijita Sarma and Amarendra K. Sarma.

be further used for quantum information processing related applications. Phonons, which are the quanta of mechanical vibrations, have lower decay rate in comparison to photons. Due to this advantage, phonons have been studied for possible applications in phononic quantum networks [85–87]. In analogy to Coulomb blockade [220] and photon blockade [175], it was proposed by Liu *et al.* that the phonons in a nanomechanical resonator coupled to superconducting charge qubit can exhibit a nonclassical phenomenon called phonon blockade [92]. In such a system, if the nonlinearity is strong enough to give rise to an anharmonic energy level, the excitation of one resonating phonon makes the second phonon off-resonant, so that the number of phonons in the resonator never exceeds one. Phonon blockade based on this mechanism has been studied in a nanomechanical resonator coupled to a qubit [94, 221] or a two-level defect [222], and also in quadratically coupled optomechanical systems [95, 223], which requires a strong anharmonicity of the eigenstates corresponding to large coupling strength. Another method has been proposed to obtain phonon blockade in the weak coupling regime via interference of phonon transition pathways [98, 99, 224], which is analogous to the unconventional photon blockade effect explored in several systems [80–82, 225].

Conventional phonon blockade has been studied in a mechanical resonator with a Kerr-type nonlinearity. [93] The realization of phonon blockade in this system demands strong Kerr-type nonlinearity in order to obtain an anharmonic energy-level. Different from this, here we show that phonon blockade in a weakly nonlinear mechanical resonator can be realized by coupling it to another weakly nonlinear mechanical resonator via Coulomb interaction [226–228]. Although the nonlinearities in the mechanical resonators are weak, owing to the presence of quantum interference pathways, the system can exhibit phonon blockade. We first discuss the effect of driving only one of the resonators and then driving both the resonators. In case of a single drive, we show that under optimal conditions for the detuning, Δ, and Kerr nonlinearity, U, phonon blockade could be achieved. However, by driving both the resonators, one can tune the blockade characteristics by using the optimal values of the drive amplitude and the phase, which can be controlled more conveniently. Also, this modification gives more robustness towards the temperature dependence of the second order correlation function. The detection of phonon blockade by measuring the photon correlations in the presence of an optomechanical interaction is also discussed.

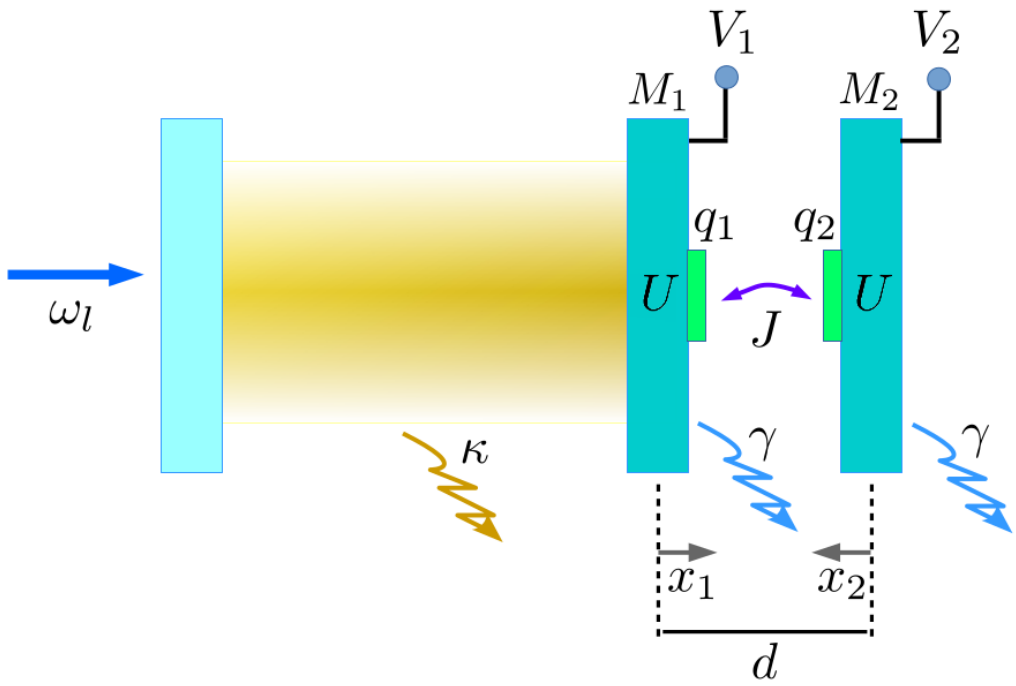

Figure 5.1: Schematic representation of the optomechanical system, where, M_1 is the weakly nonlinear movable end-mirror coupled to another weakly nonlinear mechanical resonator M_2 by Coulomb interaction. The electrodes on the resonators carrying charge q_1 and q_2 are charged by the bias gate voltages V_1 and V_2. The equilibrium separation of the resonators is d. The small deviations of M_1 and M_2 from their equilibrium positions due to the optomechanical and Coulomb interactions are denoted by x_1 and x_2 respectively. The cavity linewidth is κ and the damping rate of the mechanical resonators is considered to be γ.

5.2 Model and Hamiltonian

We consider an optomechanical cavity where the movable end-mirror denoted by M_1, is weakly nonlinear, and is coupled to another weakly nonlinear mechanical resonator, M_2 via a Coulomb interaction as shown in Fig. 5.1. The cavity mode with annihilation operator, a, and frequency, ω_a, is driven by a coherent drive with frequency, ω_l. The total Hamiltonian of the system is given by

$$H = H_{\rm om} + H_{\rm m}, \tag{5.1}$$

where, $H_{\rm om}$ describes the standard linearized optomechanical interaction [222] as given below, with effective optomechanical coupling, G, and detuning, Δ_a, in a frame rotating

at the drive frequency ω_l

$$H_{\rm om} = \Delta_a a^\dagger a + G(a + a^\dagger)(b_1 + b_1^\dagger). \tag{5.2}$$

The Hamiltonian for the mechanical resonators is given by

$$H_{\rm m} \;=\; H_{\rm free} + H_{\rm nl} + H_{\rm co} + H_{\rm drive}, \tag{5.3}$$

with, $H_{\rm free} = \omega_m(b_1^\dagger b_1 + b_2^\dagger b_2)$, $H_{\rm nl} = U(b_1^\dagger b_1^\dagger b_1 b_1 + b_2^\dagger b_2^\dagger b_2 b_2)$, $H_{\rm co} = \frac{k_e q_1 q_2}{|d + x_1 - x_2|}$, and $H_{\rm drive} = \Omega_1(b_1^\dagger e^{-i\omega_p t} + b_1 e^{i\omega_p t}) + \Omega_2(b_2^\dagger e^{-i\phi} e^{-i\omega_q t} + b_2 e^{i\phi} e^{i\omega_q t})$.
Here, b_1 ($b_1^\dagger$) and b_2 ($b_2^\dagger$) are the annihilation (creation) operators for the two mechanical resonator modes with damping rate γ. Hereafter, we will call the mode 'b_1' as the primary mode and the mode 'b_2' as the secondary mode. Here, $H_{\rm free}$ is the free Hamiltonian of the two mechanical resonators, $H_{\rm nl}$ is the Hamiltonian describing the Kerr nonlinearity, U, in both the mechanical resonators and $H_{\rm co}$ represents the Coulomb interaction Hamiltonian of the two charged mechanical oscillators. The primary and the secondary mechanical modes are driven by pumps with frequencies ω_p and ω_q respectively with the corresponding pump amplitudes Ω_1 and Ω_2 and an initial phase difference ϕ; which is described by the term $H_{\rm drive}$. Hereafter, we will assume that $\omega_q \;=\; \omega_p$.

In the Coulomb interaction Hamiltonian, $H_{\rm co}$, k_e denotes the electrostatic constant, d is the equilibrium separation of the two charged oscillators in absence of any interaction between them, and x_1 and x_2 are the small oscillations of the two mechanical oscillators from their equilibrium positions. Now, assuming that the deviations are small compared to the equilibrium separation, i.e. $\{x_1,\, x_2\} \ll d$, one can expand

$$H_{\rm co} \;=\; \frac{k_e q_1 q_2}{d}\left[1 - \left(\frac{x_1 - x_2}{d}\right) + \left(\frac{x_1 - x_2}{d}\right)^2\right].$$

Here, the first term is a constant term and the second one is a linear term which can be absorbed into the definition of the equilibrium positions. The last term consists of two parts: one part refers to the small frequency shift of the original frequencies and can be neglected by renormalising the mechanical frequencies, and the other part is the coupling term between the oscillators. Therefore, we obtain the Coulomb interaction between the mechanical oscillators as [226–228]

$$H_{\rm co} \;=\; -\frac{2k_e q_1 q_2}{d^3} x_1 x_2.$$

The charge contained in the electrodes are given by $q_1 = C_1 V_1$, and $q_2 = -C_2 V_2$, where C_j is the capacitance of the bias gate on the resonator M_j. Therefore, $H_{\rm co}$ can be obtained as

$H_{\rm co} = J(b_1 + b_1^\dagger)(b_2 + b_2^\dagger)$, where, $J = \frac{k_e C_1 V_1 C_2 V_2}{d^3}\sqrt{\frac{1}{m_1 m_2 \omega_m^2}}$. In the weak-coupling regime, considering only the resonant terms, the Coulomb interaction Hamiltonian reduces to

$$H_{\rm co} \;=\; J(b_1^\dagger b_2 + b_1 b_2^\dagger).$$

In the following, we will study the occurrence of phonon blockade in the primary resonator by analyzing the phonon statistics by means of the zero-time delay second-order correlation function given by, $g_b^{(2)}(0) = \langle b_1^\dagger(t) b_1^\dagger(t) b_1(t) b_1(t)\rangle / \langle b_1^\dagger(t) b_1(t)\rangle^2$.

5.3 Phonon blockade with a single drive

First, we will consider the case when there is no optomechanical interaction. The master equation describing the evolution of the system is given by:

$$\dot{\rho} \;=\; i[\rho, H_m'] + \gamma(n_{\rm th,1}+1)L[b_1]\rho + \gamma n_{\rm th,1} L[b_1^\dagger]\rho + \gamma(n_{\rm th,2}+1)L[b_2]\rho + \gamma n_{\rm th,2} L[b_2^\dagger]\rho, \tag{5.4}$$

where $L[b_i]\rho \;=\; b_i \rho b_i^\dagger - \frac{1}{2} b_i^\dagger b_i \rho - \frac{1}{2}\rho b_i^\dagger b_i$ is the Liouvillian operator for the mode b_i and $n_{\rm th,i} = 1/[\exp(\omega_m/k_B T) - 1]$ denotes the thermal phonon number in that mode at environmental temperature, T. We will consider $n_{\rm th,1} = n_{\rm th,2} = n_{\rm th}$ for the rest of the chapter. The Hamiltonian describing the mechanical resonators in a rotating frame with the mechanical drive frequency is given by

$$\begin{aligned} H_m' \;=\; & \Delta b_1^\dagger b_1 + \Delta b_2^\dagger b_2 + U b_1^\dagger b_1^\dagger b_1 b_1 + U b_2^\dagger b_2^\dagger b_2 b_2 + J(b_1^\dagger b_2 + b_1 b_2^\dagger) + \Omega_1(b_1^\dagger + b_1) \\ & + \Omega_2(b_2^\dagger e^{-i\phi} + b_2 e^{i\phi}), \end{aligned} \tag{5.5}$$

where, $\Delta = \omega_m - \omega_p$ is the detuning from the mechanical pump frequency. We will calculate $g_b^{(2)}(0)$ numerically by solving Eq. (5.4) in the weak-driving limit i.e. for $\{\Omega_1, \Omega_2\} \ll \gamma$, from $g_b^{(2)}(0) = {\rm Tr}(b_1^\dagger b_1^\dagger b_1 b_1 \rho_{\rm ss})/[{\rm Tr}(b_1^\dagger b_1 \rho_{\rm ss})]^2$, where $\rho_{\rm ss}$ is the steady-state density matrix [212–214]. Before solving the master equation numerically, in order to obtain the optimal parameters for unconventional phonon blockade, we develop an analytical model in the following. Firstly, we consider the case when the secondary mechanical resonator is not driven, i.e. $\Omega_2 = 0$. At low temperature, and assuming a weak pumping condition, the low-energy levels dictated by the Hamiltonian is shown in Fig. 5.2(a). Assuming that the system is initially prepared in the $|00\rangle$ state, we consider the following ansatz for the state of the system:

$$|\psi\rangle = C_{00}|00\rangle + C_{10}|10\rangle + C_{01}|01\rangle + C_{20}|20\rangle + C_{11}|11\rangle + C_{02}|02\rangle. \tag{5.6}$$

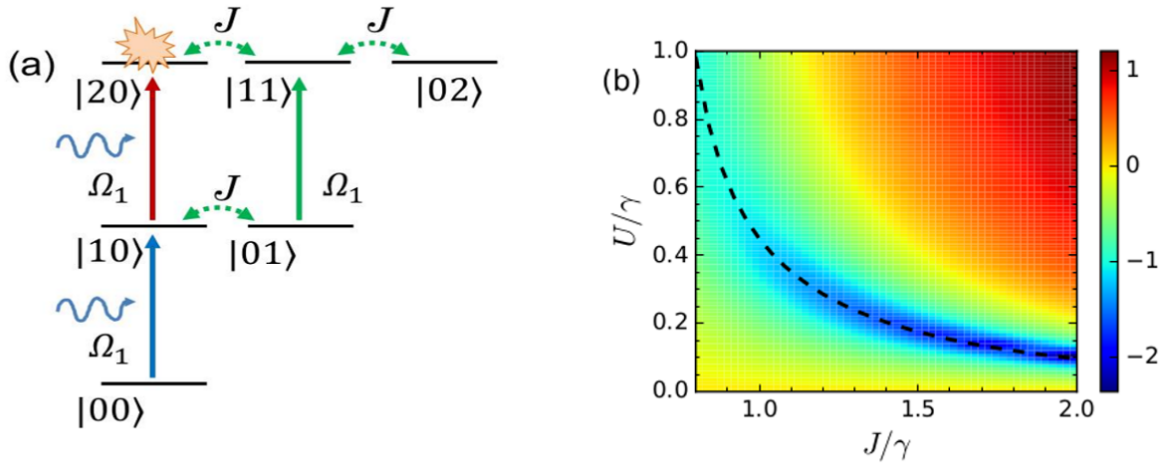

Figure 5.2: (a) Different two-phonon excitation paths that can lead to interference-based phonon blockade for a single pump applied on the primary resonator, and (b) logarithmic plot of $g_b^{(2)}(0)$ as functions of normalized U and J with optimum values of Δ. The black dashed line represents the optimum values of U/γ corresponding to the values of J/γ.

The coefficients C_{ij}'s can be obtained by solving the Schrödinger equation, $i\frac{d|\psi\rangle}{dt} = H_{\rm eff}|\psi\rangle$, where, $H_{\rm eff} = H'_m - i\frac{\gamma}{2}b_1^\dagger b_1 - i\frac{\gamma}{2}b_2^\dagger b_2$ is the non-Hermitian Hamiltonian that includes the damping of the mechanical oscillators. Following an iterative method prescribed by Bamba *et al.* in connection with photon blockade in coupled photonic molecules [81], in the limit of weak Ω_1, at steady-state, the optimal parameters are obtained as follows:

$$\Delta_{\rm opt} = \pm\frac{1}{2}\sqrt{\sqrt{9J^4+8\gamma^2J^2}-\gamma^2-3J^2}\,, \qquad U_{\rm opt} = \frac{\Delta_{\rm opt}(5\gamma^2+4\Delta_{\rm opt}^2)}{2(2J^2-\gamma^2)}. \tag{5.7}$$

The limit for the coupling, J, in this case is that the value of J must be larger than $\gamma/\sqrt{2}$. In Fig. 5.2(b), we show the variation of the zero time-delay second-order correlation function, $g_b^{(2)}(0)$, by solving the master equation, i.e. Eq. (5.4), in a truncated Fock space. Here, $g_b^{(2)}(0)$ is plotted as functions of the normalized coupling strength, J/γ and nonlinearity, U/γ for $U \le \gamma$, with optimal values of Δ as derived in Eq. (5.7). The black dashed curve shows the optimal values of U calculated in Eq. (5.7). It is observed that for the optimal conditions, phonon blockade can be obtained in the weakly nonlinear regime.

To demonstrate these results more clearly, in Fig. 5.3(a), $g_b^{(2)}(0)$ is depicted as a function of Δ/γ for different values of J/γ. The value of U is considered to be $U_{\rm opt}$. For $J/\gamma = 0.8$, 0.95, and 1.5, the optimal values of Δ/γ found from the analytical calculations are ≈ 0.11, 0.16, and 0.24 respectively. The corresponding optimal values of U/γ are 0.98, 0.52, and 0.18 respectively. From the plots, it is evident that the numerically calculated

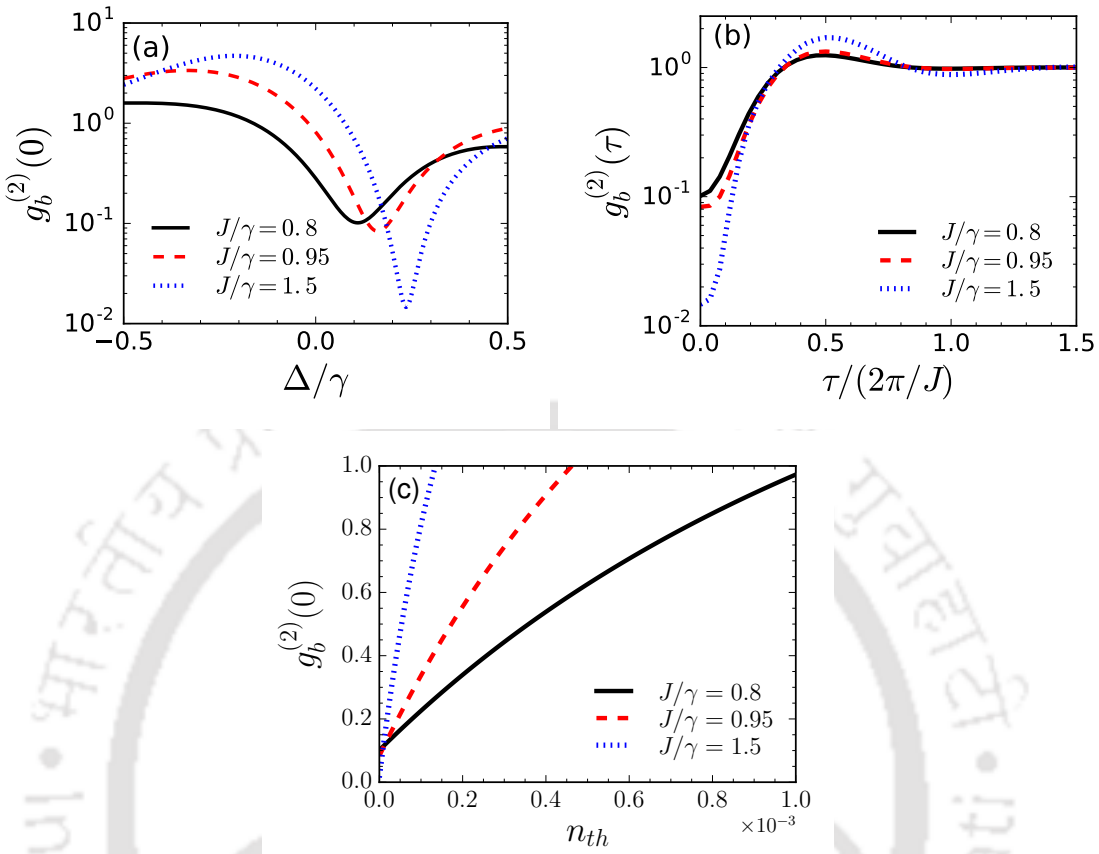

Figure 5.3: (a) Plot showing the variation of $g_b^{(2)}(0)$ as a function of Δ/γ with $U = U_{\text{opt}}$ for different values of J. (b) Second-order correlation function with finite time-delay, $g_b^{(2)}(\tau)$ and (c) temperature dependence of $g_b^{(2)}(0)$. Other parameters are: $\Omega_1 = 0.1\gamma$, $U = U_{\text{opt}}$ and $\Delta = \Delta_{\text{opt}}$.

results show complete agreement with the optimal values of the parameters calculated from the approximate analytical model. With weak coupling strengths of $J/\gamma = 0.8$ and 0.95, $g_b^{(2)}(0) \approx 0.1$,while for a moderate value of $J/\gamma = 1.5$, $g_b^{(2)}(0)$ is on the order of 0.01. We also demonstrate the second-order correlation function, $g_b^{(2)}(\tau) = \langle b_1^\dagger(t) b_1^\dagger(t+\tau) b_1(t+\tau) b_1(t)\rangle / \langle b_1^\dagger(t) b_1(t)\rangle^2$, as a function of the normalized time delay $\tau/(2\pi/J)$ in Fig. 5.3(b). Considering optimal parameters, when $J/\gamma = 0.8$ and 0.95, $g_b^{(2)}(0) \approx 0.1$ at $\tau = 0$, and for increasing delay times $g_b^{(2)}(\tau) > g_b^{(2)}(0)$. Similarly, for $J/\gamma = 1.5$, $g_b^{(2)}(0) \approx 0.01$ at $\tau = 0$, and for higher delay times, $g_b^{(2)}(\tau) > g^{(2)}(0)$ and finally reaches the value 1. Therefore, the plots demonstrate that the phonons are antibunched and have sub-Poissonian distribution. Now, in order to see the influence of environmental phonon population on the phonon

blockade characteristics, in Fig. 5.3(c), we show the variation of $g_b^{(2)}(0)$ as a function of the bath phonon number, n_{th}. For $J/\gamma = 0.8$, $g_b^{(2)}(0)$ reaches 1 at $n_{\text{th}} \approx 0.001$, whereas, for $J/\gamma = 0.95$ and 1.5, $g_b^{(2)}(0) \leq 1$ upto $n_{\text{th}} = 4.5 \times 10^{-4}$ and $n_{\text{th}} = 1.5 \times 10^{-4}$ respectively. Therefore, it is evident that the environmental thermal population has undesirable effect on the observation of phonon blockade.

5.4 Phonon blockade with two drives

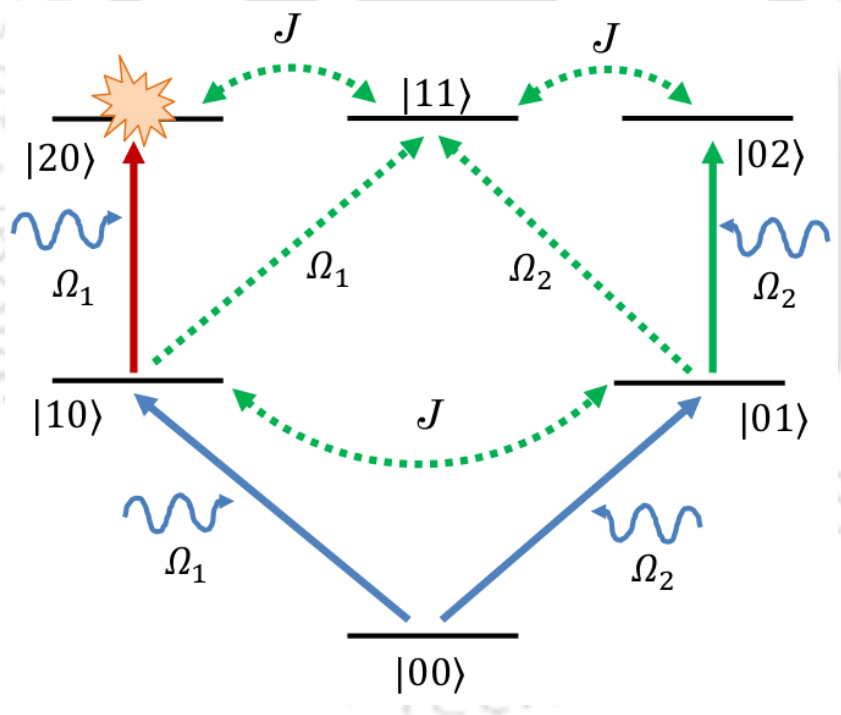

Figure 5.4: Different paths for two-phonon excitation when an additional pump is applied on the secondary mechanical resonator.

We now turn to study the phonon correlations by applying an additional drive, Ω_2 on the secondary mechanical resonator. The transition paths leading to two-phonon excitation, are shown in Fig. 5.4. The optimal conditions for phonon blockade could be determined

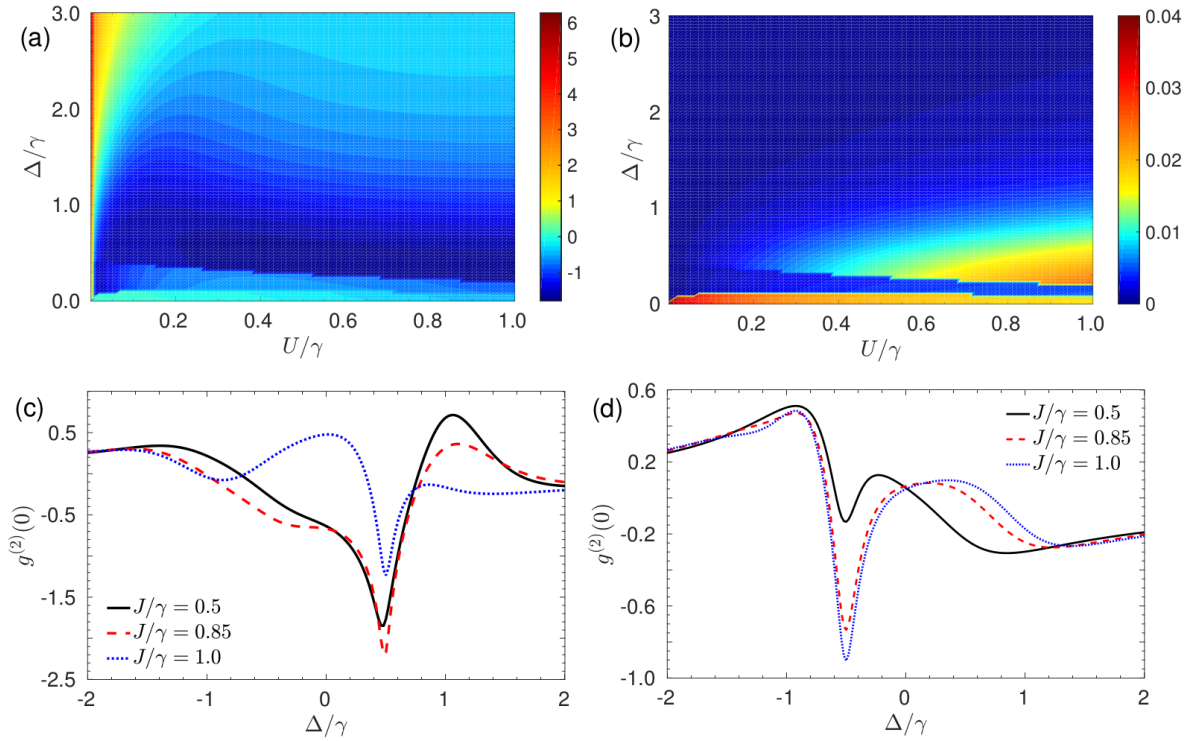

Figure 5.5: (a) Contour plot showing the variation of zero-time-delay second-order correlation function $g_b^{(2)}(0)$ as function of normalized detuning Δ_a/κ and U/κ and (b) phonon number in the primary resonator for ζ_+, ϕ_+. (c) Variation of $g_b^{(2)}(0)$ for different values of J with $U = 0.5\gamma$ and $\Delta = 0.5\gamma$. The black solid, red dashed and blue dotted lines correspond to $J = 0.5\gamma$, 0.85γ and γ, and the corresponding values of $\{\zeta_+, \phi_+/\pi\}$ are $\{2.59, 0.20\}$, $\{1.60, 0.23\}$ and $\{0.39, 0.06\}$ respectively. (d) shows the variation of $g_b^{(2)}(0)$ for $U_{\text{opt}} = 0.5\gamma$ and $\Delta_{\text{opt}} = -0.5\gamma$ for $J = 0.5\gamma$ (black solid line), 0.85γ (red dashed line) and γ (blue dotted line). The respective values of $\{\zeta_+, \phi_+/\pi\}$ are $\{1.09, 0.88\}$, $\{0.82, 0.93\}$ and $\{0.77, 0.95\}$.

by solving the equations for the coefficients obtained from Schrödinger equation:

$$i\dot{C}_{10} = \left(\Delta - i\frac{\gamma}{2}\right) C_{10} + JC_{01} + \Omega_1(C_{00} + \sqrt{2}C_{20}) + \Omega_2 e^{i\phi} C_{11}, \tag{5.8}$$

$$i\dot{C}_{01} = \left(\Delta - i\frac{\gamma}{2}\right) C_{01} + JC_{10} + \Omega_1 C_{11} + \Omega_2(e^{-i\phi} C_{00} + \sqrt{2}e^{i\phi} C_{02}), \tag{5.9}$$

$$i\dot{C}_{20} = 2\left(\Delta + U - i\frac{\gamma}{2}\right) C_{20} + \sqrt{2}JC_{11} + \sqrt{2}\Omega_1 C_{10}, \tag{5.10}$$

$$i\dot{C}_{11} = 2\left(\Delta - i\frac{\gamma}{2}\right) C_{11} + \sqrt{2}J(C_{20} + C_{02}) + \Omega_1 C_{01} + \Omega_2 e^{-i\phi} C_{10}, \tag{5.11}$$

$$i\dot{C}_{02} = 2\left(\Delta + U - i\frac{\gamma}{2}\right) C_{02} + \sqrt{2}JC_{11} + \sqrt{2}\Omega_2 e^{-i\phi} C_{01}. \tag{5.12}$$

In the limit of weak Ω_1 and Ω_2, the probability of phonon excitation to higher levels becomes subsequently lower i.e. $C_{00} \gg \{C_{10}, C_{01}\} \gg \{C_{20}, C_{11}, C_{02}\}$. The optimal condition

for the complete phonon blockade in the primary resonator corresponds to the case when the probability of a phonon in state $|20\rangle$ equals zero. Under these assumptions, solving Eqs. (5.8) and (5.9), the values of C_{10} and C_{01} at the steady-state are obtained as

$$C_{10} = \frac{J\Omega_2 e^{-i\phi} - \Omega_1(\Delta - i\frac{\gamma}{2})}{(\Delta - i\frac{\gamma}{2})^2 - J^2} C_{00}, \tag{5.13}$$

$$C_{01} = \frac{J\Omega_1 - \Omega_2 e^{-i\phi}(\Delta - i\frac{\gamma}{2})}{(\Delta - i\frac{\gamma}{2})^2 - J^2} C_{00}. \tag{5.14}$$

Now, sustituting Eqs. (5.13) and (5.14) into Eqs. (5.10)-(5.12), we obtain the following matrix equation

$$\begin{pmatrix} x_{11} & x_{12} & x_{13} \\ x_{21} & x_{22} & x_{23} \\ x_{31} & x_{32} & x_{33} \end{pmatrix} \begin{pmatrix} C_{11} \\ C_{00} \\ C_{02} \end{pmatrix} = 0, \tag{5.15}$$

where, the matrix elements are given by

$$\begin{aligned} x_{11} &= J, \quad x_{12} = \frac{J\Omega_1\Omega_2 e^{-i\phi} - \Omega_1^2(\Delta - i\frac{\gamma}{2})}{(\Delta - i\frac{\gamma}{2})^2 - J^2}, \quad x_{13} = 0, \\ x_{21} &= 2(\Delta - i\frac{\gamma}{2}), \quad x_{22} = \frac{J\left(\Omega_1^2 + \Omega_2^2 e^{-i\phi}\right) - 2\Omega_1\Omega_2 e^{-i\phi}(\Delta - i\frac{\gamma}{2})}{(\Delta - i\frac{\gamma}{2})^2 - J^2}, \quad x_{23} = \sqrt{2}J, \\ x_{31} &= J, \quad x_{32} = \frac{J\Omega_1\Omega_2 e^{-i\phi} - \Omega_2^2 e^{-2i\phi}(\Delta - i\frac{\gamma}{2})}{(\Delta - i\frac{\gamma}{2})^2 - J^2}, \quad x_{33} = \sqrt{2}\left(\Delta + U - i\frac{\gamma}{2}\right). \end{aligned} \tag{5.16}$$

To obtain nontrivial solutions for C_{11}, C_{00} and C_{02}, the determinant of the coefficient matrix must be zero, which gives rise to a quadratic equation in $\zeta e^{-i\phi}$:

$$a_2\zeta^2 e^{-2i\phi} + a_1\zeta e^{-i\phi} + a_0 = 0, \tag{5.17}$$

with $\zeta = \Omega_2/\Omega_1$, $a_2 = 2J^2(\Delta' + U/2)$, $a_1 = -4J\Delta'(\Delta' + U)$, $a_0 = 2\Delta'^3 + U(J^2 + 2\Delta'^2)$ and $\Delta' = \Delta - i\frac{\gamma}{2}$. The solutions of the quadratic equation are given by:

$$\zeta_\pm e^{-i\phi_\pm} = \frac{1}{J^2(U + 2\Delta')}\left[2J\Delta'(U + \Delta') \pm \sqrt{J^2U(2U\Delta'^2 + 2\Delta'^3 - J^2U - 2J^2\Delta')}\right]. \tag{5.18}$$

From Eq. (5.18), it can be seen that for specific values of the parameters, U, J and Δ, the optimal values of ζ and ϕ could be obtained, and there are two optimal values of ζ and ϕ for a specific set of system parameters. Therefore, by applying the additional pump we can choose the optimal values of the amplitude and the phase of the second drive for different coupling strengths and detuning in the system.

Fig. 5.5(a) depicts $g_b^{(2)}(0)$ as functions of the rescaled detuning Δ/γ and U/γ corresponding to ζ_+, ϕ_+ for a weak coupling value of $J = 0.5\gamma$. In Fig. 5.5(b), we show the corresponding average phonon number in the primary resonator. From these plots, it is observed that for the parameter regime where $g_b^{(2)}(0)$ is found to be on the order of 0.01, average phonon number on the order of 0.01 could be obtained. We show the variation of $g_b^{(2)}(0)$ as a function of Δ/γ, for different values of J in Fig. 5.5(c), with $U_{\rm opt}/\gamma = 0.5$ and $\Delta_{\rm opt}/\gamma = 0.5$, and $J/\gamma = 0.5$, 0.85 and 1. It is observed that phonon blockade could be obtained at $\Delta = 0.5\gamma$, which is in agreement with $\Delta_{\rm opt}$, as predicted by the analytical calculations. Fig. 5.5(d) shows the variation of $g_b^{(2)}(0)$, with $U_{\rm opt} = 0.5\gamma$, and $\Delta_{\rm opt} = -0.5\gamma$, and it is observed that phonon blockade could be obtained at $\Delta = -0.5\gamma$.

Similarly, in Figs. 5.6(a) and (b), we show $g_b^{(2)}(0)$ and the average phonon number in the primary resonator, as functions of the rescaled detuning, Δ/γ and nonlinearity, U/γ corresponding to ζ_-, ϕ_- for $J = 0.5\gamma$. Here also, $g_b^{(2)}(0)$ on the order of 0.01 is obtained with average phonon number ≈ 0.01. In Fig. 5.6(c), we discuss the variation of $g_b^{(2)}(0)$ with respect to Δ/γ for $U_{\rm opt} = 0.5\gamma$ and $\Delta_{\rm opt} = 0.15\gamma$ and different values of $J/\gamma = 0.5$, 0.85 and 1. It is observed that phonon blockade can be obtained at $\Delta_{\rm opt} = 0.15\gamma$. Fig. 5.6(d) shows the variation of $g_b^{(2)}(0)$ for $U_{\rm opt} = 0.5\gamma$ and $\Delta_{\rm opt} = -0.15\gamma$. In this case, phonon blockade is obtained at $\Delta = -0.15\gamma$.

Next, we discuss the variation of the second-order correlation function with finite time-delay, $g_b^{(2)}(\tau)$. In Figs. 5.7(a) and (c), we show $g_b^{(2)}(\tau)$ as a function of the normalized time delay $\tau/(2\pi/J)$ with different values of J for ζ_+, ϕ_+ and ζ_-, ϕ_- respectively. It shows that the value of $g_b^{(2)}(0)$ is the lowest at $\tau = 0$ and for increasing delay times $g_b^{(2)}(\tau) > g_b^{(2)}(0)$, which demonstrates that the phonons are antibunched and sub-Poissonian in nature. In Figs. 5.7(b) and (d), we discuss the effect of environmental phonon number on $g_b^{(2)}(0)$ for different values of U/γ, with (ζ_+, ϕ_+, $\Delta_{\rm opt}/\gamma = 0.5$, $J/\gamma = 0.5$) and (ζ_-, ϕ_-, $\Delta_{\rm opt}/\gamma = 0.15$, $J/\gamma = 0.5$) respectively. As observed in Fig. 5.7(b), for optimum values of ζ_+, ϕ_+, the phonon blockade effect can be sustained upto $n_{\rm th} \approx 0.01$ for $U = 0.9\gamma$ whereas for $U = 0.1\gamma$ and 0.5γ, $g_b^{(2)}(0) \leq 1$ for values of $n_{\rm th}$ upto ≈ 0.001 and 0.006 respectively. On the other hand, for optimum values of ζ_-, ϕ_-, as shown in Fig. 5.7(d), the phonon blockade effect can be sustained upto $n_{\rm th} \approx 0.02$ for $U = 0.9\gamma$. For $U = 0.1\gamma$ and 0.5γ, $g_b^{(2)}(0) \leq 1$ for $n_{\rm th}$ upto ≈ 0.001 and 0.01 respectively.

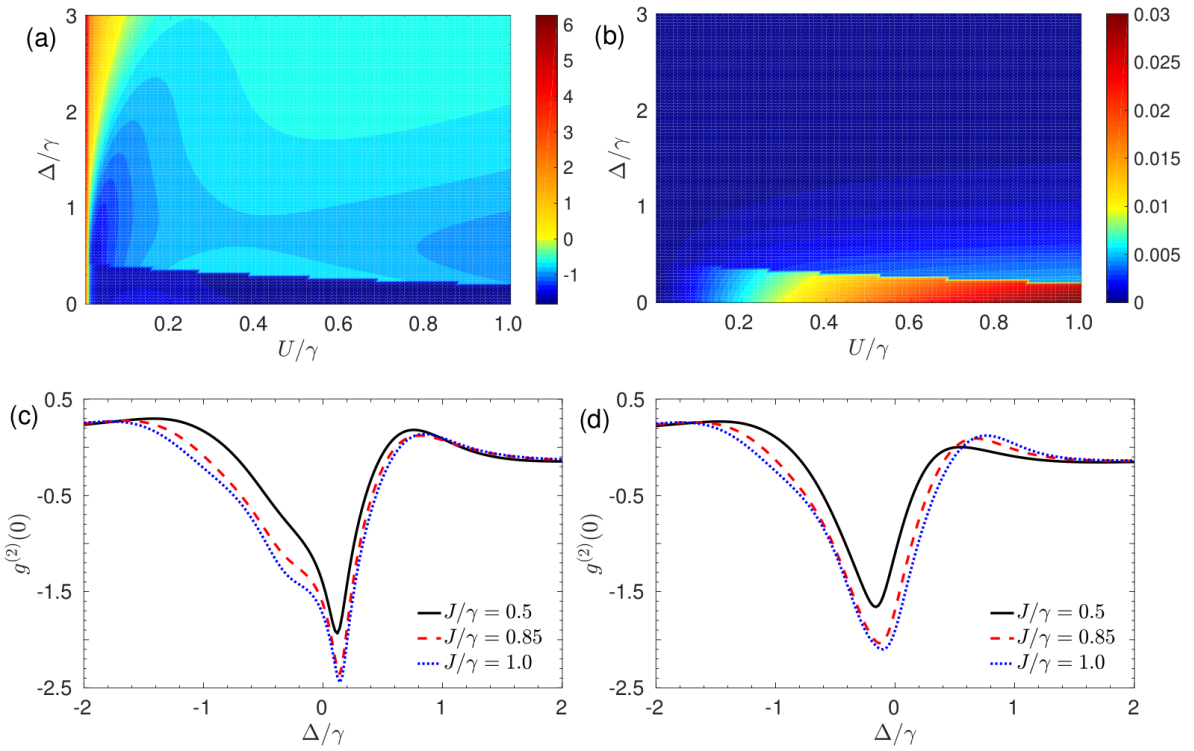

Figure 5.6: (a) Contour plot showing the variation of zero-time-delay second-order correlation function $g_b^{(2)}(0)$ as function of normalized detuning Δ_a/κ and U/κ and (b) phonon number in the primary resonator for ζ_-, ϕ_-. (c) Variation of $g_b^{(2)}(0)$ for different values of J with $U = 0.5\gamma$ and $\Delta = 0.15\gamma$. The black solid, red dashed and blue dotted lines correspond to $J = 0.5\gamma$, 0.85γ and γ, and the corresponding values of $\{\zeta_-, \phi_-/\pi\}$ are $\{2.25, 0.30\}$, $\{1.51, 0.32\}$ and $\{1.37, 0.33\}$ respectively. (d) shows the variation of $g_b^{(2)}(0)$ for $U_{\text{opt}} = 0.5\gamma$ and $\Delta_{\text{opt}} = -0.15\gamma$ for $J = 0.5\gamma$ (black solid line), 0.85γ (red dashed line) and γ (blue dotted line). The corresponding values of $\{\zeta_-, \phi_-/\pi\}$ are $\{2.23, 0.38\}$, $\{1.52, 0.37\}$ and $\{1.37, 0.36\}$ respectively.

5.5 Measurement of phonon blockade via photon correlations

Now, we study the phonon statistics in presence of the optomechanical interaction. Here, we will show that phonon blockade in the primary mechanical resonator can be detected by studying photon statistics of the optical mode in the cavity. Considering the cavity to be at the red sideband, the Langevin equation for the cavity mode fluctuation is given by

$$\dot{a} = -(i\omega_m + \frac{\kappa}{2}) - iGb_1 + \sqrt{\kappa}a_{\text{in}}. \tag{5.19}$$

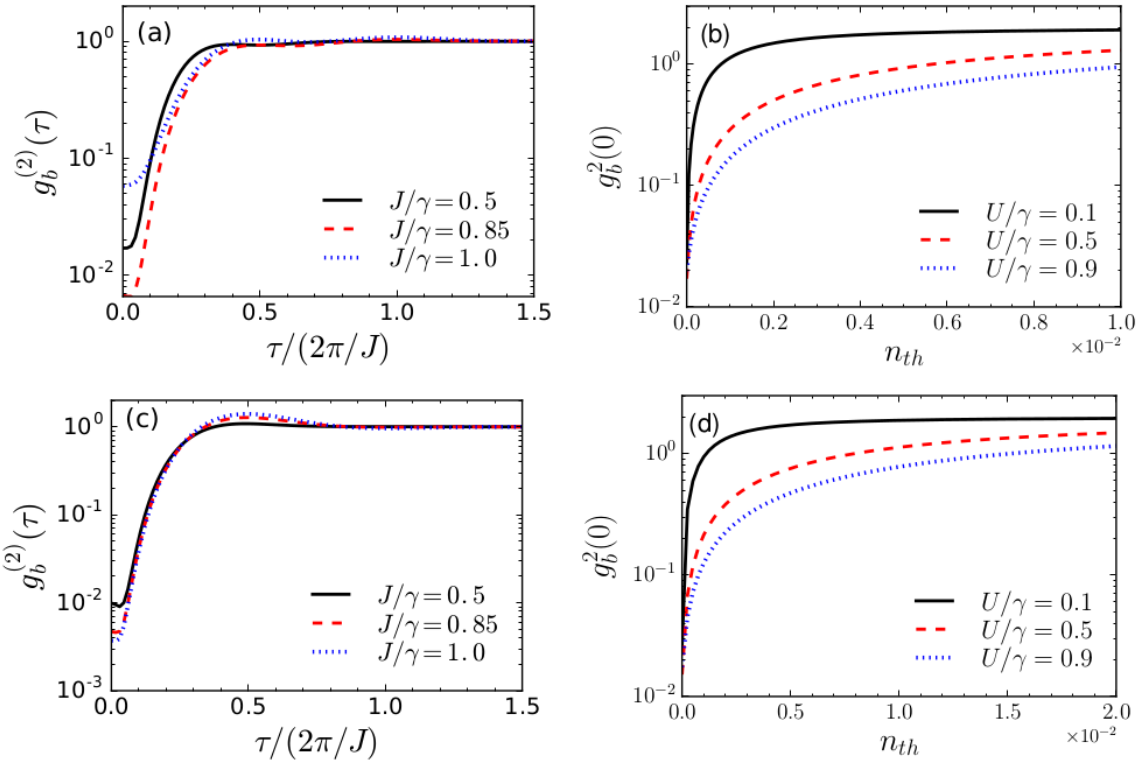

Figure 5.7: (a) Second-order correlation function with finite time-delay $g_b^{(2)}(\tau)$, and (b) effect of environmental temperature on $g_b^{(2)}(0)$ for ζ_+, ϕ_+. (c) Second-order correlation function with finite time-delay $g_b^{(2)}(\tau)$, and (d) effect of environmental temperature on $g_b^{(2)}(0)$ for ζ_-, ϕ_-. Other parameters are considered to be same as in Figs. 5.6(c) and (d).

Here, a_{in} is the input vacuum noise with the correlation function, $\langle a^\dagger{}_{\rm in}(t)a_{\rm in}(t')\rangle = 0$. In the resolved sideband regime, i.e. $\kappa \ll \omega_m$, and also for $\kappa \gg \{G, J, \gamma(n_{\rm th}+1)\}$, the cavity field follows the mechanical mode adiabatically [98, 222, 229]

$$a = -i\frac{2G}{\kappa}b_1 + \text{noise}, \tag{5.20}$$

Therefore, $g_b^{(2)}(0) \approx g_a^{(2)}(0) = \langle a^\dagger a^\dagger a a\rangle / \langle a^\dagger a\rangle^2$, so that the phonon correlation can be studied by evaluating the second-order correlation function for photons. We calculate $g_b^{(2)}(0)$ and also the zero time-delay second-order correlation function for photon, $g_a^{(2)}(0)$, by solving the following master equation:

$$\begin{aligned}\dot{\rho}_{tot} &= i[\rho_{tot}, H'] + \kappa L[a]\rho_{tot} + \gamma(n_{\rm th}+1)L[b_1]\rho_{tot} + \gamma n_{\rm th}L[b_1^\dagger]\rho_{tot} + \gamma(n_{\rm th}+1)L[b_2]\rho_{tot} \\ &\quad + \gamma n_{\rm th}L[b_2^\dagger]\rho_{tot},\end{aligned} \tag{5.21}$$

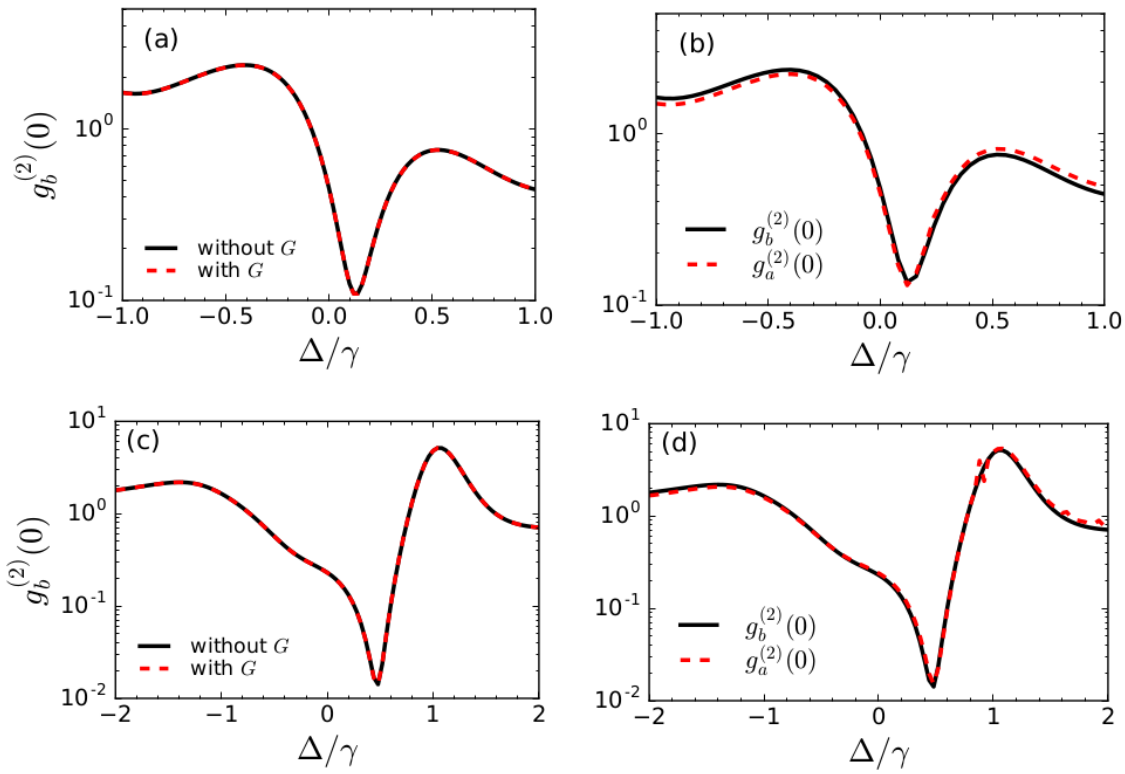

Figure 5.8: (a) The phonon correlations when the drive is applied only on the primary resonator i.e. $\Omega_2 = 0$, showing $g_b^{(2)}(0)$ in absence of the optomechanical coupling (black solid line) and in presence of optomechanical coupling (red dashed line). (b) The phonon and photon correlations calculated for the total Hamiltonian in presence of the optomechanical coupling. (c) $g_b^{(2)}(0)$ in absence of the optomechanical coupling (black solid line) and in presence of optomechanical coupling (red dashed line) for additional driving of the secondary mode. (d) The phonon and photon correlations with two drives in presence of the optomechanical coupling. Other parameters are $\kappa = 10\gamma$, $G = 0.1\kappa$.

where the total Hamiltonian of the system, in a frame rotating at the mechanical pump frequency ω_p is given by

$$H' = \Delta a^\dagger a + \Delta b_1^\dagger b_1 + \Delta b_2^\dagger b_2 + U b_1^\dagger b_1^\dagger b_1 b_1 + U b_2^\dagger b_2^\dagger b_2 b_2 + J(b_1^\dagger b_2 + b_1 b_2^\dagger) + G(a^\dagger b_1 + a b_1^\dagger) + \Omega_1(b_1^\dagger + b_1) + \Omega_2(b_2^\dagger e^{-i\phi} + b_2 e^{i\phi}). \quad (5.22)$$

In Fig. 5.8(a), we discuss the phonon correlations for only one drive applied on the primary resonator. We consider $G = 0.1\kappa$, that lies in the weak coupling regime and $\kappa = 10\gamma$ for typical optomechanical systems. The black solid line shows $g_b^{(2)}(0)$ in absence of the optomechanical coupling and the red dashed line shows the one in presence of the

optomechanical coupling. It is observed that both the values agree well with each other in this parameter regime. Therefore, there is not any modification in the phonon blockade characteristics due to the additional coupling term induced by the optomechanical interaction in the adiabatic regime. In Fig. 5.8(b), we compare the phonon and photon correlations calculated by solving the master equation for the total Hamiltonian in presence of the optomechanical coupling. We observe that both the correlation functions show evidence of blockade at the same detuning value. Therefore, the photon blockade characteristics for the cavity mode can serve as an evidence of phonon blockade in the primary mechanical resonator. Further, in Figs. 5.8(c)-(d), we show $g_b^{(2)}(0)$ for additional driving of the secondary mode i.e for $\Omega_2 \neq 0$, which also show similar features as the single-driving case.

5.6 Summary

In conclusion, we have proposed schemes for the realization of phonon blockade in a weakly nonlinear mechanical end-mirror in an optomechanical cavity, coupled by Coulomb interaction to another weakly nonlinear mechanical resonator. Phonon correlations are characterised in terms of the second-order correlation function. Firstly, we studied the phonon blockade characteristics without considering the optomechanical interaction. By applying a single drive on the primary mechanical resonator, strong phonon blockade could be obtained with optimum values of the mechanical drive detuning and Kerr-nonlinearity. However, the phonon blockade effect is very fragile towards environmental thermal phonon number. Next, we discussed the scenario where both the mechanical resonators were driven simultaneously. In this case, the optimum values could be obtained in terms of the amplitude and the phase of the second mechanical drive, which allows more controllability of phonon blockade. Also, the phonon blockade effect could be sustained upto higher number of thermal phonons. Finally, we discussed the blockade characteristics to be observed when the optomechanical interaction was switched on. It was demonstrated that when the cavity optical field follows the resonator dynamics adiabatically, for both the single and the double mechanical drives, phonon blockade could be detected in terms of the photon correlations of the cavity mode.

CHAPTER 6

CONCLUSION

In this thesis, we have discussed the optomechanical bistability, mechanical resonator cooling, and photon and phonon antibunching effects in cavity optomechanical systems. In chapter 2, we studied the bistable behavior shown by the intracavity optical field and mechanical mirror motion in a hybrid optomechanical system consisting of a driven optomechanical cavity and another cavity containing an ultracold two-level atomic ensemble serving as feedback to the optomechanical cavity. We observe that the bistability of the intracavity field in the optomechanical cavity can be tuned by the power of the driving laser as well as the frequency of the driving laser which controls both the cavity-field detuning in the optomechanical cavity and the atom-field detuning in the atomic cavity. Compared to a generic optomechanical system, this allows more flexibility in the control of bistability. We also observed that due to the feedback from the atomic cavity, bistability can occur for much lower threshold power compared to the single-cavity optomechanical system.

In chapter 3, we discussed the unresolved-sideband cooling of a mechanical resonator in an optomechanical cavity in the presence of a quantum well with lower decay rate. Although the excitons in the quantum well and mechanical mode are not coupled directly, but due to their interaction with the common optical mode, there arises an indirect coupling between them and as a result, the system comes back to the resolved-sideband regime. Due to the presence of the quantum well, the cavity noise spectrum is modified and one can obtain asymmetric cooling and heating rates. Therefore the requirement

of the resolved-sideband condition for cooling is relaxed significantly. We observed that the cooling rate could be enhanced by tuning the cavity-field detuning. We also studied the time evolution of the average phonon number in the mechanical resonator using the quantum master equation approach. It was observed that with time, the average phonon number in the mechanical resonator tend towards the ground-state.

In chapter 4, we studied the photon antibunching effect in a weakly driven three-mode optomechanical system, where two nonlinear optical modes and one mechanical mode interact via a three-mode mixing. In addition to the resonant pathways, new two-photon excitation paths in the higher-frequency optical mode are created due to this coupling. One can harness these two-photon excitation processes to obtain the desired photon blockade characteristics in the system via destructive quantum interference mechanism. We studied the photon statistics in terms of second-order correlation function, and we derived the optimal parameters required for strong photon blockade by solving the non-Hermitian Schrödinger equation describing the damping in the system. Also, we performed numerical calculations by solving the master equation, which show complete agreement with the analytical calculations. In conventional photon blockade mechanism, strong antibunching is obtained only in the strong-coupling regime. Here we observed that even when the Kerr-nonlinearity in the optical modes is weak, under the optimal conditions fulfilling the criteria for quantum interference mechanism, strong photon antibunching is possible in the system. In the next part of the chapter, we explored another system that can give rise to photon blockade in the weak-coupling regime. We considered a weakly driven optomechanical cavity containing a degenerate optical parametric amplifier, which gives rise additional two-photon excitation paths in the cavity mode. Using analytical calculations, we found that optimal antibunching can be obtained in the system by tuning the parametric amplifier pump gain and phase. We observed a red-blue detuning asymmetry in the photon blockade characteristics for the pump phase. The numerical calculations were found to be consistent with the analytical results.

In chapter 5, we explored the occurrence of phonon blockade in a weakly nonlinear mechanical resonator in an optomechanical cavity, coupled to another weakly nonlinear mechanical resonator via Coulomb interaction. We analyzed the situations where in one case, only one of the mechanical resonators is driven, and in the other case, both the mechanical resonators are driven. Phonon blockade characteristics are studied in terms of the second-order correlation function. Firstly, we studied phonon blockade in absence of

the optomechanical interaction. Under a single drive, optimum values of the mechanical drive detuning and Kerr-nonlinearity were determined for strong phonon antibunching. However, the phonon blockade effect was found to be very fragile towards environmental thermal phonon number. In the case of double drive, the optimum values are obtained in terms of the amplitude and the phase of the second mechanical drive, which allows more controllability of phonon blockade. Also, the phonon blockade effect could be sustained upto higher number of thermal phonons in comparison to the earlier case, and we also discussed the blockade characteristics in presence of the optomechanical interaction. We observed that when the cavity field follows the resonator dynamics adiabatically, phonon blockade can be studied in terms of the photon correlations of the cavity mode.

With new theoretical studies and experiments coming up, the area of cavity optomechanics has been proven to be a promising platform where quantum mechanics in mesoscopic scale might be utilized in device-based applications. For example, cavity cooling has possibilities in suppressing thermalization effects in spintronic devices by cooling mechanical modes in semiconductor nanomembranes [15, 155]. One particular interesting aspect of optomechanical systems is its coupling via the mechanical motion to other quantum systems, which are not compatible otherwise [15, 230, 231]. There is possibility of exploring antibunching phenomena in various hybrid quantum systems with particular emphasis on solid-state platform, owing to the tremendous potential in quantum communication related applications. Therefore, combining the developments in the field of cavity optomechanics to the parallel developments in analogous areas like circuit-QED systems, cold atoms etc., one may explore newer possibilities in transduction and quantum information processing as a whole.

BIBLIOGRAPHY

[1] J. Kepler, "Comet," *De cometis libelli tres (Typis Andreae Apergiri)*, 1619.

[2] J. C. Maxwell, *A treatise on electricity and magnetism*, vol. 2. Clarendon press, Oxford, 1873.

[3] A. G. Bartoli, *Sopra i movimenti prodotti dalla luce e dal calore: e sopra il radiometro di Crookes*. Le Monnier, Florence, 1876.

[4] P. Lebedev, "Untersuchungen über die druckkräfte des lichtes," *Ann. Phys. (Berl.)*, vol. 311, no. 11, pp. 433–458, 1901.

[5] E. F. Nichols and G. F. Hull, "A preliminary communication on the pressure of heat and light radiation," *Phys. Rev.*, vol. 13, no. 5, p. 307, 1901.

[6] V. Braginski and A. Manukin, "Ponderomotive effects of electromagnetic radiation," *Sov. Phys. JETP*, vol. 25, no. 4, pp. 653–655, 1967.

[7] C. Fabre, M. Pinard, S. Bourzeix, A. Heidmann, E. Giacobino, and S. Reynaud, "Quantum-noise reduction using a cavity with a movable mirror," *Phys. Rev. A*, vol. 49, no. 2, p. 1337, 1994.

[8] M. Pinard, C. Fabre, and A. Heidmann, "Quantum-nondemolition measurement of light by a piezoelectric crystal," *Phys. Rev. A*, vol. 51, no. 3, p. 2443, 1995.

[9] S. Mancini, D. Vitali, and P. Tombesi, "Optomechanical cooling of a macroscopic oscillator by homodyne feedback," *Phys. Rev. Lett.*, vol. 80, no. 4, p. 688, 1998.

[10] S. Bose, K. Jacobs, and P. Knight, "Preparation of nonclassical states in cavities with a moving mirror," *Phys. Rev. A*, vol. 56, no. 5, p. 4175, 1997.

[11] A. Dorsel, J. D. McCullen, P. Meystre, E. Vignes, and H. Walther, "Optical bistability and mirror confinement induced by radiation pressure," *Phys. Rev. Lett.*, vol. 51, no. 17, p. 1550, 1983.

[12] P.-F. Cohadon, A. Heidmann, and M. Pinard, "Cooling of a mirror by radiation pressure," *Phys. Rev. Lett.*, vol. 83, no. 16, p. 3174, 1999.

[13] T. J. Kippenberg and K. J. Vahala, "Cavity optomechanics: back-action at the

mesoscale," *Science*, vol. 321, no. 5893, pp. 1172–1176, 2008.

[14] A. Ashkin, "Trapping of atoms by resonance radiation pressure," *Phys. Rev. Lett.*, vol. 40, no. 12, p. 729, 1978.

[15] M. Aspelmeyer, T. J. Kippenberg, and F. Marquardt, "Cavity optomechanics," *Rev. Mod. Phys.*, vol. 86, no. 4, p. 1391, 2014.

[16] W. Bowen and G. J. Milburn, *Quantum optomechanics*. CRC Press, 2015.

[17] C. K. Law, "Interaction between a moving mirror and radiation pressure: A Hamiltonian formulation," *Phys. Rev. A*, vol. 51, no. 3, p. 2537, 1995.

[18] O. Arcizet, P.-F. Cohadon, T. Briant, M. Pinard, and A. Heidmann, "Radiation-pressure cooling and optomechanical instability of a micromirror," *Nature*, vol. 444, no. 7115, pp. 71–74, 2006.

[19] D. Kleckner and D. Bouwmeester, "Sub-kelvin optical cooling of a micromechanical resonator," *Nature*, vol. 444, no. 7115, p. 75, 2006.

[20] S. Groeblacher, S. Gigan, H. R. Böhm, A. Zeilinger, and M. Aspelmeyer, "Radiation-pressure self-cooling of a micromirror in a cryogenic environment," *EPL*, vol. 81, no. 5, p. 54003, 2008.

[21] S. Gröblacher, K. Hammerer, M. R. Vanner, and M. Aspelmeyer, "Observation of strong coupling between a micromechanical resonator and an optical cavity field," *Nature*, vol. 460, no. 7256, pp. 724–727, 2009.

[22] T. Corbitt, Y. Chen, E. Innerhofer, H. Müller-Ebhardt, D. Ottaway, H. Rehbein, D. Sigg, S. Whitcomb, C. Wipf, and N. Mavalvala, "An all-optical trap for a gram-scale mirror," *Phys. Rev. Lett.*, vol. 98, no. 15, p. 150802, 2007.

[23] B. Abbott, R. Abbott, R. Adhikari, A. Ageev, B. Allen, R. Amin, S. Anderson, W. Anderson, M. Araya, H. Armandula, *et al.*, "Detector description and performance for the first coincidence observations between ligo and geo," *Nuclear Instruments and Methods in Physics Research Section A: Accelerators, Spectrometers, Detectors and Associated Equipment*, vol. 517, no. 1-3, pp. 154–179, 2004.

[24] A. Jayich, J. Sankey, B. Zwickl, C. Yang, J. Thompson, S. Girvin, A. Clerk, F. Marquardt, and J. Harris, "Dispersive optomechanics: a membrane inside a cavity," *New J. Phys.*, vol. 10, no. 9, p. 095008, 2008.

[25] M. Karuza, M. Galassi, C. Biancofiore, C. Molinelli, R. Natali, P. Tombesi, G. Di Giuseppe, and D. Vitali, "Tunable linear and quadratic optomechanical coupling for a tilted membrane within an optical cavity: theory and experiment," *J. Opt.*, vol. 15, no. 2, p. 025704, 2012.

[26] T. Purdy, P.-L. Yu, R. Peterson, N. Kampel, and C. Regal, "Strong optomechanical squeezing of light," *Phys. Rev. X*, vol. 3, no. 3, p. 031012, 2013.

[27] I. Favero, S. Stapfner, D. Hunger, P. Paulitschke, J. Reichel, H. Lorenz, E. M. Weig, and K. Karrai, "Fluctuating nanomechanical system in a high finesse optical microcavity," *Opt. Express*, vol. 17, no. 15, pp. 12813–12820, 2009.

[28] T. Kippenberg, S. Spillane, D. Armani, and K. Vahala, "Fabrication and coupling to planar high-q silica disk microcavities," *Appl. Phys. Lett.*, vol. 83, no. 4, pp. 797–799, 2003.

[29] E. Verhagen, S. Deléglise, S. Weis, A. Schliesser, and T. J. Kippenberg, "Quantum-coherent coupling of a mechanical oscillator to an optical cavity mode," *Nature*, vol. 482, no. 7383, p. 63, 2012.

[30] L. Ding, C. Baker, P. Senellart, A. Lemaitre, S. Ducci, G. Leo, and I. Favero, "High frequency gaas nano-optomechanical disk resonator," *Phys. Rev. Lett.*, vol. 105, no. 26, p. 263903, 2010.

[31] M. Zhang, G. S. Wiederhecker, S. Manipatruni, A. Barnard, P. McEuen, and M. Lipson, "Synchronization of micromechanical oscillators using light," *Phys. Rev. Lett.*, vol. 109, no. 23, p. 233906, 2012.

[32] X. Sun, K. Y. Fong, C. Xiong, W. H. Pernice, and H. X. Tang, "Ghz optomechanical resonators with high mechanical q factor in air," *Opt. Express*, vol. 19, no. 22, pp. 22316–22321, 2011.

[33] M. Tomes and T. Carmon, "Photonic micro-electromechanical systems vibrating at x-band (11-ghz) rates," *Phys. Rev. Lett.*, vol. 102, no. 11, p. 113601, 2009.

[34] Y.-S. Park and H. Wang, "Resolved-sideband and cryogenic cooling of an optomechanical resonator," *Nat. Phys.*, vol. 5, no. 7, p. 489, 2009.

[35] T. Palomaki, J. Teufel, R. Simmonds, and K. Lehnert, "Entangling mechanical motion with microwave fields," *Science*, p. 1244563, 2013.

[36] J. Teufel, T. Donner, D. Li, J. Harlow, M. Allman, K. Cicak, A. Sirois, J. D. Whittaker, K. Lehnert, and R. W. Simmonds, "Sideband cooling of micromechanical motion to the quantum ground state," *Nature*, vol. 475, no. 7356, p. 359, 2011.

[37] J. Hertzberg, T. Rocheleau, T. Ndukum, M. Savva, A. Clerk, and K. Schwab, "Back-action-evading measurements of nanomechanical motion," *Nat. Phys.*, vol. 6, no. 3, p. 213, 2010.

[38] M. Eichenfield, J. Chan, A. H. Safavi-Naeini, K. J. Vahala, and O. Painter, "Modeling dispersive coupling and losses of localized optical and mechanical modes in

optomechanical crystals," *Opt. Express*, vol. 17, no. 22, pp. 20078–20098, 2009.

[39] J. Chan, T. M. Alegre, A. H. Safavi-Naeini, J. T. Hill, A. Krause, S. Gröblacher, M. Aspelmeyer, and O. Painter, "Laser cooling of a nanomechanical oscillator into its quantum ground state," *Nature*, vol. 478, no. 7367, p. 89, 2011.

[40] N. Kiesel, F. Blaser, U. Delić, D. Grass, R. Kaltenbaek, and M. Aspelmeyer, "Cavity cooling of an optically levitated submicron particle," *Proc. Natl. Acad. Sci. U.S.A.*, vol. 110, no. 35, pp. 14180–14185, 2013.

[41] T. Monteiro, J. Millen, G. Pender, F. Marquardt, D. Chang, and P. Barker, "Dynamics of levitated nanospheres: towards the strong coupling regime," *New J. Phys.*, vol. 15, no. 1, p. 015001, 2013.

[42] K. W. Murch, K. L. Moore, S. Gupta, and D. M. Stamper-Kurn, "Observation of quantum-measurement backaction with an ultracold atomic gas," *Nat. Phys.*, vol. 4, no. 7, p. 561, 2008.

[43] F. Brennecke, S. Ritter, T. Donner, and T. Esslinger, "Cavity optomechanics with a bose-einstein condensate," *Science*, vol. 322, no. 5899, pp. 235–238, 2008.

[44] D. W. Brooks, T. Botter, S. Schreppler, T. P. Purdy, N. Brahms, and D. M. Stamper-Kurn, "Non-classical light generated by quantum-noise-driven cavity optomechanics," *Nature*, vol. 488, no. 7412, p. 476, 2012.

[45] F. Marquardt, J. Harris, and S. M. Girvin, "Dynamical multistability induced by radiation pressure in high-finesse micromechanical optical cavities," *Phys. Rev. Lett.*, vol. 96, no. 10, p. 103901, 2006.

[46] M. Mikkelsen, T. Fogarty, J. Twamley, and T. Busch, "Optomechanics with a position-modulated kerr-type nonlinear coupling," *Phys. Rev. A*, vol. 96, no. 4, p. 043832, 2017.

[47] R. Ghobadi, A. Bahrampour, and C. Simon, "Quantum optomechanics in the bistable regime," *Phys. Rev. A*, vol. 84, no. 3, p. 033846, 2011.

[48] H. Gibbs, S. Tarng, J. Jewell, D. Weinberger, K. Tai, A. Gossard, S. McCall, A. Passner, and W. Wiegmann, "Room-temperature excitonic optical bistability in a GaAs-GaAlAs superlattice étalon," *Appl. Phys. Lett.*, vol. 41, no. 3, pp. 221–222, 1982.

[49] A. Baas, J. P. Karr, H. Eleuch, and E. Giacobino, "Optical bistability in semiconductor microcavities," *Phys. Rev. A*, vol. 69, no. 2, p. 023809, 2004.

[50] A. Gozzini, F. Maccarrone, F. Mango, I. Longo, and S. Barbarino, "Light-pressure bistability at microwave frequencies," *J. Opt. Soc. Am. B*, vol. 2, no. 11, pp. 1841–1845, 1985.

[51] C. Jiang, H. Liu, Y. Cui, X. Li, G. Chen, and X. Shuai, "Controllable optical bistability based on photons and phonons in a two-mode optomechanical system," *Phys. Rev. A*, vol. 88, no. 5, p. 055801, 2013.

[52] T. P. Purdy, D. Brooks, T. Botter, N. Brahms, Z.-Y. Ma, and D. M. Stamper-Kurn, "Tunable cavity optomechanics with ultracold atoms," *Phys. Rev. Lett.*, vol. 105, no. 13, p. 133602, 2010.

[53] E. A. Sete and H. Eleuch, "Controllable nonlinear effects in an optomechanical resonator containing a quantum well," *Phys. Rev. A*, vol. 85, no. 4, p. 043824, 2012.

[54] A. Schliesser, R. Rivière, G. Anetsberger, O. Arcizet, and T. J. Kippenberg, "Resolved-sideband cooling of a micromechanical oscillator," *Nat. Phys.*, vol. 4, no. 5, p. 415, 2008.

[55] D. J. Wineland and W. M. Itano, "Laser cooling of atoms," *Phys. Rev. A*, vol. 20, no. 4, p. 1521, 1979.

[56] F. Marquardt, J. P. Chen, A. Clerk, and S. Girvin, "Quantum theory of cavity-assisted sideband cooling of mechanical motion," *Phys. Rev. Lett.*, vol. 99, no. 9, p. 093902, 2007.

[57] F. Elste, S. Girvin, and A. Clerk, "Quantum noise interference and backaction cooling in cavity nanomechanics," *Phys. Rev. Lett.*, vol. 102, no. 20, p. 207209, 2009.

[58] T. Weiss and A. Nunnenkamp, "Quantum limit of laser cooling in dispersively and dissipatively coupled optomechanical systems," *Phys. Rev. A*, vol. 88, no. 2, p. 023850, 2013.

[59] M.-Y. Yan, H.-K. Li, Y.-C. Liu, W.-L. Jin, and Y.-F. Xiao, "Dissipative optomechanical coupling between a single-wall carbon nanotube and a high-q microcavity," *Phys. Rev. A*, vol. 88, no. 2, p. 023802, 2013.

[60] W.-J. Gu and G.-X. Li, "Quantum interference effects on ground-state optomechanical cooling," *Phys. Rev. A*, vol. 87, no. 2, p. 025804, 2013.

[61] Y. Guo, K. Li, W. Nie, and Y. Li, "Electromagnetically-induced-transparency-like ground-state cooling in a double-cavity optomechanical system," *Phys. Rev. A*, vol. 90, no. 5, p. 053841, 2014.

[62] Y.-C. Liu, Y.-F. Xiao, X. Luan, Q. Gong, and C. W. Wong, "Coupled cavities for motional ground-state cooling and strong optomechanical coupling," *Phys. Rev. A*, vol. 91, no. 3, p. 033818, 2015.

[63] C. Genes, H. Ritsch, and D. Vitali, "Micromechanical oscillator ground-state cooling via resonant intracavity optical gain or absorption," *Phys. Rev. A*, vol. 80, no. 6,

p. 061803, 2009.

[64] C. Genes, H. Ritsch, M. Drewsen, and A. Dantan, "Atom-membrane cooling and entanglement using cavity electromagnetically induced transparency," *Phys. Rev. A*, vol. 84, no. 5, p. 051801, 2011.

[65] B. Vogell, K. Stannigel, P. Zoller, K. Hammerer, M. T. Rakher, M. Korppi, A. Jöckel, and P. Treutlein, "Cavity-enhanced long-distance coupling of an atomic ensemble to a micromechanical membrane," *Phys. Rev. A*, vol. 87, no. 2, p. 023816, 2013.

[66] T. Ojanen and K. Børkje, "Ground-state cooling of mechanical motion in the unresolved sideband regime by use of optomechanically induced transparency," *Phys. Rev. A*, vol. 90, no. 1, p. 013824, 2014.

[67] E. Knill, R. Laflamme, and G. J. Milburn, "A scheme for efficient quantum computation with linear optics," *Nature*, vol. 409, no. 6816, p. 46, 2001.

[68] M. Toishi, D. Englund, A. Faraon, and J. Vučković, "High-brightness single photon source from a quantum dot in a directional-emission nanocavity," *Opt. Express*, vol. 17, no. 17, pp. 14618–14626, 2009.

[69] X. Xu, I. Toft, R. T. Phillips, J. Mar, K. Hammura, and D. A. Williams, ""plug and play" single-photon sources," *Appl. Phys. Lett.*, vol. 90, no. 6, p. 061103, 2007.

[70] J. McKeever, A. Boca, A. Boozer, R. Miller, J. Buck, A. Kuzmich, and H. Kimble, "Deterministic generation of single photons from one atom trapped in a cavity," *Science*, vol. 303, no. 5666, pp. 1992–1994, 2004.

[71] K. M. Birnbaum, A. Boca, R. Miller, A. D. Boozer, T. E. Northup, and H. J. Kimble, "Photon blockade in an optical cavity with one trapped atom," *Nature*, vol. 436, no. 7047, p. 87, 2005.

[72] A. Faraon, I. Fushman, D. Englund, N. Stoltz, P. Petroff, and J. Vučković, "Coherent generation of non-classical light on a chip via photon-induced tunnelling and blockade," *Nat. Phys.*, vol. 4, no. 11, p. 859, 2008.

[73] D. G. Angelakis, M. F. Santos, and S. Bose, "Photon-blockade-induced mott transitions and x y spin models in coupled cavity arrays," *Phys. Rev. A*, vol. 76, no. 3, p. 031805, 2007.

[74] Y.-X. Liu, X.-W. Xu, A. Miranowicz, and F. Nori, "From blockade to transparency: Controllable photon transmission through a circuit-QED system," *Phys. Rev. A*, vol. 89, no. 4, p. 043818, 2014.

[75] P. Rabl, "Photon blockade effect in optomechanical systems," *Phys. Rev. Lett.*, vol. 107, no. 6, p. 063601, 2011.

[76] P. Komar, S. Bennett, K. Stannigel, S. Habraken, P. Rabl, P. Zoller, and M. D. Lukin, "Single-photon nonlinearities in two-mode optomechanics," *Phys. Rev. A*, vol. 87, no. 1, p. 013839, 2013.

[77] J.-Q. Liao, F. Nori, *et al.*, "Photon blockade in quadratically coupled optomechanical systems," *Phys. Rev. A*, vol. 88, no. 2, p. 023853, 2013.

[78] H. Wang, X. Gu, Y.-X. Liu, A. Miranowicz, and F. Nori, "Tunable photon blockade in a hybrid system consisting of an optomechanical device coupled to a two-level system," *Phys. Rev. A*, vol. 92, no. 3, p. 033806, 2015.

[79] M. Fox, *Quantum optics: an introduction*, vol. 15. Oxford University Press, 2006.

[80] T. Liew and V. Savona, "Single photons from coupled quantum modes," *Phys. Rev. Lett.*, vol. 104, no. 18, p. 183601, 2010.

[81] M. Bamba, A. Imamoğlu, I. Carusotto, and C. Ciuti, "Origin of strong photon antibunching in weakly nonlinear photonic molecules," *Phys. Rev. A*, vol. 83, no. 2, p. 021802, 2011.

[82] J. Tang, W. Geng, and X. Xu, "Quantum interference induced photon blockade in a coupled single quantum dot-cavity system," *Sci. Rep.*, vol. 5, p. 9252, 2015.

[83] H. Shen, Y. Zhou, H. Liu, G. Wang, and X. Yi, "Exact optimal control of photon blockade with weakly nonlinear coupled cavities," *Opt. Express*, vol. 23, no. 25, pp. 32835–32858, 2015.

[84] X.-W. Xu and Y.-J. Li, "Antibunching photons in a cavity coupled to an optomechanical system," *J. Phys. B: At. Mol. Opt. Phys.*, vol. 46, no. 3, p. 035502, 2013.

[85] S. Habraken, K. Stannigel, M. D. Lukin, P. Zoller, and P. Rabl, "Continuous mode cooling and phonon routers for phononic quantum networks," *New J. Phys.*, vol. 14, no. 11, p. 115004, 2012.

[86] S. Rips and M. J. Hartmann, "Quantum information processing with nanomechanical qubits," *Phys. Rev. Lett.*, vol. 110, no. 12, p. 120503, 2013.

[87] M. V. Gustafsson, T. Aref, A. F. Kockum, M. K. Ekström, G. Johansson, and P. Delsing, "Propagating phonons coupled to an artificial atom," *Science*, vol. 346, no. 6206, pp. 207–211, 2014.

[88] K. Børkje, "Scheme for steady-state preparation of a harmonic oscillator in the first excited state," *Phys. Rev. A*, vol. 90, no. 2, p. 023806, 2014.

[89] M. R. Vanner, I. Pikovski, G. D. Cole, M. Kim, Č. Brukner, K. Hammerer, G. J. Milburn, and M. Aspelmeyer, "Pulsed quantum optomechanics," *Proc. Natl. Acad. Sci.*, vol. 108, no. 39, pp. 16182–16187, 2011.

[90] R. Riedinger, S. Hong, R. A. Norte, J. A. Slater, J. Shang, A. G. Krause, V. Anant, M. Aspelmeyer, and S. Gröblacher, "Non-classical correlations between single photons and phonons from a mechanical oscillator," *Nature*, vol. 530, no. 7590, p. 313, 2016.

[91] C. Galland, N. Sangouard, N. Piro, N. Gisin, and T. J. Kippenberg, "Heralded single-phonon preparation, storage, and readout in cavity optomechanics," *Phys. Rev. Lett.*, vol. 112, no. 14, p. 143602, 2014.

[92] Y.-X. Liu, A. Miranowicz, Y. Gao, J. Bajer, C. Sun, and F. Nori, "Qubit-induced phonon blockade as a signature of quantum behavior in nanomechanical resonators," *Phys. Rev. A*, vol. 82, no. 3, p. 032101, 2010.

[93] N. Didier, S. Pugnetti, Y. M. Blanter, and R. Fazio, "Detecting phonon blockade with photons," *Phys. Rev. B*, vol. 84, no. 5, p. 054503, 2011.

[94] A. Miranowicz, J. Bajer, N. Lambert, Y.-X. Liu, and F. Nori, "Tunable multiphonon blockade in coupled nanomechanical resonators," *Phys. Rev. A*, vol. 93, no. 1, p. 013808, 2016.

[95] H. Seok and E. Wright, "Antibunching in an optomechanical oscillator," *Phys. Rev. A*, vol. 95, no. 5, p. 053844, 2017.

[96] G.-W. Deng, D. Zhu, X.-H. Wang, C.-L. Zou, J.-T. Wang, H.-O. Li, G. Cao, D. Liu, Y. Li, M. Xiao, *et al.*, "Strongly coupled nanotube electromechanical resonators," *Nano Lett.*, vol. 16, no. 9, pp. 5456–5462, 2016.

[97] E. Babourina-Brooks, A. Doherty, and G. Milburn, "Quantum noise in a nanomechanical duffing resonator," *New J. Phys.*, vol. 10, no. 10, p. 105020, 2008.

[98] X.-W. Xu, A.-X. Chen, and Y.-X. Liu, "Phonon blockade in a nanomechanical resonator resonantly coupled to a qubit," *Phys. Rev. A*, vol. 94, no. 6, p. 063853, 2016.

[99] S. Guan, W. P. Bowen, C. Liu, and Z. Duan, "Phonon antibunching effect in coupled nonlinear micro/nanomechanical resonator at finite temperature," *EPL*, vol. 119, no. 5, p. 58001, 2017.

[100] C. Hohberger and K. Karrai, "Self-oscillation of micromechanical resonators," in *Nanotechnology, 2004. Proceedings of the 4th IEEE conference on nanotechnology*, pp. 419–421, IEEE, 2004.

[101] T. Carmon, H. Rokhsari, L. Yang, T. J. Kippenberg, and K. J. Vahala, "Temporal behavior of radiation-pressure-induced vibrations of an optical microcavity phonon mode," *Phys. Rev. Lett.*, vol. 94, no. 22, p. 223902, 2005.

[102] T. Kippenberg, H. Rokhsari, T. Carmon, A. Scherer, and K. Vahala, "Analysis of radiation-pressure induced mechanical oscillation of an optical microcavity," *Phys. Rev. Lett.*, vol. 95, no. 3, p. 033901, 2005.

[103] C. Metzger, M. Ludwig, C. Neuenhahn, A. Ortlieb, I. Favero, K. Karrai, and F. Marquardt, "Self-induced oscillations in an optomechanical system driven by bolometric backaction," *Phys. Rev. Lett.*, vol. 101, no. 13, p. 133903, 2008.

[104] M. Ludwig, B. Kubala, and F. Marquardt, "The optomechanical instability in the quantum regime," *New J. Phys.*, vol. 10, no. 9, p. 095013, 2008.

[105] G. Anetsberger, O. Arcizet, Q. P. Unterreithmeier, R. Rivière, A. Schliesser, E. M. Weig, J. P. Kotthaus, and T. J. Kippenberg, "Near-field cavity optomechanics with nanomechanical oscillators," *Nat. Phys.*, vol. 5, no. 12, p. 909, 2009.

[106] M. Eichenfield, J. Chan, R. M. Camacho, K. J. Vahala, and O. Painter, "Optomechanical crystals," *Nature*, vol. 462, no. 7269, p. 78, 2009.

[107] Q. Lin, J. Rosenberg, X. Jiang, K. J. Vahala, and O. Painter, "Mechanical oscillation and cooling actuated by the optical gradient force," *Phys. Rev. Lett.*, vol. 103, no. 10, p. 103601, 2009.

[108] T. Antoni, K. Makles, R. Braive, T. Briant, P.-F. Cohadon, I. Sagnes, I. Robert-Philip, and A. Heidmann, "Nonlinear mechanics with suspended nanomembranes," *EPL*, vol. 100, no. 6, p. 68005, 2013.

[109] G. S. Agarwal and S. Huang, "Electromagnetically induced transparency in mechanical effects of light," *Phys. Rev. A*, vol. 81, no. 4, p. 041803, 2010.

[110] S. Weis, R. Rivière, S. Deléglise, E. Gavartin, O. Arcizet, A. Schliesser, and T. J. Kippenberg, "Optomechanically induced transparency," *Science*, vol. 330, no. 6010, pp. 1520–1523, 2010.

[111] J. Teufel, D. Li, M. Allman, K. Cicak, A. Sirois, J. Whittaker, and R. Simmonds, "Circuit cavity electromechanics in the strong-coupling regime," *Nature*, vol. 471, no. 7337, p. 204, 2011.

[112] A. H. Safavi-Naeini, T. M. Alegre, J. Chan, M. Eichenfield, M. Winger, Q. Lin, J. T. Hill, D. E. Chang, and O. Painter, "Electromagnetically induced transparency and slow light with optomechanics," *Nature*, vol. 472, no. 7341, p. 69, 2011.

[113] X. Zhou, F. Hocke, A. Schliesser, A. Marx, H. Huebl, R. Gross, and T. J. Kippenberg, "Slowing, advancing and switching of microwave signals using circuit nanoelectromechanics," *Nat. Phys.*, vol. 9, no. 3, p. 179, 2013.

[114] D. Vitali, S. Gigan, A. Ferreira, H. Böhm, P. Tombesi, A. Guerreiro, V. Vedral,

A. Zeilinger, and M. Aspelmeyer, "Optomechanical entanglement between a movable mirror and a cavity field," *Phys. Rev. Lett.*, vol. 98, no. 3, p. 030405, 2007.

[115] A. Mari and J. Eisert, "Opto-and electro-mechanical entanglement improved by modulation," *New J. Phys.*, vol. 14, no. 7, p. 075014, 2012.

[116] S. Mancini, V. Giovannetti, D. Vitali, and P. Tombesi, "Entangling macroscopic oscillators exploiting radiation pressure," *Phys. Rev. Lett.*, vol. 88, no. 12, p. 120401, 2002.

[117] C. Genes, A. Mari, P. Tombesi, and D. Vitali, "Robust entanglement of a micromechanical resonator with output optical fields," *Phys. Rev. A*, vol. 78, no. 3, p. 032316, 2008.

[118] A. Clerk, F. Marquardt, and K. Jacobs, "Back-action evasion and squeezing of a mechanical resonator using a cavity detector," *New J. Phys.*, vol. 10, no. 9, p. 095010, 2008.

[119] M. Woolley, A. Doherty, G. Milburn, and K. Schwab, "Nanomechanical squeezing with detection via a microwave cavity," *Phys. Rev. A*, vol. 78, no. 6, p. 062303, 2008.

[120] A. Mari and J. Eisert, "Gently modulating optomechanical systems," *Phys. Rev. Lett.*, vol. 103, no. 21, p. 213603, 2009.

[121] U. Akram, N. Kiesel, M. Aspelmeyer, and G. J. Milburn, "Single-photon optomechanics in the strong coupling regime," *New J. Phys.*, vol. 12, no. 8, p. 083030, 2010.

[122] M. Vanner, M. Aspelmeyer, and M. Kim, "Quantum state orthogonalization and a toolset for quantum optomechanical phonon control," *Phys. Rev. Lett.*, vol. 110, no. 1, p. 010504, 2013.

[123] F. Khalili, S. Danilishin, H. Miao, H. Müller-Ebhardt, H. Yang, and Y. Chen, "Preparing a mechanical oscillator in non-gaussian quantum states," *Phys. Rev. Lett.*, vol. 105, no. 7, p. 070403, 2010.

[124] M. Vengalattore, M. Hafezi, M. Lukin, and M. Prentiss, "Optical bistability at low light level due to collective atomic recoil," *Phys. Rev. Lett.*, vol. 101, no. 6, p. 063901, 2008.

[125] A. Dalafi, M. Naderi, M. Soltanolkotabi, and S. Barzanjeh, "Controllability of optical bistability, cooling and entanglement in hybrid cavity optomechanical systems by nonlinear atom–atom interaction," *J. Phys. B: At. Mol. Opt. Phys.*, vol. 46, no. 23, p. 235502, 2013.

[126] Y. He, "Optomechanically induced transparency associated with steady-state en-

tanglement," *Phys. Rev. A*, vol. 91, no. 1, p. 013827, 2015.

[127] M. Aspelmeyer, S. Gröblacher, K. Hammerer, and N. Kiesel, "Quantum optomechanics—throwing a glance," *J. Opt. Soc. Am. B*, vol. 27, no. 6, pp. A189–A197, 2010.

[128] M. Wallquist, K. Hammerer, P. Rabl, M. Lukin, and P. Zoller, "Hybrid quantum devices and quantum engineering," *Phys. Scr.*, vol. 2009, no. T137, p. 014001, 2009.

[129] D. E. Chang, C. Regal, S. Papp, D. Wilson, J. Ye, O. Painter, H. J. Kimble, and P. Zoller, "Cavity opto-mechanics using an optically levitated nanosphere," *Proc. Natl. Acad. Sci. U.S.A.*, vol. 107, no. 3, pp. 1005–1010, 2010.

[130] P. Barker, "Doppler cooling a microsphere," *Phys. Rev. Lett.*, vol. 105, no. 7, p. 073002, 2010.

[131] K. Stannigel, P. Rabl, A. S. Sørensen, P. Zoller, and M. D. Lukin, "Optomechanical transducers for long-distance quantum communication," *Phys. Rev. Lett.*, vol. 105, no. 22, p. 220501, 2010.

[132] S. Camerer, M. Korppi, A. Jöckel, D. Hunger, T. W. Hänsch, and P. Treutlein, "Realization of an optomechanical interface between ultracold atoms and a membrane," *Phys. Rev. Lett.*, vol. 107, no. 22, p. 223001, 2011.

[133] A. Dantan, B. Nair, G. Pupillo, and C. Genes, "Hybrid cavity mechanics with doped systems," *Phys. Rev. A*, vol. 90, no. 3, p. 033820, 2014.

[134] Q. Xu, S. Sandhu, M. L. Povinelli, J. Shakya, S. Fan, and M. Lipson, "Experimental realization of an on-chip all-optical analogue to electromagnetically induced transparency," *Phys. Rev. Lett.*, vol. 96, no. 12, p. 123901, 2006.

[135] J. Cho, D. G. Angelakis, and S. Bose, "Heralded generation of entanglement with coupled cavities," *Phys. Rev. A*, vol. 78, no. 2, p. 022323, 2008.

[136] Y. Sato, Y. Tanaka, J. Upham, Y. Takahashi, T. Asano, and S. Noda, "Strong coupling between distant photonic nanocavities and its dynamic control," *Nat. Photonics*, vol. 6, no. 1, p. 56, 2012.

[137] C. Zheng, X. Jiang, S. Hua, L. Chang, G. Li, H. Fan, and M. Xiao, "Controllable optical analog to electromagnetically induced transparency in coupled high-q microtoroid cavities," *Opt. Express*, vol. 20, no. 16, pp. 18319–18325, 2012.

[138] B. Peng, Ş. K. Özdemir, F. Lei, F. Monifi, M. Gianfreda, G. L. Long, S. Fan, F. Nori, C. M. Bender, and L. Yang, "Parity–time-symmetric whispering-gallery microcavities," *Nat. Phys.*, vol. 10, no. 5, p. 394, 2014.

[139] C. W. Gardiner and P. Zoller, *Quantum noise: a handbook of Markovian and*

non-Markovian quantum stochastic methods with applications to quantum optics, vol. 56. Springer Science & Business Media, 2004.

[140] V. Giovannetti and D. Vitali, "Phase-noise measurement in a cavity with a movable mirror undergoing quantum brownian motion," *Phys. Rev. A*, vol. 63, no. 2, p. 023812, 2001.

[141] S. Chakram, Y. Patil, L. Chang, and M. Vengalattore, "Dissipation in ultrahigh quality factor sin membrane resonators," *Phys. Rev. Lett.*, vol. 112, no. 12, p. 127201, 2014.

[142] F. Bariani, S. Singh, L. Buchmann, M. Vengalattore, and P. Meystre, "Hybrid optomechanical cooling by atomic λ systems," *Phys. Rev. A*, vol. 90, no. 3, p. 033838, 2014.

[143] A. H. Safavi-Naeini, J. Chan, J. T. Hill, T. P. M. Alegre, A. Krause, and O. Painter, "Observation of quantum motion of a nanomechanical resonator," *Phys. Rev. Lett.*, vol. 108, no. 3, p. 033602, 2012.

[144] I. Wilson-Rae, N. Nooshi, W. Zwerger, and T. J. Kippenberg, "Theory of ground state cooling of a mechanical oscillator using dynamical backaction," *Phys. Rev. Lett.*, vol. 99, no. 9, p. 093901, 2007.

[145] J. Teufel, J. Harlow, C. Regal, and K. Lehnert, "Dynamical backaction of microwave fields on a nanomechanical oscillator," *Phys. Rev. Lett.*, vol. 101, no. 19, p. 197203, 2008.

[146] M. Li, W. H. Pernice, and H. X. Tang, "Reactive cavity optical force on microdisk-coupled nanomechanical beam waveguides," *Phys. Rev. Lett.*, vol. 103, no. 22, p. 223901, 2009.

[147] A. Xuereb, R. Schnabel, and K. Hammerer, "Dissipative optomechanics in a michelson-sagnac interferometer," *Phys. Rev. Lett.*, vol. 107, no. 21, p. 213604, 2011.

[148] K. Hammerer, K. Stannigel, C. Genes, P. Zoller, P. Treutlein, S. Camerer, D. Hunger, and T. W. Hänsch, "Optical lattices with micromechanical mirrors," *Phys. Rev. A*, vol. 82, no. 2, p. 021803, 2010.

[149] L. Ding, C. Baker, P. Senellart, A. Lemaitre, S. Ducci, G. Leo, and I. Favero, "Wavelength-sized gaas optomechanical resonators with gigahertz frequency," *Appl. Phys. Lett.*, vol. 98, no. 11, p. 113108, 2011.

[150] J. S. Bennett, L. S. Madsen, M. Baker, H. Rubinsztein-Dunlop, and W. P. Bowen, "Coherent control and feedback cooling in a remotely coupled hybrid atom–

optomechanical system," *New J. Phys.*, vol. 16, no. 8, p. 083036, 2014.

[151] X. Chen, Y.-C. Liu, P. Peng, Y. Zhi, and Y.-F. Xiao, "Cooling of macroscopic mechanical resonators in hybrid atom-optomechanical systems," *Phys. Rev. A*, vol. 92, no. 3, p. 033841, 2015.

[152] Y.-C. Liu, Y.-F. Xiao, X. Luan, and C. W. Wong, "Optomechanically-induced-transparency cooling of massive mechanical resonators to the quantum ground state," *Sci. China-Phys. Mech. Astron.*, vol. 58, no. 5, pp. 1–6, 2015.

[153] M. Nomura, N. Kumagai, S. Iwamoto, Y. Ota, and Y. Arakawa, "Laser oscillation in a strongly coupled single-quantum-dot–nanocavity system," *Nat. Phys.*, vol. 6, no. 4, p. 279, 2010.

[154] S. Hughes and H. Carmichael, "Phonon-mediated population inversion in a semiconductor quantum-dot cavity system," *New J. Phys.*, vol. 15, no. 5, p. 053039, 2013.

[155] K. Usami, A. Naesby, T. Bagci, B. M. Nielsen, J. Liu, S. Stobbe, P. Lodahl, and E. S. Polzik, "Optical cavity cooling of mechanical modes of a semiconductor nanomembrane," *Nat. Phys.*, vol. 8, no. 2, p. 168, 2012.

[156] S. Anguiano, G. Rozas, A. Bruchhausen, A. Fainstein, B. Jusserand, P. Senellart, and A. Lemaitre, "Spectra of mechanical cavity modes in distributed bragg reflector based vertical gaas resonators," *Phys. Rev. B*, vol. 90, no. 4, p. 045314, 2014.

[157] O. Kyriienko, T. C. H. Liew, and I. A. Shelykh, "Optomechanics with cavity polaritons: dissipative coupling and unconventional bistability," *Phys. Rev. Lett.*, vol. 112, no. 7, p. 076402, 2014.

[158] E. A. Sete, H. Eleuch, and C. R. Ooi, "Entanglement between exciton and mechanical modes via dissipation-induced coupling," *Phys. Rev. A*, vol. 92, no. 3, p. 033843, 2015.

[159] Y.-D. Wang and A. A. Clerk, "Using interference for high fidelity quantum state transfer in optomechanics," *Phys. Rev. Lett.*, vol. 108, no. 15, p. 153603, 2012.

[160] S. McGee, D. Meiser, C. Regal, K. Lehnert, and M. Holland, "Mechanical resonators for storage and transfer of electrical and optical quantum states," *Phys. Rev. A*, vol. 87, no. 5, p. 053818, 2013.

[161] K. Bergmann, H. Theuer, and B. Shore, "Coherent population transfer among quantum states of atoms and molecules," *Rev. Mod. Phys.*, vol. 70, no. 3, p. 1003, 1998.

[162] Y.-C. Liu, Y.-F. Xiao, X. Luan, and C. W. Wong, "Dynamic dissipative cooling of a

mechanical resonator in strong coupling optomechanics," *Phys. Rev. Lett.*, vol. 110, no. 15, p. 153606, 2013.

[163] A. Fainstein, N. D. Lanzillotti-Kimura, B. Jusserand, and B. Perrin, "Strong optical-mechanical coupling in a vertical gaas/alas microcavity for subterahertz phonons and near-infrared light," *Phys. Rev. Lett.*, vol. 110, no. 3, p. 037403, 2013.

[164] J. M. Dobrindt, I. Wilson-Rae, and T. J. Kippenberg, "Parametric normal-mode splitting in cavity optomechanics," *Phys. Rev. Lett.*, vol. 101, no. 26, p. 263602, 2008.

[165] C. H. Metzger and K. Karrai, "Cavity cooling of a microlever," *Nature*, vol. 432, no. 7020, p. 1002, 2004.

[166] S. Gigan, H. Böhm, M. Paternostro, F. Blaser, G. Langer, J. Hertzberg, K. C. Schwab, D. Bäuerle, M. Aspelmeyer, and A. Zeilinger, "Self-cooling of a micromirror by radiation pressure," *Nature*, vol. 444, no. 7115, p. 67, 2006.

[167] T. Corbitt, C. Wipf, T. Bodiya, D. Ottaway, D. Sigg, N. Smith, S. Whitcomb, and N. Mavalvala, "Optical dilution and feedback cooling of a gram-scale oscillator to 6.9 mk," *Phys. Rev. Lett.*, vol. 99, no. 16, p. 160801, 2007.

[168] J. Thompson, B. Zwickl, A. Jayich, F. Marquardt, S. Girvin, and J. Harris, "Strong dispersive coupling of a high-finesse cavity to a micromechanical membrane," *Nature*, vol. 452, no. 7183, p. 72, 2008.

[169] D. Wilson, C. Regal, S. Papp, and H. Kimble, "Cavity optomechanics with stoichiometric sin films," *Phys. Rev. Lett.*, vol. 103, no. 20, p. 207204, 2009.

[170] A. D. O'Connell, M. Hofheinz, M. Ansmann, R. C. Bialczak, M. Lenander, E. Lucero, M. Neeley, D. Sank, H. Wang, M. Weides, *et al.*, "Quantum ground state and single-phonon control of a mechanical resonator," *Nature*, vol. 464, no. 7289, p. 697, 2010.

[171] M. Schmidt, M. Ludwig, and F. Marquardt, "Optomechanical circuits for nanomechanical continuous variable quantum state processing," *New J. Phys.*, vol. 14, no. 12, p. 125005, 2012.

[172] A. H. Safavi-Naeini and O. Painter, "Proposal for an optomechanical traveling wave phonon–photon translator," *New J. Phys.*, vol. 13, no. 1, p. 013017, 2011.

[173] A. Nunnenkamp, K. Børkje, and S. M. Girvin, "Single-photon optomechanics," *Phys. Rev. Lett.*, vol. 107, no. 6, p. 063602, 2011.

[174] B. Dayan, A. S. Parkins, T. Aoki, E. P. Ostby, K. J. Vahala, and H. J. Kimble, "A photon turnstile dynamically regulated by one atom," *Science*, vol. 319, no. 5866,

pp. 1062–1065, 2008.

[175] A. Imamoglu, H. Schmidt, G. Woods, and M. Deutsch, "Strongly interacting photons in a nonlinear cavity," *Phys. Rev. Lett.*, vol. 79, no. 8, p. 1467, 1997.

[176] D. E. Chang, V. Gritsev, G. Morigi, V. Vuletić, M. D. Lukin, and E. A. Demler, "Crystallization of strongly interacting photons in a nonlinear optical fibre," *Nat. Phys.*, vol. 4, no. 11, pp. 884–889, 2008.

[177] M. J. Hartmann, F. G. S. L. Brandao, and M. B. Plenio, "Strongly interacting polaritons in coupled arrays of cavities," *Nat. Phys.*, vol. 2, no. 12, pp. 849–855, 2006.

[178] A. D. Greentree, C. Tahan, J. H. Cole, and L. C. L. Hollenberg, "Quantum phase transitions of light," *Nat. Phys.*, vol. 2, no. 12, pp. 856–861, 2006.

[179] A. Miranowicz, J. Bajer, M. Paprzycka, Y. Liu, A. M. Zagoskin, and F. Nori, "State-dependent photon blockade via quantum-reservoir engineering," *Phys. Rev. A*, vol. 90, no. 3, p. 033831, 2014.

[180] C. Lang *et al.*, "Observation of resonant photon blockade at microwave frequencies using correlation function measurements," *Phys. Rev. Lett.*, vol. 106, no. 24, p. 243601, 2011.

[181] A. J. Hoffman, S. J. Srinivasan, S. Schmidt, L. Spietz, J. Aumentado, H. E. Türeci, and A. A. Houck, "Dispersive photon blockade in a superconducting circuit," *Phys. Rev. Lett.*, vol. 107, no. 5, p. 053602, 2011.

[182] Y. Zhou, H. Shen, X. Zhang, and X. Yi, "Zero eigenvalues of a photon blockade induced by a non-hermitian hamiltonian with a gain cavity," *Phys. Rev. A*, vol. 97, no. 4, p. 043819, 2018.

[183] O. Kyriienko and T. C. Liew, "Triggered single-photon emitters based on stimulated parametric scattering in weakly nonlinear systems," *Phys. Rev. A*, vol. 90, no. 6, p. 063805, 2014.

[184] A. Miranowicz, M. Paprzycka, Y. Liu, J. Bajer, and F. Nori, "Two-photon and three-photon blockades in driven nonlinear systems," *Phys. Rev. A*, vol. 87, no. 2, p. 023809, 2013.

[185] G. H. Hovsepyan, A. R. Shahinyan, and G. Y. Kryuchkyan, "Multiphoton blockades in pulsed regimes beyond stationary limits," *Phys. Rev. A*, vol. 90, no. 1, p. 013839, 2014.

[186] W.-W. Deng, G.-X. Li, and H. Qin, "Enhancement of the two-photon blockade in a strong-coupling qubit-cavity system," *Phys. Rev. A*, vol. 91, no. 4, p. 043831, 2015.

[187] F.-Y. Hong and S.-J. Xiong, "Single-photon transistor using microtoroidal resonators," *Phys. Rev. A*, vol. 78, no. 1, p. 013812, 2008.

[188] Y. Han, B. He, K. Heshami, C.-Z. Li, and C. Simon, "Quantum repeaters based on rydberg-blockade-coupled atomic ensembles," *Phys. Rev. A*, vol. 81, no. 5, p. 052311, 2010.

[189] H.-Z. Wu, Z.-B. Yang, and S.-B. Zheng, "Implementation of a multiqubit quantum phase gate in a neutral atomic ensemble via the asymmetric rydberg blockade," *Phys. Rev. A*, vol. 82, no. 3, p. 034307, 2010.

[190] D. Gerace, H. E. Türeci, A. Imamoglu, V. Giovannetti, and R. Fazio, "The quantum-optical josephson interferometer," *Nat. Phys.*, vol. 5, no. 4, pp. 281–284, 2009.

[191] I. Carusotto, D. Gerace, H. E. Tureci, S. De Liberato, C. Ciuti, and A. Imamoglu, "Fermionized photons in an array of driven dissipative nonlinear cavities," *Phys. Rev. Lett.*, vol. 103, no. 3, p. 033601, 2009.

[192] M. J. Hartmann, "Polariton crystallization in driven arrays of lossy nonlinear resonators," *Phys. Rev. Lett.*, vol. 104, no. 11, p. 113601, 2010.

[193] L.-M. Duan, M. Lukin, J. I. Cirac, and P. Zoller, "Long-distance quantum communication with atomic ensembles and linear optics," *Nature*, vol. 414, no. 6862, pp. 413–418, 2001.

[194] H. J. Kimble, "The quantum internet," *Nature*, vol. 453, no. 7198, pp. 1023–1030, 2008.

[195] J. L. O'Brien, A. Furusawa, and J. Vučković, "Photonic quantum technologies," *Nat. Photonics*, vol. 3, no. 12, pp. 687–695, 2009.

[196] S. Gupta, K. L. Moore, K. W. Murch, and D. M. Stamper-Kurn, "Cavity nonlinear optics at low photon numbers from collective atomic motion," *Phys. Rev. Lett.*, vol. 99, no. 21, p. 213601, 2007.

[197] S. Ferretti, V. Savona, and D. Gerace, "Optimal antibunching in passive photonic devices based on coupled nonlinear resonators," *New J. Phys.*, vol. 15, no. 2, p. 025012, 2013.

[198] H. Flayac, D. Gerace, and V. Savona, "An all-silicon single-photon source by unconventional photon blockade," *Sci. Rep.*, vol. 5, p. srep11223, 2015.

[199] H. Z. Shen, Y. H. Zhou, and X. X. Yi, "Tunable photon blockade in coupled semiconductor cavities," *Phys. Rev. A*, vol. 91, no. 6, p. 063808, 2015.

[200] H. Flayac and V. Savona, "Single photons from dissipation in coupled cavities," *Phys. Rev. A*, vol. 94, no. 1, p. 013815, 2016.

[201] F. Zou, D.-G. Lai, and J.-Q. Liao, "Photon blockade effect in a coupled cavity system," *arXiv:1803.06642*, 2018.

[202] V. Savona, "Unconventional photon blockade in coupled optomechanical systems," *arXiv:1302.5937*, 2013.

[203] A. Majumdar, M. Bajcsy, A. Rundquist, and J. Vučković, "Loss-enabled sub-poissonian light generation in a bimodal nanocavity," *Phys. Rev. Lett.*, vol. 108, no. 18, p. 183601, 2012.

[204] W. Zhang, Z. Yu, Y. Liu, Y. Peng, *et al.*, "Optimal photon antibunching in a quantum-dot–bimodal-cavity system," *Phys. Rev. A*, vol. 89, no. 4, p. 043832, 2014.

[205] X.-W. Xu and Y. Li, "Strong photon antibunching of symmetric and antisymmetric modes in weakly nonlinear photonic molecules," *Phys. Rev. A*, vol. 90, no. 3, p. 033809, 2014.

[206] M.-A. Lemonde, N. Didier, and A. A. Clerk, "Antibunching and unconventional photon blockade with gaussian squeezed states," *Phys. Rev. A*, vol. 90, no. 6, p. 063824, 2014.

[207] O. Kyriienko, I. A. Shelykh, and T. C. H. Liew, "Tunable single-photon emission from dipolaritons," *Phys. Rev. A*, vol. 90, no. 3, p. 033807, 2014.

[208] D. Gerace and V. Savona, "Unconventional photon blockade in doubly resonant microcavities with second-order nonlinearity," *Phys. Rev. A*, vol. 89, no. 3, p. 031803, 2014.

[209] Y. H. Zhou, H. Z. Shen, and X. X. Yi, "Unconventional photon blockade with second-order nonlinearity," *Phys. Rev. A*, vol. 92, no. 2, p. 023838, 2015.

[210] H. Snijders, J. Frey, J. Norman, H. Flayac, V. Savona, A. Gossard, J. Bowers, M. van Exter, D. Bouwmeester, and W. Löffler, "Single photons and unconventional photon blockade in quantum dot cavity-QED," *arXiv:1803.10992*, 2018.

[211] D. Chang, A. H. Safavi-Naeini, M. Hafezi, and O. Painter, "Slowing and stopping light using an optomechanical crystal array," *New J. Phys.*, vol. 13, no. 2, p. 023003, 2011.

[212] S. M. Tan, "A computational toolbox for quantum and atomic optics," *J. Opt. B: Quantum Semiclass. Opt.*, vol. 1, no. 4, p. 424, 1999.

[213] J. Johansson, P. Nation, and F. Nori, "Qutip: An open-source python framework for the dynamics of open quantum systems," *Comput. Phys. Commun.*, vol. 183, no. 8, pp. 1760–1772, 2012.

[214] J. Johansson, P. Nation, and F. Nori, "Qutip 2: A python framework for the dynam-

ics of open quantum systems," *Comput. Phys. Commun.*, vol. 184, no. 4, pp. 1234–1240, 2013.

[215] P. Knight and G. Gerry, *Introductory Quantum Optics*. Cambridge University Press, 2005.

[216] C. M. Caves, K. S. Thorne, R. W. Drever, V. D. Sandberg, and M. Zimmermann, "On the measurement of a weak classical force coupled to a quantum-mechanical oscillator. I. issues of principle," *Rev. Mod. Phys.*, vol. 52, no. 2, p. 341, 1980.

[217] M. F. Bocko and R. Onofrio, "On the measurement of a weak classical force coupled to a harmonic oscillator: experimental progress," *Rev. Mod. Phys.*, vol. 68, no. 3, p. 755, 1996.

[218] M. A. Nielsen and I. L. Chuang, *Quantum computation and quantum information*. Cambridge university press, 2010.

[219] K. Stannigel, P. Komar, S. Habraken, S. Bennett, M. D. Lukin, P. Zoller, and P. Rabl, "Optomechanical quantum information processing with photons and phonons," *Phys. Rev. Lett.*, vol. 109, no. 1, p. 013603, 2012.

[220] M. A. Kastner, "Artificial atoms," *Phys. Today*, vol. 46, pp. 24–24, 1993.

[221] X. Wang, A. Miranowicz, H.-R. Li, and F. Nori, "Method for observing robust and tunable phonon blockade in a nanomechanical resonator coupled to a charge qubit," *Phys. Rev. A*, vol. 93, no. 6, p. 063861, 2016.

[222] T. Ramos, V. Sudhir, K. Stannigel, P. Zoller, and T. J. Kippenberg, "Nonlinear quantum optomechanics via individual intrinsic two-level defects," *Phys. Rev. Lett.*, vol. 110, no. 19, p. 193602, 2013.

[223] H. Xie, C.-G. Liao, X. Shang, M.-Y. Ye, and X.-M. Lin, "Phonon blockade in a quadratically coupled optomechanical system," *Phys. Rev. A*, vol. 96, no. 1, p. 013861, 2017.

[224] H.-Q. Shi, X.-T. Zhou, X.-W. Xu, and N.-H. Liu, "Tunable phonon blockade in quadratically coupled optomechanical systems," *Sci. Rep.*, vol. 8, no. 1, p. 2212, 2018.

[225] H. Flayac and V. Savona, "Unconventional photon blockade," *Phys. Rev. A*, vol. 96, no. 5, p. 053810, 2017.

[226] W. Hensinger, D. W. Utami, H.-S. Goan, K. Schwab, C. Monroe, and G. Milburn, "Ion trap transducers for quantum electromechanical oscillators," *Phys. Rev. A*, vol. 72, no. 4, p. 041405, 2005.

[227] P.-C. Ma, J.-Q. Zhang, Y. Xiao, M. Feng, and Z.-M. Zhang, "Tunable double op-

tomechanically induced transparency in an optomechanical system," *Phys. Rev. A*, vol. 90, no. 4, p. 043825, 2014.

[228] R.-X. Chen, L.-T. Shen, and S.-B. Zheng, "Dissipation-induced optomechanical entanglement with the assistance of coulomb interaction," *Phys. Rev. A*, vol. 91, no. 2, p. 022326, 2015.

[229] X.-W. Xu, Y.-X. Liu, C.-P. Sun, and Y. Li, "Mechanical PT symmetry in coupled optomechanical systems," *Phys. Rev. A*, vol. 92, no. 1, p. 013852, 2015.

[230] J. Bochmann, A. Vainsencher, D. D. Awschalom, and A. N. Cleland, "Nanomechanical coupling between microwave and optical photons," *Nat. Phys.*, vol. 9, no. 11, p. 712, 2013.

[231] R. W. Andrews, R. W. Peterson, T. P. Purdy, K. Cicak, R. W. Simmonds, C. A. Regal, and K. W. Lehnert, "Bidirectional and efficient conversion between microwave and optical light," *Nat. Phys.*, vol. 10, no. 4, p. 321, 2014.

Journal Publications

1. **Bijita Sarma** and Amarendra K. Sarma, 'Ground-state cooling of micromechanical oscillators in the unresolved sideband regime induced by a quantum well,' *Phys. Rev. A* **93**, 033845 (2016).

2. **Bijita Sarma** and Amarendra K. Sarma, 'Controllable optical bistability in a hybrid optomechanical system,' *J. Opt. Soc. Am. B* **33**, 1335 (2016).

3. **Bijita Sarma** and Amarendra K. Sarma, 'Quantum-interference-assisted photon blockade in a cavity via parametric interactions,' *Phys. Rev. A* **96**, 053827 (2017).

4. **Bijita Sarma** and Amarendra K. Sarma, 'Single-photon blockade in a hybrid cavity-optomechanical system via third-order nonlinearity,' *J. Phys. B: At. Mol. Opt. Phys.* **51**, 075505 (2018).

5. **Bijita Sarma** and Amarendra K. Sarma, 'Unconventional photon blockade in three-mode optomechanics,' *Phys. Rev. A* **98**, 013826 (2018).

6. **Bijita Sarma** and Amarendra K. Sarma, 'Tunable phonon blockade in weakly nonlinear coupled mechanical resonators via Coulomb interaction,' arXiv:1803.10403 (under review).

Conference Publications

1. **Bijita Sarma** and Amarendra K. Sarma, 'Atom assisted cavity cooling of a micromechanical oscillator in the unresolved sideband regime,' *Journal of Physics: Conference series (IOP)* **759**, 012059 (2016).

2. **Bijita Sarma** and Amarendra K. Sarma, 'Strong Antibunching in a Kerr-type Optomechanical Cavity,' in 13th International Conference on Fiber Optics and Photonics, *OSA Technical Digest* (online) (Optical Society of America, 2016), paper P1A.19.

Bijita Sarma

Curriculum Vitae

Doctoral Student,
Department of Physics,
Indian Institute of Technology (IIT) Guwahati
Guwahati, Assam-781039, India
✉ *bijitasarma@gmail.com, s.bijita@iitg.ernet.in*

Education

2013–now **IIT Guwahati**, *Ph.D.*, Physics.
Advisor: Prof. Amarendra Kumar Sarma.
Thesis Title: Ground-State Cooling and Photon Antibunching in Cavity Optomechanical Systems.

2011–2013 **IIT Guwahati**, *M.Sc.*, Physics.
Courses: Classical Mechanics, Electrodynamics, Quantum Mechanics, Mathematical Physics, Atomic and Molecular Physics, Statistical Mechanics, Computer Programming, Numerical Methods and Computational Physics, Solid State Physics, Nonlinear Optics, Quantum Field Theory, Nanostructured Materials.
CGPI: 9.39/10 (1st rank in the batch)

2007–2010 **Cotton College**, *B.Sc.*, Physics.
Courses: Physics (Major), Mathematics, Statistics, English.
Percentage: 81.3 (1st rank in the university with distinction)

2005–2007 **Cotton College**, *Higher Secondary*, Science.
Courses: Physics, Chemistry, Mathematics, English, Assamese.
Percentage: 82.0

2005 **Dharmapur Jnanadayini High School**, *High School*.
Courses: Science, Mathematics, Social Studies, Advanced Mathematics, English, Assamese.
Percentage: 92.5 (3rd rank in the state of Assam)

Achievements

2013 **Institute silver medal**, *IIT Guwahati, for obtaining 1st rank in M.Sc. Physics, batch of 2013*.

2013 **Qualified GATE**, *Graduate Aptitude Test in Engineering, for pursuing Ph.D. in IITs/IISc*.

2013 **Qualified NET**, *National Eligibility Test for lectureship*.

2013 **Merit Scholarship of 1 Lakh Rupees**, *Chief Minister's Scheme for Financial Assistance to Meritorious Students of Assam*.

2012-13 **Merit-cum-means Scholarship**, *IIT Guwahati, awarded to top 25% students of the class*.

2012 **Scholarship from ONGC**, *awarded for obtaining highest mark in M.Sc. 1st year*.

2011 **Qualified JAM**, *Joint Admission Test for M.Sc., for joining IITs/IISc for M.Sc*.

2010 **Dr. H. C. Bhuyan memorial gold medal**, *Gauhati University, for obtaining 1st rank in B.Sc. Physics, batch of 2010*.

2007 **Merit Scholarship from Director of Higher Education, Assam**, *for excellence at the Class XII examination across the state of Assam*.

2005 **Shantiram Das memorial gold medal from Assam Science Society**, *for obtaining highest mark in Mathematics in the state of Assam in Class X examination*.

2005 **Anundoram Borooah Award from Government of Assam**, *for excellence at the Class X level examination across the state of Assam*.

Teaching Experience

2015 – 2017 Teaching assistant for Numerical programming courses for M.Sc. and B.Tech students in IIT Guwahati.

2014 – 2015 Teaching assistant for General Physics and Advanced Physics laboratories for B.Tech and M.Sc. students in IIT Guwahati.

Presentations (Conferences/Seminars)

Apr. 2018 **Participation**, *C3QS: Coherent Control of Complex Quantum Systems*, 17-20 April, 2018, OIST Graduate University, Okinawa, Japan.

Mar. 2018 **Poster presentation**, *Recent Trends in Cold and Ultracold Matter*, 27-29 March, 2018, IIT Guwahati, India.
Topic: Optomechanical ground-state cooling in the unresolved sideband regime.

Feb. 2018 **Invited talk**, *National Science Day*, 28 February, 2018, IIT Guwahati, India.
Topic: Phonon blockade in weakly nonlinear mechanical resonators in an optomechanical cavity.

Jul. 2017 **Poster presentation**, *ICTS school on Open Quantum Systems*, 24-29 July, 2017, ICTS Bangalore, India.
Topic: Ground-state cooling in cavity optomechanics.

Dec. 2016 **Poster presentation**, *PHOTONICS 2016*, 04-08 December, 2016, IIT Kanpur, India.
Topic: Strong antibunching in a Kerr-type optomechanical cavity.

Nov. 2016 **Oral presentation**, *International Conference on Light and Light-based Technologies, ICLLT-2016*, 26-28 November, 2016, Tezpur University, India.
Topic: Photon blockade in optomechanical systems.

Mar. 2016 **Poster presentation**, *Research Conclave*, 17-20 March, 2016, IIT Guwahati, India.
Topic: Sideband cooling of micromechanical resonators in cavity optomechanics.

Dec. 2015 **Poster presentation**, *XXVII IUPAP Conference on Computational Physics (CCP-2015)*, 2-5 December, 2015, IIT Guwahati, India.
Topic: Atom assisted cavity cooling of a micromechanical oscillator in the unresolved sideband regime.

Nov. 2015 **Participation**, *South Asian Workshop on Optics & Photonics, 'SAWOP-2015'*, 17-18 November, 2015, IIT Guwahati, India..

Oct. 2015 **Poster presentation**, *TEQIP symposium on International Year of Light and Light based Technologies*, 31 October, 2015, IIT Guwahati, India.
Topic: Quantum Optics with Cavity Optomechanical Systems.

School attended

2017 **DST-SERB School on Frontiers in Quantum Optics**, 1-19 December, 2017, IIT Guwahati, India.

2017 **ICTS School on Open Quantum Systems**, 17 July-04 August, 2017, ICTS Bangalore, India.

2014 **ICTS School and Discussion Meeting on Frontiers in Light-Matter Interactions**, 8-12 December, 2014, IACS, Kolkata, India.